Titre: Title:	Multi(six)-port impulse ultra-wideband radio system
Auteur: Author:	Yan Yang Zhao
Date:	2006
Type:	Mémoire ou thèse / Dissertation or Thesis
Référence: Citation:	Zhao, Y. Y. (2006). Multi(six)-port impulse ultra-wideband radio system [Thèse de doctorat, École Polytechnique de Montréal]. PolyPublie. https://publications.polymtl.ca/7789/

UNIVERSITÉ DE MONTRÉAL

MULTI(SIX)-PORT IMPULSE ULTRA-WIDEBAND RADIO SYSTEM

YAN YANG ZHAO
DÉPARTEMENT DE GÉNIE ÉLECTRIQUE
ÉCOLE POLYTECHNIQUE DE MONTRÉAL

THÈSE PRÉSENTÉE EN VUE DE L'OBTENTION
DU DIPLÔME DE PHILOSOPHIAE DOCTOR (Ph.D.)
(GÉNIE ÉLECTRIQUE)
SEPTEMBRE 2006

Your file Votre référence
ISBN: 978-0-494-24554-5
Our file Notre référence
ISBN: 978-0-494-24554-5

UNIVERSITÉ DE MONTRÉAL

ÉCOLE POLYTECHNIQUE DE MONTRÉAL

Cette thèse intitulée :

MULTI(SIX)-PORT IMPULSE ULTRA-WIDEBAND RADIO SYSTEM

présente par : YAN YANG ZHAO

En vue de l'obtention du diplôme de : PHILOSOPHIAE DOCTOR (Ph. D.)

A été dûment accepte par le jury d'examen constitué de :

M. KE, WU, Ph.D., président

M. CHARLES DESPINS, Ph. D., membre externe

M. CHRISTOPHE CALOZ, Ph. D., membre

M. RENATO G. BOSISIO, M. SC. A, membre et directeur de recherche

M. JEAN-FRANÇOIS FRIGON, Ph.D., membre et co-directeur de recherche

DEDICATION

To my parents

To my wife: Lijuan

To my sons: Dezheng and Boyu

To my sisters: Yanlin and Yanjun

To my niece: Yinfeng and Yibao

ACKNOWLEDGEMENTS

The research work presented in this dissertation was completed during my doctoral project at the Centre de recherché Poly-Grames (CRP), Départment de Génie Électrique, École Polytechnique de Montréal, Université de Montréal, Montréal, Québec, Canada.

I would like to express my sincere gratitude to my current (2003-2006) thesis director, Professor Renato G. Bosisio, co-director Professor Jean-François Frigon, and my previous director - Professor Ke Wu (from 2002 to 2003) for offering me the opportunity and financial support to pursue Ph.D. programme and for their fruitful advice, guidance, and encouragement throughout my doctoral project and course work.

I would also like to thank all thesis jury members for their time and remarks in reviewing this thesis.

Recognition and immense gratitude to Prof. Christophe Caloz is also acknowledged for equipment loan and his leadership in UWB research activities at CRP.

Thanks to Professor Bozzi and Professor Perregrini for loan of UWB antenna developed at University of Pavia, Pavia, Italy.

My gratitude is also due to my colleagues: Abielmona Samer, Cornelius Viereck, Ding Yan, Hu Xiao, Jiang Xiaoma, Li Duochuan, Li Lin, Li Zhaolong, Munir Ashad, Nguyen Van Hoang, Wang Ligen, Xu Feng, Xu Xinyu, Yang Ping, and Zhang Hui for their generous help.

I would like to thank staff members and technicians from CPR for their assistance and collaboration.

RÉSUMÉ

La technologie de transmission à large bande (en anglais "UWB") attire l'intérêt de plusieurs chercheurs et industries pour ses multiples avantages. Par exemple, la possibilité de combiner un système de communications avec un système de positionnement simple. La faible probabilité d'interception rend cette technologie prometteuse. Des études antérieures ont démontré les avantages que la technologie six-port apporte, soit une large bande passante, les faibles coûts et sa simplicité. De plus, des travaux ont poussé l'analyse de cette technologie dans le but d'explorer son utilisation dans des systèmes de communication à bande étroite. L'objectif de ce présent projet est d'étudier la technologie six-port de point de vue d'un système d'impulsion-UWB. Dans ce sens, cette thèse porte sur l'utilisation de la technologie UWB pour un système radio à impulsion six-port (MIR). Les contributions du projet sont un modulateur six-port à bande passante ultra large, un démodulateur, de nouvelles technologies de modulation spectrales en phase et des algorithmes de traitement de signal. Les résultats des simulations et expérimentaux sont présentés dans cette thèse.

Le système MIR possédant une bande passante de 500 MHz a été réalisé en utilisant des composantes commerciales. Une confirmation des résultats de simulations a été effectuée en mesurant un signal d'impulsions UWB (I-UWB). Le système MIR est utilisé pour valider les nouveaux algorithmes de modulation spectrale de phase binaire (BPSM) et la quadrature (QPSM) à large bande (3-4GHz), utilisant le modulateur et démodulateur six-port. Étant donné l'absence d'un générateur monocycle, le spectre de phase de 1 GHz est généré à l'aide d'un signal d'impulsion carré et par la suite, monté en

fréquence par des filtres, un mélangeur et un oscillateur local. Le signal d'impulsion de 3 à 4 GHz est appliqué à l'entrée RF du modulateur six-port et les données numériques synchronisées sont envoyées à une matrice de commutation terminant soit avec un court-circuit ou un circuit ouvert, les quatre autres ports du modulateur. Cette opération permet d'obtenir un signal de sortie modulé en BPSM ou QPSM. À la réception, la première entrée du démodulateur reçoit la phase modulée du signal tandis que la deuxième reçoit le signal non modulé servant de référence. Les quatre sorties du démodulateur six-port fournissent les signaux de différentes amplitudes utilisés par le DSP pour déterminer l'état de modulation avec les algorithmes de traitement de signal. Les algorithmes de modélisation, de démodulation et de synchronisation sont implémentés sur une plateforme de traitement de signal DSP basées sur une matrice FPGA et équipées de quatre convertisseur analogiques et numériques. Le MIR a été préalablement simulé avec le logiciel ADS de la compagnie Agilent Technologies en utilisant un canal de bruit blanc Gaussien (AWGN). Le banc d'essais utilisé a été utilisé pour déterminer le taux d'erreur par bit (BER) avec un canal AWGN avec et sans fils. Un débit binaire de 20 Mbps fut choisi en conformité avec les instruments utilisés. Le taux d'erreur par bit obtenu est comparable aux valeurs théoriques calculées et aux résultats de simulation. D'autres facteurs de dégradation de performance du système, tels que les interférences et les propagations multiples ont été étudié et des méthodes de mitigation ont été intégré. Le MIR UWB peut coexister avec les systèmes radio existant même s'il augmente le planché de bruit. Une courte comparaison avec d'autres systèmes UWB est aussi présentée. Dans le futur, le système MIR pourra être intégré avec des méthodes de

communications multi-bande OFDM pour créer une plateforme unique UWB.

ABSTRACT

Ultra-wideband (UWB) technology has attracted the interest of research institutions and the industry due to its numerous advantages such as low probability of interception and the possibility of combining data communication with positioning in a single system. Previous studies have shown that six-port technology can be used for single carrier communications and has several advantages such as wideband operation, low cost, and simplicity. The objective of this project is to study the multi(six)-port technology for impulse-UWB communications. In this thesis, original contributions are made on a multi(six)-port impulse radio (MIR) system including ultra-wideband six-port modulator, demodulator, novel phase spectrum modulation (PSM) schemes, and signal processing algorithms. Simulation and experimental results have been obtained and are presented in this thesis.

A MIR platform operating over a limited bandwidth of 1 GHz has been designed and implemented with commercial components. The MIR was used to validate wide band (3GHz–4GHz) new binary phase spectrum modulation (BPSM) and quaternary phase spectrum modulation (QPSM) schemes using wideband six-port modulator and demodulator circuits. Due to the lack of a monocycle generator, the 1-GHz spectral phase channel is generated from a rectangular pulse signal, upconverted using filters, mixer, and local oscillator. The 3–4GHz pulsed signal is applied to the RF input of a six-port modulator and digital data is simultaneously fed to a switch matrix terminating four ports of the new modulator with either a short circuit or open circuit. This technique produces an output RF signal in BPSM or QPSM scheme. At the receiver, one input port

of the six-port demodulator is fed with the RF phase modulated signal and the second input port is fed with a reference non-modulated signal. The demodulator's four outputs provide signals of different amplitudes, which are used by a DSP to determine the modulation state with proper digital signal processing (DSP) algorithms. Modulation, demodulation algorithms and synchronization control are implemented on a field-programmable gate-array (FPGA) based DSP platform fitted with four analog-to-digital converters (ADCs). Assuming an additive white Gaussian noise (AWGN) channel, the proposed MIR was first simulated with the advanced design system (ADS) software tool of Agilent Technologies. The test bench version was then used for bit error rate (BER) measurements with both wired and wireless AWGN channels. A data rate of 20 Mbps was used for this measurement in conformity with the available instruments. The measured BER results have been successfully compared with simulation and theoretical results. Also other factors degrading the system performance, such as signal interference and multipath propagation were investigated and mitigation methods have been proposed. The MIR UWB is able to coexist with exiting radio system although it raises the noise floor to a certain degree. A brief comparison with other UWB systems is also given.

In future, a single integrated MIR UWB prototype is expected to accommodate both impulse-UWB and multi-band UWB standards.

CONDENSÉ EN FRANÇAIS

SYSTÈME DE RADIO MULTI (SIX)-PORTES À IMPULSION ULTRA-LARGE BANDE

0.1 Introduction

La technologie de transmission à large bande (UWB) a attiré une attention considérable dans le domaine des communications sans fil à courte portée et des applications d'identification de positionnement par la fréquence radio (RF). Les avantages principaux de cette technologie incluent la résolution d'intervalle de temps fin, l'immunité à l'interférence par trajets multiples, la basse probabilité d'interception du signal, la basse complexité et le prix réduit, et les possibilités de combiner la communication de données avec le positionnement dans un système simple.

Un signal UWB est défini comme un signal avec une largeur de bande partielle instantanée (B_f) plus grande que 0.20. La largeur de bande partielle est déterminée comme suit:

$$B_f = 2\frac{f_H - f_L}{f_H + f_L}\ , \tag{1}$$

où f_L et f_H sont les points $-3\ dB$ inférieurs et supérieurs dans le spectre de signal, respectivement. Le rapport de la Commission fédérale de communications (FCC) des États-Unis d'Amérique sur l'UWB définit un signal UWB comme un signal ayant une largeur de bande, à -10dB, de 500MHz (ou plus), cela indépendamment de la valeur de la largeur de bande partielle instantanée. La FCC fixe aussi la limite maximum de la puissance de rayonnement à $-41.3\ dBm/MHz$ entre 3.1GHz et 10.6GHz pour les

applications UWB d'intérieur.

Les types d'émetteur pour les présents systèmes UWB sont sans porteuse et avec porteuse. Le sans porteuse UWB, également connu sous le nom d'UWB à impulsion (I-UWB), utilise des impulsions très courtes pour la transmission d'information. Les modulations les plus communes pour la communication d'I-UWB incluent la modulation de position de l'impulsion (PPM), la modulation d'amplitude de l'impulsion (PAM), et la modulation de la forme de l'impulsion. Dans les modulations mentionnées ci-dessus, les données d'information sont transmises soit par la position, l'amplitude ou la forme de l'impulsion. Et la norme la plus reconnue pour l'I-UWB est la séquence directe UWB (DS-UWB). D'autre part, l'UWB avec porteuse utilise de multiples porteuses simultanées pour la transmission. Plusieurs formes communes d'UWB avec porteuse existent, comme l'UWB à multi-bandes (MB-UWB). Dans cette catégorie, l'OFDM à multi-bandes (MB-OFDM) est la norme dominante.

La technologie six-portes a été employée pour la première fois dans les systèmes de mesure micro-ondes pour déterminer le coefficient de réflexion complexe d'un circuit. La technologie six-portes a également été appliquée aux récepteurs de communication en obtenant le rapport complexe d'un signal reçue inconnu avec le signal connu de l'oscillateur local (LO). L'information d'amplitude et de phase fournie par ce rapport complexe peut être employée pour obtenir la phase et l'amplitude du signal modulé. Le récepteur six-portes démodule directement l'information provenant d'un signal avec porteuse modulé soit en quadrature de phase (QPSK) ou en quadrature d'amplitude (QAM).

En plus du récepteur six-portes, un modulateur de phase en quadrature basé sur la technologie six-portes a été récemment introduit pour un signal à une seule porteuse. Des radars basés sur la technologie six-portes ont également été étudiés comme alternative à la sonde standard utilisée dans les radars à onde continue par modulation de fréquence (FMCW). En effet l'information sur la distance et la fréquence de Doppler contenue dans le vecteur complexe du rapport entre le signal transmis et celui reçu peut être extrait en utilisant un discriminateur phase/fréquence six-portes.

L'aspect le plus important d'un circuit six-portes est la capacité d'exécuter la discrimination précise de phase autant dans la bande de la fréquence radio (RF) que dans la bande de fréquence à ondes millimétriques, ce circuit pouvant être facilement conçu pour opérer sur une large bande de fréquence.

Les études précédentes sur la technologie six-portes ont prouvé que cette technologie a plusieurs avantages tels que l'opération à large bande, le faible coût, et la simplicité. Cependant l'utilisation d'une radio à large bande basée sur un circuit six-portes pour traiter un signal UWB occupant une largeur de bande absolue de plus de 500 mégahertz n'a pas encore été réalisée. Le présent projet comblera cette lacune.

Dans ce travail, une plateforme de radio multi(six)-portes à impulsion (MIR) pour la communication UWB est conçue et mise en application. La plateforme adopte une architecture quasi-symétrique de récepteur et d'émetteur (à l'aide des circuits six-portes pour moduler et démoduler digitalement un plein spectre de phase de 1 GHz conformément à la définition du FCC UWB). Une nouvelle modulation spectrale de phase (PSM) est proposée pour la plateforme de radio multi(six)-portes à impulsion pour

une opération en UWB. Cette nouvelle modulation spectrale de phase code l'information dans le spectre de phase d'un signal à impulsion sur un canal large bande. Dans des méthodes précédentes de modulation, l'information est codée par la position, par l'amplitude ou par la forme d'une impulsion, mais n'emploie pas la modulation à large bande du spectre de phase du canal.

Des algorithmes de modulation et de démodulation développés sont programmés dans une plateforme de traitement de signal digital (DSP) utilisant des circuits programmables (FPGA). La plateforme de la MIR UWB est simulée et mesurée en assumant un canal gaussien avec bruit blanc (AWGN). Les mesures sont effectuées pour ces deux raccordements : lien direct par câble et lien sans fil à l'aide d'une antenne UWB appropriée. Des résultats expérimentaux sur les effets d'interférence par trajets multiples à bande étroite, et de coexistence avec des signaux radios standards à bande étroite sont également obtenus.

0.2 Description de système et génération de signal de l'impulsion UWB

Un système de communication UWB doit avoir une occupation spectrale instantanée au-dessus de 500 mégahertz ou une largeur de bande partielle de plus de 20%. La définition d'UWB par la FCC ne limite pas la génération des signaux d'UWB, à condition que la largeur partielle de bande ou la bande minimum (500 mégahertz) soient vérifiées à tout temps de la transmission.

Une façon de produire des signaux UWB est d'employer des transitions de signal très pointues en temps suivi d'un filtre passe-bande. Le signal pointu peut être une impulsion

rectangulaire étroite qui a un spectre à large bande pouvant être ajusté utilisant le filtre passe-bande désiré. C'est une méthode simple et efficace pour produire des signaux UWB, qui est approprié pour certains genres de systèmes UWB. Cependant, la méthode manque d'exactitude pour former et placer avec précision l'énergie de signal UWB dans le spectre de fréquence.

Des signaux UWB peuvent également être produits en utilisant la méthode de génération d'impulsion de précision. Dans cette approche, des signaux UWB sont synthétisés avec précision tant en forme qu'en position dans le spectre de fréquence. Pour ce faire, des signaux sont formés à la bande de base et puis décalés en fréquence à l'endroit désiré dans le spectre en utilisant une technique hétérodyne. Il est beaucoup plus facile de construire le signal dans la bande de base qu'à des fréquences radio plus élevées.

Une autre approche pour produire des signaux UWB est de générer l'impulsion avec une série de Fourier. Dans cette approche, un signal UWB est produit dans le domaine de fréquence en additionnant des harmoniques du signal désiré au lieu de produire le signal avec une seule source de haute puissance dans le domaine du temps. La série de Fourier est normalement employée pour décomposer les signaux périodiques sinusoïdaux. Elle peut être employée à l'envers pour synthétiser un signal périodique. En effet, le train d'impulsion à émettre peut être produit en calculant l'expansion de la série de Fourier du signal puis en générant et émettant chacune des composantes sinusoïdales de l'expansion. Chaque composant harmonique de l'expansion de série de Fourier est produite par un oscillateur et la somme de tous les oscillateurs reproduira les impulsions

périodiques désirées. Seulement des termes finis des séries de Fourier sont employés en raison du nombre fini des oscillateurs. Avec ces contraintes, nous synthétisons approximativement le train d'impulsion désiré.

D'autres méthodes telles que le multiplexage de division fréquentielle orthogonal de bande multiple (MB-OFDM) sont capables de produire des signaux UWB. Au lieu d'employer le principe d'impulsion, les signaux MB-OFDM UWB comprennent la transmission en parallèle de plusieurs signaux qui sont modulés à différentes fréquences porteuses occupant l'attribution correcte de spectre.

Dans l'expérience de la plateforme proposée, un signal d'impulsion s'assortissant avec la largeur de bande du matériel et les équipements disponibles est nécessaire. Par conséquent, la méthode de génération d'impulsion de précision a été adoptée pour produire le signal UWB.

0.3 Modulateur de six-port d'UWB

Les circuits six-portes peuvent être utilisés pour réaliser la modulation directe de phase quand quatre des sorties d'un circuit six-portes sont terminées avec certaines charges. Un tel modulateur direct se compose d'un circuit six-portes, d'une matrice de commutation, des terminaisons court-circuit et circuit-ouvert. Le circuit six-portes est fait de composants passifs, c.-à-d., un diviseur de puissance et trois coupleurs hybrides. Le diviseur de puissance n'a aucune différence de phase entre ses deux portes de sortie. Chaque coupleur hybride fournit en sortie des signaux d'amplitude égale, mais déphasés de 90°. Le modulateur direct six-portes fonctionne comme suit : la porte 1 est alimentée avec un signal non modulé qui est transféré aux portes 3 à 6 par les différentes branches

du circuit six-portes. Les portes 3 à 6 sont reliés aux terminaisons circuit-ouverts ou court-circuit par une matrice de commutation commandée par les données de bande de base à transmettre. Les signaux reflétés sont alors additionnés à la porte 2, qui est le signal modulé. Ce modulateur direct six-portes peut être employé pour moduler un signal avec porteuse ou un signal non sinusoïdal (impulsion) selon la largeur de bande de fonctionnement du modulateur.

Dans ce travail, on propose une nouvelle technique de modulation, appelé la modulation spectrale de phase, pour moduler un signal à impulsion UWB en binaire ou en quadrature. La fonction de modulation d'un modulateur six-portes a été dérivée la première fois en utilisant un signal convoyeur simple. Alors le résultat est prolongé à la modulation spectrale de phase des signaux à impulsion UWB.

La fonction de modulation de phase est décrite en utilisant une fonction de transfert entre les ports 1 et 2. Selon la structure du circuit six-portes, la fonction de transfert entre le port 1 et le port 2 du modulateur peut être dérivée et exprimée comme suit:

$$H_i(f_c) = 0.707 \times e^{-j(\phi_1 + 3\phi_2 + 2\theta + 45^\circ + i \cdot 90^\circ)}, \quad i = 0,1,2,3 \qquad (2)$$

où ϕ_1 est le changement de phase d'une branche de diviseur de puissance, ϕ_2 est le changement de phase d'une branche hybride de coupleur, θ est le changement de phase d'une ligne de transmission, i représente la i^{th} configuration de quatre configurations différentes de terminaisons. Pour une seule porteuse à la fréquence f_c, les valeurs de phase sont constantes. La valeur de $(\phi_1 + 3\phi_2 + 2\theta)$ est le changement de phase total non désiré des composants et des lignes de transmission. Cette valeur peut être ajustée dans

la conception du modulateur pour être un multiple discret de 360° afin d'éliminer la variation de phase du signal modulé.

Quand le signal de référence est un signal à large bande, la phase en (2) change linéairement avec la fréquence. Elle peut être décrite en utilisant la fonction linéaire suivante:

$$\phi(f) = K \cdot f \tag{3}$$

où $\phi(f)$ représente la réponse linéaire idéale de la phase du modulateur en fonction de la fréquence, K est une constante qui dépend des composants du modulateur, et f représente des points de fréquence dans la largeur de bande désirée, par exemple, 3-4 GHz pour la plateforme étudiée.

De l'eq. (2) et (3), on peut voir que la différence de phase entre les états de modulation est satisfaite à n'importe quelle fréquence, alors que la constante K dépend seulement du circuit lui-même. Par conséquent, les courbes de phases sous les quatre états de modulation sont linéaires avec la fréquence et sont parallèles avec une différence de phase 90° entre les états successifs de modulation à n'importe quelle fréquence dans le canal de fonctionnement. La fonction de transfert à quatre états de modulation avec le signal à large bande, tel qu'une impulsion UWB, est exprimée par:

$$H_i(f) = 0.707 \times e^{-j\left[\phi(f)+i\cdot 90^\circ\right]}, \quad i = 0,1,2,3 \tag{4}$$

où i représente i^{th} l'état des quatre états différents de modulation pour la modulation spectrale de phase en quadrature (QPSM).

Si le signal d'entrée est un signal sinusoïdal, le signal de sortie acquiert différentes

phases selon les terminaisons appliquées aux portes 3 à 6. Comparé au modulateur six-portes pour les signaux sinusoïdaux, les différences essentielles quand le modulateur six-portes fonctionne avec les signaux non-sinusoïdaux se situent dans la réponse de phase linéaire à travers la large bande et la modulation spectrale de phase uniforme à travers la largeur de bande du canal. Donc si le signal d'entrée est un signal à large bande, le spectre de phase du signal entier doit être uniformément modulé à n'importe quelle fréquence dans le canal de fonctionnement avec une différence de phase 90° entre les états successifs de modulation.

Les modèles idéal et pratique du six-portes ont été développés pour simuler le modulateur six-portes proposé. Le modèle idéal emploie des paramètres S idéaux du diviseur de puissance et des coupleurs d'hybride du six-port. Le modèle pratique du six-portes a été développé pour faciliter la conception, la fabrication, et la vérification des circuits six-portes. Dans ce modèle, chaque composant (les coupleurs hybrides et le diviseur de puissance) est simulé en utilisant les paramètres S mesurés. Le modulateur six-portes a été simulé pour QPSK et QPSM. Les résultats de simulation sont conformes à la dérivation des eq. (2) et (4). Dans la simulation, une analyse de vecteur d'erreur est également faite pour mesurer les performances du modulateur en termes d'erreurs d'amplitude et de phase. On propose également une méthode de conception optimale pour réduire la contribution du déséquilibre de la phase et d'amplitude à la grandeur du vecteur d'erreur (EVM).

Pour les expériences du modulateur six-portes, les paramètres S ont été mesurés la première fois pour caractériser le modulateur six-portes fabriqué et pour estimer sa

largeur de bande opérationnelle. Des mesures de fonction de modulation ont été également effectuées avec des signaux non-sinusoïdaux à large bande et des signaux sinusoïdaux. Les résultats de mesure sont en accord avec les précédents résultats théoriques et de simulation.

0.4 Démodulateur de six-port d'UWB

Le démodulateur six-portes se compose d'un circuit six-portes utilisant la même structure que le modulateur précédent. Cette quasi-symétrie entre le modulateur et le démodulateur facilite la conception et la fabrication. Les portes 1 et 2 sont alimentées respectivement avec le signal de référence et le signal inconnu à être démodulé. Les quatre signaux de sortie sont simultanément disponibles aux portes 3 à 6, qui sont reliés aux détecteurs de puissance. Les détecteurs de puissance se composent de diodes Schottky zéro-décentrées. Les signaux de sortie des détecteurs de puissance sont alors employés pour la démodulation par méthode analogique ou numérique.

La méthode de démodulation est trouvée en analysant les signaux de sortie du circuit six-portes et des détecteurs de puissance. Selon la structure du circuit, les grandeurs normalisées des sorties des détecteurs de puissance par rapport à la différence de phase $\Delta\theta$ entre les portes 1 et 2 peuvent être dérivées et exprimées en (5).

$$\begin{aligned} s_3 &= 0.5\left|\cos\Delta\theta - 1\right| \\ s_4 &= 0.5\left|-\sin\Delta\theta + 1\right| \\ s_5 &= 0.5\left|\cos\Delta\theta + 1\right| \\ s_6 &= 0.5\left|\sin\Delta\theta + 1\right| \end{aligned} \tag{5}$$

Dans cette équation, s_3 - s_6 sont les grandeurs normalisée normalisées des signaux

aux portes 3-6 respectivement. L'équation (5) est valide pour n'importe quelle fréquence dans le canal.

Pour une certaine différence de phase entre la référence et le signal inconnu, les quatre signaux de sortie ont une amplitude différente qui sera employée pour mettre en application l'algorithme de démodulation. Comme exemple, quand la différence de phase entre le signal de référence et le signal inconnu est $\pi/2$, s_4 a une amplitude minimum et s_6 a une amplitude maximum. Aux portes 3 et 5, les amplitudes du signal de sortie ont des valeurs médianes (entre les amplitudes minimum et maximum). Pour un signal à impulsion modulé par la modulation spectrale de phase, un changement fixe de phase à chaque point de fréquence est maintenu. Ainsi, le profil d'amplitude est également valide.

Le démodulateur six-portes a été simulé avec des signaux avec porteuse et sans porteuses (à impulsion). Les signaux de sortie simulés sont conformes au résultat de dérivation en (5). Un démodulateur six-portes a été conçu et fabriqué en utilisant des composants commerciaux. Pour estimer la largeur de bande efficace du démodulateur six-portes, des mesures de paramètres S ont été effectuées. Des mesures des signaux de sortie pour les quatre états de modulation ont été faites à l'aide du circuit de démodulateur six-portes et des instruments disponibles. Les résultats de mesure sont conformes aux résultats de modélisation et de simulation.

En se basant sur l'analyse et la vérification ci-dessus (simulation et expériences) de la fonction de démodulation six-portes, la démodulation peut être faite en comparant les amplitudes des signaux de sortie et en choisissant la valeur minimale. Des algorithmes

de démodulation ont été programmés dans un circuit FPGA sur la plateforme de DSP. En plus des algorithmes ci-dessus, la gestion d'horloge de bande de base est également intégrée dans la programmation du FPGA.

0.5 Étude d'exécution de système

La performance du système UWB proposé est étudiée pour caractériser la probabilité d'erreur de bit. La relation entre l'énergie par bit par rapport à la densité de puissance du bruit et la probabilité d'erreur de bit pour la modulation spectrale de phase est dérivée en utilisant l'hypothèse suivante - durée limitée d'impulsion, absence de l'interférence entre symbole, pas de multi-trajets, aucune interférence à utilisateurs multiples, et une synchronisation parfaite entre l'émetteur et le récepteur.

Pour le système de modulation spectrale de phase UWB, une analyse dans le domaine fréquentielle est appropriée pour le signal à impulsion utilisé pour la transmission. Premièrement, le spectre d'amplitude et de phase du signal à impulsion modulé a été dérivé en utilisant une expression d'une suite périodique d'impulsion et des théorèmes de transformée de Fourier. Dans la transmission d'un signal MIR UWB, chaque impulsion représente un symbole et la transmission se produit seulement pendant la durée de l'impulsion. L'énergie du symbole peut être calculée en multipliant le temps de durée d'impulsion avec la puissance maximale. Pour le signal pulsé, la puissance maximale est le taux auquel de l'énergie est fournie pendant chaque impulsion. La puissance maximale dans le système de MIR est calculée en intégrant la densité spectrale de puissance sur la largeur de bande utilisée pour la transmission. En supposant que la seule source au récepteur est le bruit gaussien blanc additif (AWGN), la densité spectrale de puissance

du bruit à la température ambiante standard est utilisée dans le calcul de l'énergie par bit par rapport à la densité de puissance du bruit.

L'analyse d'un point de fréquence d'un signal modulé QPSM est équivalente à l'analyse d'un signal avec porteuse modulé QPSK à la même fréquence. Bien que la phase absolue change avec la fréquence, la différence de phase à une fréquence donnée est identique en ce qui concerne la fréquence pendant une période de symbole. En outre, la densité spectrale de puissance du bruit est la même dans le spectre. Par conséquent nous pouvons employer le résultat de performance du taux d'erreur de bit (BER) de la modulation QPSK d'une seule porteuse pour évaluer la modulation QPSM.

Supposons que le signal se propage dans un canal de propagation dans l'air. Par l'analyse de budget du lien, nous pouvons déterminer la puissance de transmission et le rapport signal sur bruit moyen nécessaires pour obtenir un niveau donné de performance à un certain débit désiré. D'une façon similaire, étant donnée la puissance permise, nous pouvons évaluer la distance maximale pour laquelle une probabilité d'erreur prédéterminée peut être garantie au récepteur pour débit donnée.

Le système de radio multi(six)-portes à impulsion UWB complet a été simulé pour obtenir le taux d'erreurs des bits (BER). Dans la simulation, nous avons utilisé la méthode de Monte Carlo pour estimer le BER. Pour que le résultat estimé soit statistiquement significatif, le nombre de bits exigé est typiquement de l'ordre de 10/BER (en règle générale). La fiabilité de l'évaluation du BER est habituellement qualifiée en termes d'intervalles de confiance. Ainsi une certaine variation observée sur les résultats de simulation du BER est raisonnable aussi longtemps que le résultat du

BER est dans l'intervalle de confiance.

Pour prouver le concept du système, un montage utilisant des câbles coaxiaux pour relier directement un émetteur et un récepteur six-portes à impulsion UWB a été réalisé. Le délai dans le circuit de référence est manuellement ajusté pour qu'il corresponde au délai du circuit de réception. Les résultats mesurés du BER sont comparés aux valeurs théoriques et de simulation. La comparaison montre l'accord étroit avec quelques variations, s'étendant typiquement de $0.3\text{x}10^{-4}$ à $1.1\text{x}10^{-4}$ pour un E_b/N_o de 8dB.

Une plateforme MIR UWB a été mise en œuvre en remplaçant la connexion directe câblée par un lien sans fil utilisant des antennes UWB ayant une réponse de phase linéaire sur la bande de fréquence. La mesure du système a été faite en utilisant la plateforme et des antennes UWB. Les résultats mesurés de BER sont comparés aux résultats théoriques, de simulation et de la mesure utilisant le lien direct câblé. L'accord parmi ces résultats prouve encore une fois la fonctionnalité du système UWB proposée dans un canal AWGN, tant avec d'un lien câblé qu'avec un lien sans fil.

Un des problèmes pratiques a considéré dans l'application de la plateforme UWB est la synchronisation. Une recherche a été faite sur le signal de sortie du démodulateur six-portes sous des situations de non-synchronisation, c.-à-d., un délai arbitraire existe entre le signal de référence et le signal reçu. Le but de la recherche est de déduire le délai en observant les signaux aux sorties du démodulateur six-portes. Les résultats de simulation et de ceux avec la plateforme UWB indiquent que la différence de temps entre deux impulsions est équivalente au délai de propagation entre l'impulsion de référence et l'impulsion reçue.

La performance du système peut se dégrader de la performance idéale lorsque d'autres contraintes sont ajoutés, telles que le bruit additif, l'interférence par trajets multiples, l'interférence de canal, et la mise en œuvre pratique de l'émetteur-récepteur, etc. Ce qui suit discute qualitativement de l'influence de certaines de ces contraintes avec les résultats expérimentaux.

Le débit du modulateur six-portes est limité par le temps de commutation. La sensibilité du récepteur six-portes est limitée par la sensibilité des détecteurs de puissance.

Pour l'effet de trajets multiples sur la plateforme MIR UWB, un canal avec deux trajets sans chevauchement a été considéré, c.-à-d., les signaux à impulsion transmis par trajets multiples sont résolubles au récepteur. Le traitement en bande de base choisit le signal le plus fort parmi les deux reçus pour la démodulation, et filtre simplement l'autre signal par commande de synchronisation. Les résultats de BER mesurés montrent que l'immunité de la plateforme MIR UWB sur l'effet de trajets multiples existe dans certaines conditions particulières. Cependant, des algorithmes plus sophistiqués peuvent être développés pour rendre fonctionnel la plateforme pour des canaux réels avec trajets multiples.

Le système MIR UWB emploie une grande largeur de bande pour transmettre l'information. Un signal à bande étroite émis dans la largeur de bande occupée par le signal UWB interférera avec ce système UWB. La dégradation de performance dépend du nombre et de la distribution du signal à bande étroite, des puissances relatives, et du type de modulation utilisé. Dans un environnement pratique, si la fréquence de

l'interférence à bande étroite est connue, plusieurs techniques peuvent être employées pour supprimer cette interférence.

Sur la coexistence avec la radio à bande étroite, la FCC a limité la puissance maximum émise par les systèmes UWB à une densité spectrale de puissance de -41.3 dBm/MHz. Un signal d'impulsion typique UWB a un spectre approximativement plat sur la largeur de bande. Par conséquent, le signal UWB a pour effet de soulever le niveau de bruit des systèmes à bande étroite qui utilisent le même spectre. Une expérience a été faite pour montrer l'effet du signal UWB sur un signal à bande étroite QPSK. Pour le signal à bande étroite, le niveau efficace de bruit est élevé au niveau du signal UWB. La dégradation de performance est visuellement observée sur les constellations mesurées et quantitativement montrée en utilisant la figure de mérite (EVM). Le système MIR UWB proposé est comparé à d'autres systèmes UWB du point de vue qualitatif comme suit :

- Pour des architectures d'émetteur/récepteur, les autres systèmes UWB incluent habituellement un circuit de contrôle de synchronisation ou de forme (dépend de la modulation) du côté de l'émetteur et un circuit de corrélation du côté du récepteur. La MIR UWB adopte une architecture quasi-symétrique d'émetteur récepteur (utilisant le circuit six-portes pour la modulation et la démodulation).
- Pour ce qui est des types de modulation, les modulations les plus répandues dans les systèmes UWB à impulsion existants incluent la modulation de position d'impulsion (PPM), la modulation d'amplitude d'impulsion (PAM), et

la modulation de forme d'impulsion. Dans le système MIR UWB, la modulation spectrale de phase proposée code l'information dans le spectre de phase d'un signal à impulsion sur toute la largeur du canal. Dans des méthodes précédentes de modulation, l'information de données est représentée par la position, l'amplitude ou la forme de l'impulsion, mais n'utilise pas la modulation à large bande du spectre de phase d'un canal seul.

- Un récepteur UWB commun est basé sur un circuit de corrélation qui se compose d'un multiplicateur et d'un intégrateur. La sortie du circuit de corrélation est alors utilisée pour la détection de bit. Dans une plateforme MIR UWB, le démodulateur six-portes à bande large réalise d'une manière équivalente la fonction de corrélation. De plus. ses quatre signaux de sortie facilitent le traitement subséquent des signaux.

0.6 Conclusion et travaux futurs

Une radio multi(six)-portes à impulsion de pour les communications UWB a été proposée et étudiée. La radio multi(six)-portes permet de valider une nouvelle méthode de modulation, soit la modulation spectrale de phase, sur un canal de 3 à 4GHz à l'aide d'un modulateur et d'un démodulateur six-portes. La plateforme UWB réalisée a été mesurée avec un lien direct câblé, un lien sans fil, et un lien avec deux trajets. Les résultats de performance du système ont été obtenus par des simulations et des mesures expérimentales. Ils sont en accord étroit avec les prédictions théoriques. D'autre part, des facteurs dégradant la performance du système ont été étudiés. La MIR UWB peut également coexister avec les systèmes radio existants bien qu'elle élève le niveau de

bruit dans une certaine mesure. Une brève comparaison avec d'autres systèmes UWB a également été donnée. Des principales contributions sont récapitulées comme suit :

- Le concept du circuit six-portes a été appliqué à l'UWB.
- Des algorithmes de modulation et de démodulation spectrale de phase ont été proposés et validés en utilisant des simulations et des résultats expérimentaux
- On a proposé une méthode optimale pour la conception des circuits six-portes
- La performance de la MIR UWB pour le lien sans fil, le canal de trajets multiples simplifiés, et la coexistence avec une radio à bande étroite standard, ont été expérimentalement caractérisés.

Les propositions pour les travaux futurs sur le prototype MIR UWB incluent :

- Conception du circuit intégré qui inclut les antennes UWB, le modulateur six-portes et le démodulateur six-portes sur une seule puce.
- Développez un algorithme de synchronisation pour la MIR.
- Étudiez la possibilité d'adapter sur une même configuration matérielle MIR les normes d'impulsion UWB et des multi-bandes UWB.
- Étudiez la possibilité de réaliser des fonctions de communication UWB et de positionnement avec la même radio MIR.

TABLE OF CONTENTS

FIGURE LIST

TABLE LIST

LIST OF SIGNS AND ABBREVIATION

3GPP	3rd generation partnership project
CPW	Co-planar waveguide
I	In-phase
LUT	Look-up table
MHMIC	Monolithic hybrid microwave integrated circuit
Q	Quadrature
ADC	Analog-to-digital converter
ADS	Advanced design system
AWGN	Additive white Gaussian noise
BER	Bit error rate
BPSK	Binary phase shift keying
BPSM	Binary phase spectrum modulation
CRLH	Composite right/left-handed
DAC	Data access component
DSP	Digital signal processing
DS-UWB	Direct-sequence UWB
DUT	Device under test
EVM	Error vector magnitude
FCC	Federal communications commission
FMCW	Frequency modulation continuous wave

FPGA	Field programmable gate array
GMAC	Giga multiply accumulate
GPS	Global positioning system
IF	Intermediate frequency
IP	Intellectual property
ISI	Inter symbol interference
I-UWB	Impulse-ultra wideband
LEs	Logic elements
LO	Local oscillator
MB-OFDM	Multiband-orthogonal frequency division multiplexing
Mbps	Mega bit per second
MB-UWB	Multiband-ultra wideband
MC-UWB	Multicarrier-ultra wideband
MIR	Multi(six)-port impulse Radio
MMIC	Monolithic microwave integrated circuit
M-PSK	M-ary phase shift keying
Msps	Mega symbol per second
NF	Noise figure
PAM	Pulse amplitude modulation
PCS	Personal communication system
PLL	Phase locked loop
PPM	Pulse position modulation

PPM	Pulse position modulation
PR	Pseudo random
PSD	Power spectral density
PSM	Phase spectrum modulation
QAM	Quadrature amplitude modulation
QPSK	Quadrature phase shift keying
QPSM	Quaternary phase spectrum modulation
RF	Radio frequency
SDR	Software defined radio
SIW	Substrate integrated waveguide
TFMA	Time frequency multiple access
TSDF	Timed synchronous data flow
U-NII	Unlicensed-national information infrastructure
UWB	Ultra wideband
WPAN	Wireless personal area network

CHAPTER 1 INTRODUCTION

1.1 Review of Ultra-Wideband (UWB) technology

Ultra-wideband (UWB) technology has attracted considerable attention in both short-range wireless communication and radio frequency (RF) location sensing applications. Major advantages of this technology include fine time resolution, immunity to multi-path interference, low probability of signal interception, low complexity and low cost, and the capability of combining data communication with positioning in a single system [1]–[4].

A UWB signal is defined as a signal with an instantaneous fractional bandwidth (B_f) greater than 0.20. The fractional bandwidth can be determined as follows [5]:

$$B_f = 2\frac{f_H - f_L}{f_H + f_L}, \tag{1.1}$$

where f_L and f_H are the lower and upper $-3\ dB$ points in the signal spectrum, respectively. The Federal Communications Commission's (FCC) report on UWB [6] also classifies a UWB signal as one having a bandwidth of 500MHz (or more) at -10 dB emission points regardless of the fractional bandwidth value. The FCC sets the maximum radiation limit at $-41.3\ dBm/MHz$ of output power between 3.1 GHz and 10.6 GHz for indoor UWB applications. Fig. 1-1 shows the FCC-mandated spectral masks for unlicensed UWB systems, in comparison with other radio standards, such as global positioning systems (GPS) and personal communication systems (PCS).

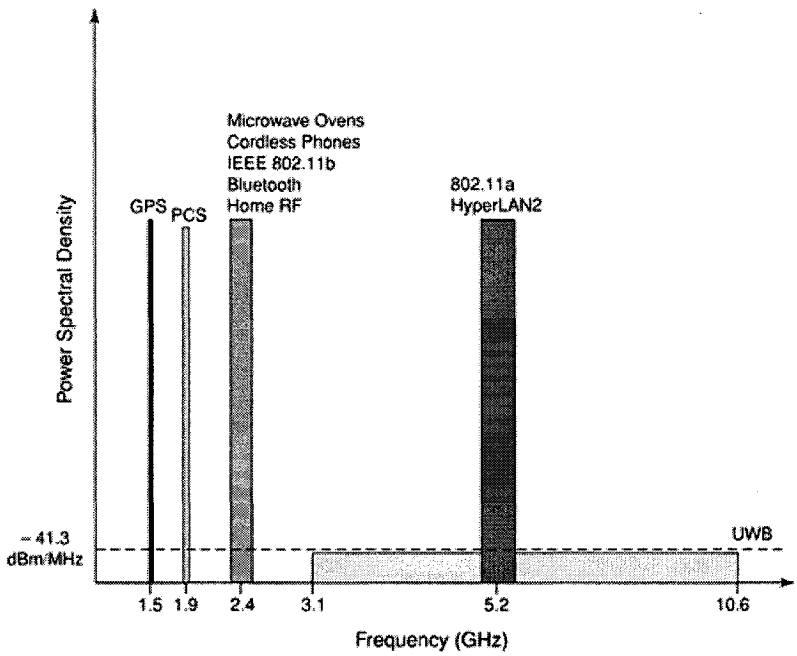

Fig. 1-1. FCC spectral masks for unlicensed UWB systems in comparison with other radio standards [7].

Current UWB systems primarily employ either a carrier-less or a carrier-based transceiver. Carrier-less UWB, also known as Impulse-UWB (I-UWB), utilizes very short pulses in transmission. Common choices for a modulation scheme in I-UWB communication include pulse position modulation (PPM), pulse amplitude modulation (PAM), and pulse shape modulation [8]. In the above modulation schemes, data information is conveyed either in position, amplitude, or shape of a pulse. In I-UWB, Direct-Sequence UWB (DS-UWB) [9] is one of the leading proposed standards for UWB communication. In the DS-UWB system, as shown in Fig. 1-2, the 3.1–10.6 GHz band is divided into a low band from 3.1–4.9 GHz and an optional high band from 6.2–9.7 GHz. The bandwidth of the high band is twice the bandwidth of the low band, resulting in narrower time-domain pulses in the high band, shown in Fig. 1-2. The 4.9–

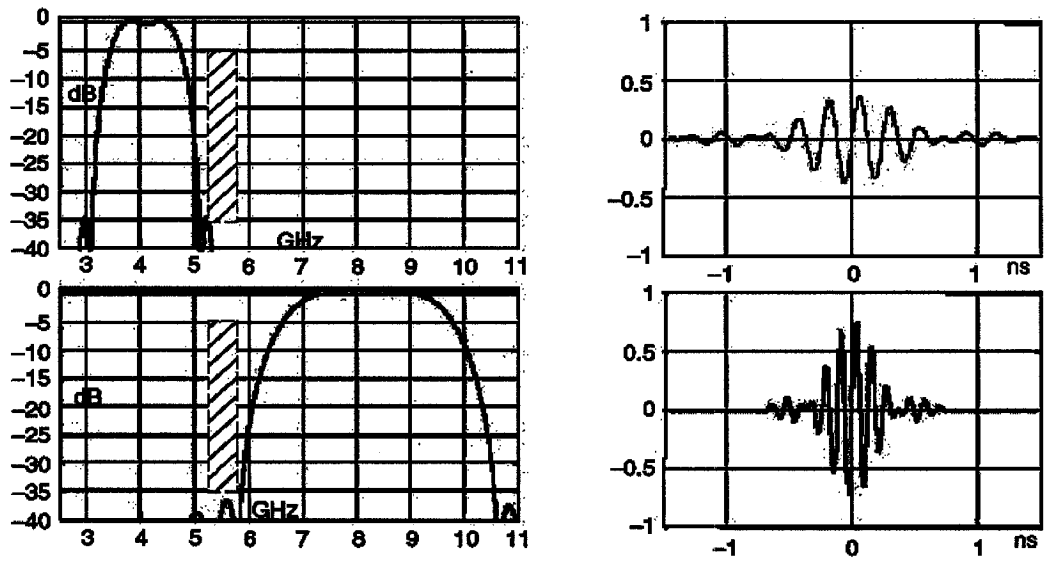

Fig. 1-2. Frequency and time response of the two basic channels in the DS-UWB proposal [9].

6.1 GHz band is purposely neglected to avoid interference with IEEE 802.11a devices operating in the 5 GHz unlicensed national information infrastructure (U-NII) bands. As for the basic cell, referred to as a picocell, it has a nominal coverage range of about 10 m. A network operating within that range is referred to as a piconet. Each piconet of the DS-UWB operates in one of the two bands, and piconets in the same band are separated by code-division multiplexing.

On the other hand, carrier-based UWB uses multiple simultaneous carriers for transmission. Common forms of carrier-based UWB exist such as multicarrier UWB (MC-UWB) and multiband UWB (MB-UWB). In this category, the leading proposed standard is multiband OFDM (MB-OFDM). The MB-OFDM system uses the OFDM technique in the UWB 3.1–10.6 GHz unlicensed bands. By first dividing the spectrum into 15 bands, each with a bandwidth of 528 MHz. In each band a 128-point OFDM

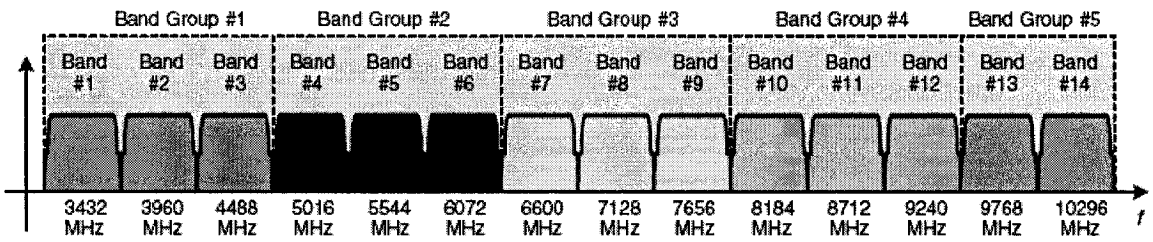

Fig. 1-3. Frequency bands, along with sub-bands, for the MB-OFDM approach to UWB communications in 3.1–10.6 GHz unlicensed UWB bands proposed to the IEEE 802.15.3a WPAN standard [9].

system using QPSK modulation is employed to limit the required precision of mathematical operations and make digital implementation at ultrahigh sampling rates feasible. Fig. 1-3 gives an overview of the MB-OFDM spectrum proposal. The 15 bands in the 3.1−10.6 GHz unlicensed UWB spectrum are divided into five groups of 528-MHz bands. Group 1 is the most desirable because group 2 interferes with U-NII bands and IEEE 802.11a devices, and higher groups have smaller coverage areas. Each physical piconet is implemented in a band group and several logical piconets share a band group using different time-frequency multiple access (TFMA) codes.

Other research and development activities on UWB include UWB channel characteristics, UWB antennas, and generation of UWB waveforms. More detail can be found in [5], [9], [10].

1.2 Review of six-port technology

The six-port technology was first used for microwave measurement to obtain the complex reflection coefficient of a device under test (DUT) [11]. The complex coefficients of the device connected at one input port of a six-port circuit can be determined by observing signal powers at the remaining four output ports which are

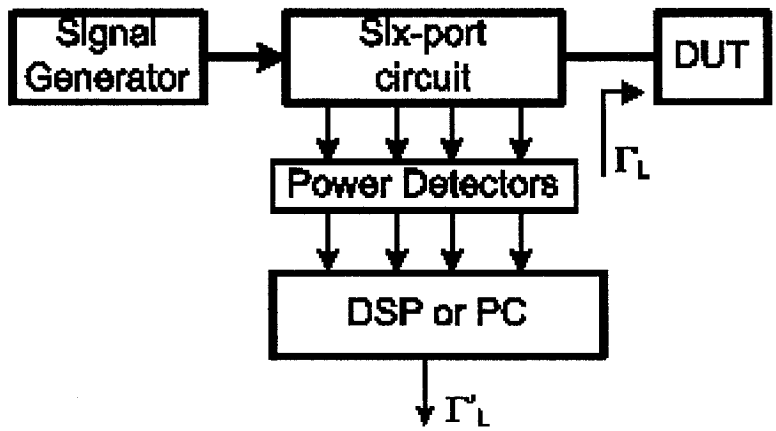

Fig. 1-4. Six-port reflectometer for microwave measurment.

called test ports. Fig. 1-4 shows the diagram of a six-port circuit used for this kind of microwave measurement. One of the benefits of the six-port based measurement technique is that the power measurements at the test ports are from locations other than the position of interest of the DUT. This feature can be utilized to avoid the violation of uniformity using a uniform transmission line or waveguide at the interface between the six-port circuit and the DUT. Other methods for observing the signal (e.g., via probes, etc.) at the position of interest violates the uniformity.

Six-port technology has also been applied to communication receivers [12]–[16], by obtaining the complex ratio of an incoming signal and a known local oscillator (LO) signal. From a communication receiver point of view, the amplitude and phase information embedded in the complex ratio can be used for obtaining the phase and amplitude of the modulated signal. In [12]–[16], the six-port technology was utilized in a direct conversion receiver operated for single carrier signals at millimeter-wave and radio frequencies (RF). The six-port receiver, shown in Fig. 1-5, directly demodulates the data information carried on a single carrier using quadrature phase shift keying

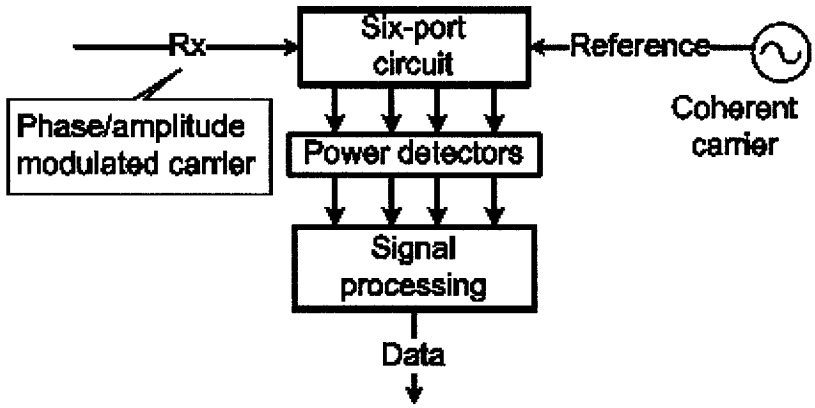

Fig. 1-5. Six-port direct conversion receiver.

(QPSK) or quadrature amplitude modulation (QAM). Standard direct conversion techniques usually use two carrier paths to do the direct conversion without intermediate frequencies (IF), i.e., the in-phase (I) and quadrature signal are separated at RF stage [17]. The previously reported six-port based direct conversion receivers, however, use only one carrier and separate the I and Q signals with signal processing of the four test-port output signals at baseband stage. This direct conversion or demodulation feature of the six-port circuit was applied to a software defined radio (SDR) platform by utilizing the flexibility of signal processing at baseband, shown in Fig. 1-6. Detailed investigations of six-port SDR applications can be found in [13] and [18].

Along with six-port based receivers, a direct quadrature phase shift keying modulator based on six-port technology was recently introduced for a single carrier signal [19]. The modulator is composed of a six-port circuit, a switch matrix and open and short terminations. A conventional QPSK modulator employs heterodyne architecture which requires two intermediate frequency (IF) mixers, in-phase and quadrature-phase carriers, and an RF upconversion section. Compared with a heterodyne

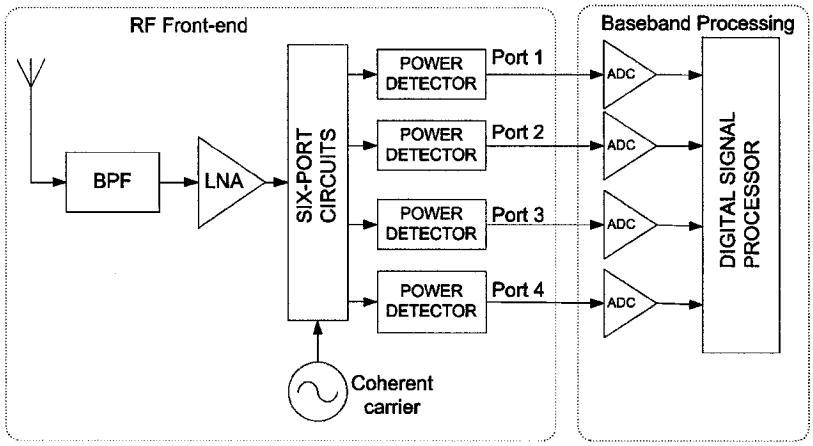

Fig. 1-6. Six-port based SDR receiver architecture.

modulator, this direct QPSK modulator eliminates the need for IF modulation and RF upconversion, consequently reducing power consumption and circuit complexity. Due to the absence of nonlinear elements, another advantage of the six-port based modulator is its dimensional scalability to operate from RF to millimeter wave frequency ranges, which is not the case for other direct modulators [20], [21]. Also, the data rate can be easily increased using M-ary phase shift keying (M-PSK) because the six-port circuit allows a variety of terminations to be applied to its ports.

Six-port based radars were also investigated in [22] and [23] as an alternative to standard frequency modulation continuous wave (FMCW) radar sensor. Range information and Doppler frequency contained in the vector of complex ratio of the transmitted and received signal can be found using six-port phase/frequency discriminator.

Several fabrication technologies have been used for six-port circuits. Tatu [14] demonstrated a six-port module fabricated using monolithic hybrid microwave integrated circuit (MHMIC). The MHMIC six-port module was used as a front-end for

QPSK demodulator operating between 26–28.5 GHz (in Ka band). Moldovan [22] demonstrated a six-port circuit fabricated in metal blocks using machined WR-10 waveguides. The six-port circuit was used at 94-GHz (in W band) as the front-end module of a collision avoidance radar. Xu [24] implemented a six-port junction operating at 24 GHz using a substrate integrated waveguide (SIW) structure. The SIW structure impresses the design and development of low-cost millimeter-wave integrated circuits by allowing the integration of planar and non-planar structures on the same planar platform [25]. Another example of a wideband (0.9–5GHz) six-port circuit is implemented using integrated circuits [15]. A recent study [26] showed a six-port circuit adopting a composite right/left-handed (CRLH) transmission line for its key components. A direct advantage of the six-port is thus that dual bands 3.96 GHz and 7.39 GHz can be covered by the proposed front-end.

1.3 Motivation and objectives

The most important feature of a six-port circuit is the ability to perform accurate phase discrimination both in radio frequency (RF) and millimeter wave frequency range. The phase discrimination capability is feasible over a wide bandwidth as long as the six-port circuit covers the wideband frequency range.

Previous studies, investigating six-port technology for sinusoidal signals, have shown that six-port technology has several advantages such as wideband operation, low cost, and simplicity. For a UWB signal occupying an absolute bandwidth of more than 500 MHz, the implementation of a wideband radio using the six-port circuit has not yet been achieved. The entire 3.1–10.6-GHz UWB band can be covered with one or two six-port

circuits fabricated with low cost integrated circuit chips. The six-port technology for UWB applications is therefore promising and this project will study this topic.

The objectives of this research are as follows:

- Design a multi(six)-port impulse radio (MIR) platform for UWB communication;
- Design and implement a transceiver based on six-port technology using commercial components;
- Propose a certain modulation scheme to access the UWB spectrum;
- Develop modulation and demodulation algorithms;
- Validate the MIR UWB platform by simulation;
- Validate experimentally the MIR UWB platform using a direct connection and a wireless link with manual synchronization adjustment.

In this work, a multi(six)-port impulse radio (MIR) platform for UWB communication is designed and implemented. The platform adopts a quasi-symmetric receiver and transmitter architecture (using six-port circuits to digitally modulate and demodulate a full 1 GHz phase spectrum in accordance with FCC UWB bandwidth). A novel phase spectrum modulation (PSM) scheme is proposed for multi(six)-port impulse radio platform for UWB. The proposed phase spectrum modulation scheme encodes the information in phase spectrum of a pulse signal over a single wideband channel. In previous modulation methods, data information is conveyed either in position, amplitude or shape of a pulse, but do not use wideband single channel phase spectrum modulation.

The MIR transceiver is fabricated using commercial coaxial and planar circuit

components. Based on previous six-port technology [15], it is believed that the entire 3.1-10.6 GHz band can be covered with one or two integrated circuit chips.

Modulation and demodulation algorithms are developed for a field programmable gate array (FPGA) digital signal processing (DSP) platform. The MIR UWB platform is simulated and measured assuming an additive white Gaussian noise (AWGN) channel. The measurements are carried out using both direct connection and wireless link using suitable UWB antenna. Experimental results on effects of multipath, narrowband interference and coexistence with standard narrow band radio are also obtained.

The thesis is organized as follows. In Chapter 2, the multi(six)-port radio platform is briefly introduced. The impulse-UWB signal generating method is also described. Chapter 3 covers detailed results of the six-port modulator. Chapter 4 details the UWB six-port demodulator. Chapter 5 discusses the results of the system performance study. Finally, conclusions and future works are summarized in Chapter 6.

CHAPTER 2 SYSTEM DESCRIPTION AND IMPULSE-UWB SIGNAL GENERATION

2.1 System description

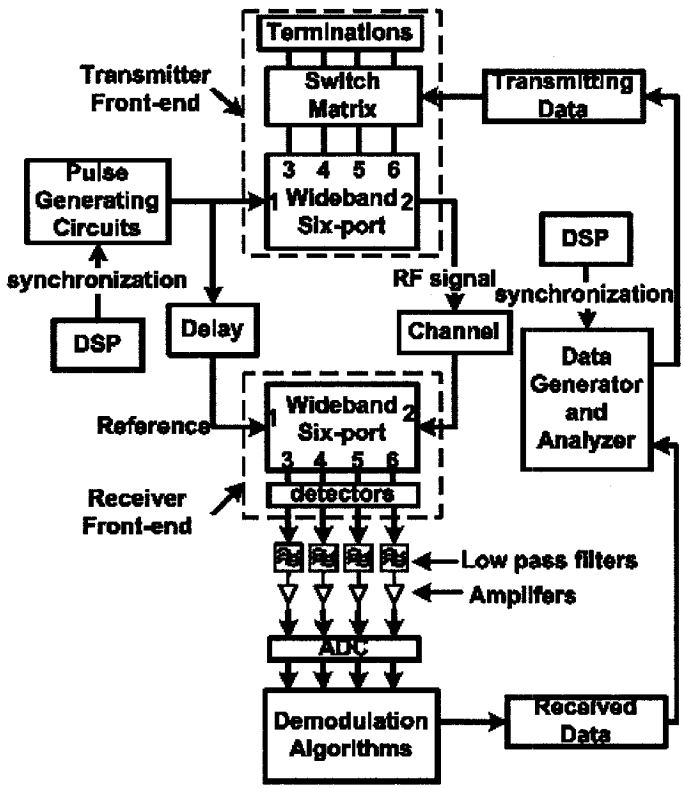

Fig. 2-1. Diagram of Multi(six)-port impulse-UWB platform.

Fig. 2-1 shows a block diagram of the multi(six)-port impulse (MIR) UWB radio platform. It consists of a pulse generating circuit, a six-port modulator as the transmitter front-end, a receiver front-end using a six-port demodulator circuit, and a digital signal processing platform with demodulation and synchronization algorithms. The functions of the platform are described next.

The pulse generating circuits in Fig. 2-1 include a rectangular pulse generator, a low pass filter, and an upconverter. The pulse generator provides a rectangular pulse train at a repetition frequency of 20 MHz with a pulse width of 2 ns. The low pass filter has a passband of 500 MHz. The filtered signal is upconverted to a center frequency of 3.5 GHz and covers the 3–4 GHz band. The above pulse generating circuits is described in details in section 2.2 and can be replaced with a generator of Gaussian monocycle derivatives to cover all channels in UWB.

Data is transmitted on the aforementioned pulse signal using a novel phase spectrum modulation scheme, i.e., binary phase spectrum modulation (BPSM) or quaternary phase spectrum modulation (QPSM). The MIR UWB platform adopts a quasi-symmetric front-end architecture which uses the six-port technology for both the modulator and the demodulator. The wideband six-port modulator provides a simple way to convert data from baseband to a 1-GHz phase modulated spectrum at the center frequency. The modulated pulse signal and non-modulated pulse signal (as a reference) are fed into the receiver front-end. Output signals at ports 3 to 6 provide different signal profiles used for PSM demodulation. The demodulation algorithm is operating on a field programmable gate array (FPGA) signal processing platform fitted with four analog-to-digital converters. The operation of the six-port, along with the phase spectrum modulation scheme and the signal processing algorithms are explained in details in Chapter 3.

2.1 Methods of generating UWB waveforms

UWB communication defines systems with an instantaneous spectral occupancy in excess of 500 MHz or a fractional bandwidth of more than 20%. The fractional bandwidth is defined as B/f_c , where $B = f_H - f_L$ denotes the $-10\,dB$ bandwidth and $f_c = (f_H + f_L)/2$, with f_H and f_L being the upper and lower frequency of the $-10\,dB$ emission points, respectively. The UWB definition released by the FCC, as mentioned in chapter 1, does not limit the generation of UWB signals, provided that the fractional bandwidth or minimum bandwidth (500 MHz) requirements are verified at all times of the transmission

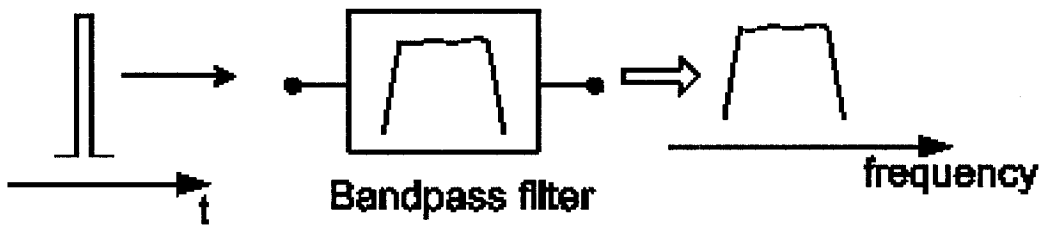

Fig. 2-2. Method 1 of pulse generation.

One way of generating UWB signals is to use very sharp signal transitions in time followed by a band-pass filter, as shown in Fig. 2-2 [30]. The sharp signal can be a narrow rectangular pulse which has a wideband spectrum that can then be shaped using the desired bandpass filter. This is a simple and effective method for generating UWB signals, which is appropriate for certain kinds of UWB systems. However, the method lacks the accuracy to precisely shape and position the UWB signal energy in the frequency spectrum.

UWB signals can also be generated using the method illustrated in Fig. 2-3. In this

approach, UWB signals are precisely synthesized in both the signal shape and position in the frequency spectrum. To that end, signals are shaped at baseband and then shifted in frequency to the desired location in the spectrum using a heterodyne technique. Band shaping is much easier to accomplish at base band than it is at higher radio frequencies.

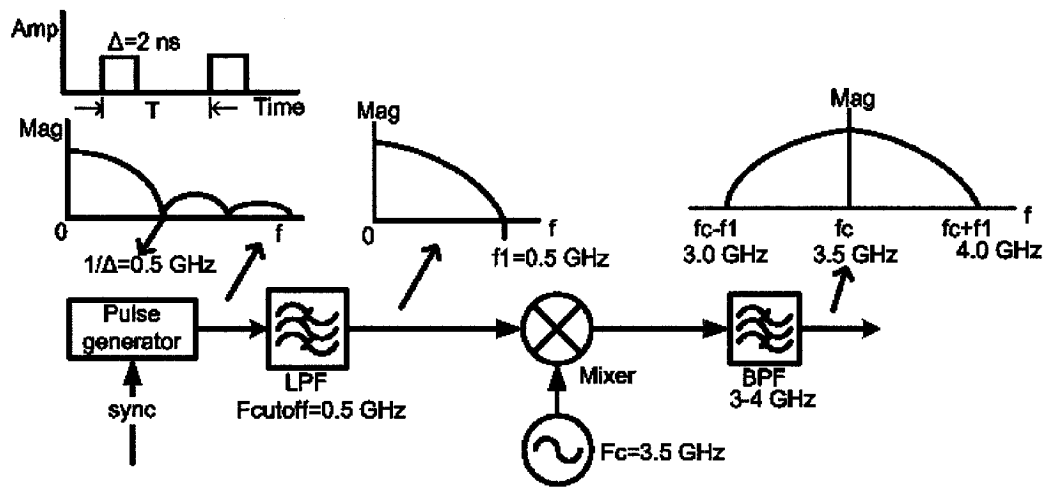

Fig. 2-3. Precision pulse generation.

Another approach to generate UWB signals is Fourier Series-Based pulse generation [31]. In this approach, a UWB signal is generated in the frequency domain by summing harmonics of the desired signal instead of generating the signal by a single high-power source in the time domain. The Fourier series is normally used to decompose periodic signals into sinusoids as described in eq. (2.1).

$$x(t) \approx \sum_{n=1}^{N} \left[a_n \cdot \cos(n\omega_0 t) + b_n \cdot \sin(n\omega_0 t) \right] \approx \sum_{n=1}^{N} c_n \cdot \cos(n\omega_0 t - \phi_n) \qquad (2.1)$$

where ω_0 is the fundamental angular frequency related with the signal repetition interval T as $\omega_0 = 2\pi / T$. The Fourier series can be used in reverse to synthesize a periodic signal. That is, generating a periodic pulse train can be done by finding the Fourier series

expansion of the pulse train to be produced and then generating and transmitting each sinusoidal component of the expansion. A separate oscillator produces each harmonic component of Fourier series expansion and the sum of all the oscillators will reproduce the desired periodic pulses. Only finite terms of Fourier series are used because of finite number of oscillators. With these constraints, we can approximately synthesize a desired pulse train from the truncated Fourier series expansion.

Other methods such as multi band orthogonal frequency-division multiplexing (MB-OFDM) are capable of generating UWB signals. Instead of using the impulse principle, the MB-OFDM UWB signal consists of the parallel transmission of several signals that are modulated at different carrier frequencies occupying the correct spectrum allocation.

2.2 Pulse generation in the experiment

In the experiment of this proposed platform, a pulse signal matching the bandwidth of the hardware and available equipments is necessary. Therefore, the precision signal design method was adopted to generate such an impulse-UWB signal. The pulse signal in the chosen channel (3–4 GHz) is generated using a rectangular pulse generator, a low pass filter, an upconverter, and a band pass filter, as shown in Fig. 2-3. The pulse generator generates a rectangular pulse train at a repetition frequency of 20 MHz. The width of each pulse is 2 ns. The generated pulse train and its spectrum are shown in Fig. 2-4 and Fig. 2-5 respectively. A low pass filter with 500 MHz cut-off frequency is used to filter out frequency points beyond 500 MHz of the rectangular pulse spectrum. The upconverter operates at a center frequency of 3.5 GHz and it converts the portion of the rectangular pulse signal spectrum to a signal spectrum occupying 1-GHz bandwidth

between 3–4 GHz. Fig. 2-6 shows the spectrum of the generated UWB signal. The above pulse generating circuits can be replaced with a generator of Gaussian monocycle derivatives to cover all channels in UWB.

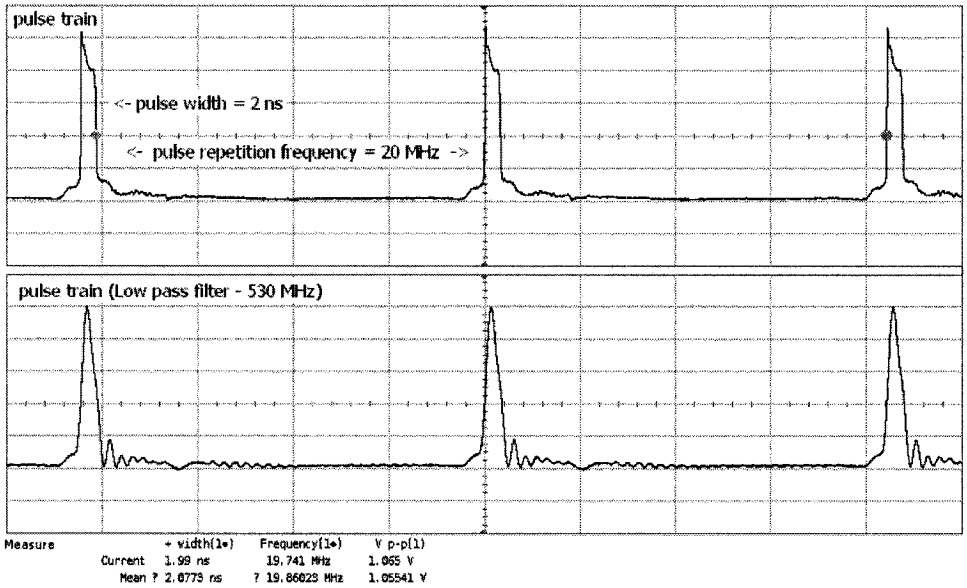

Fig. 2-4. Measured pulse train.

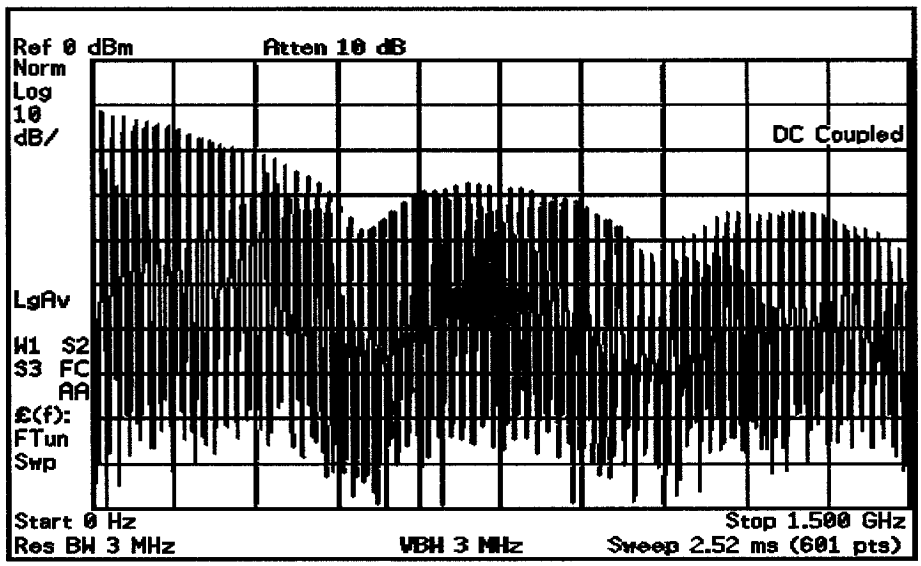

Fig. 2-5. Pulse spectrum before upconversion.

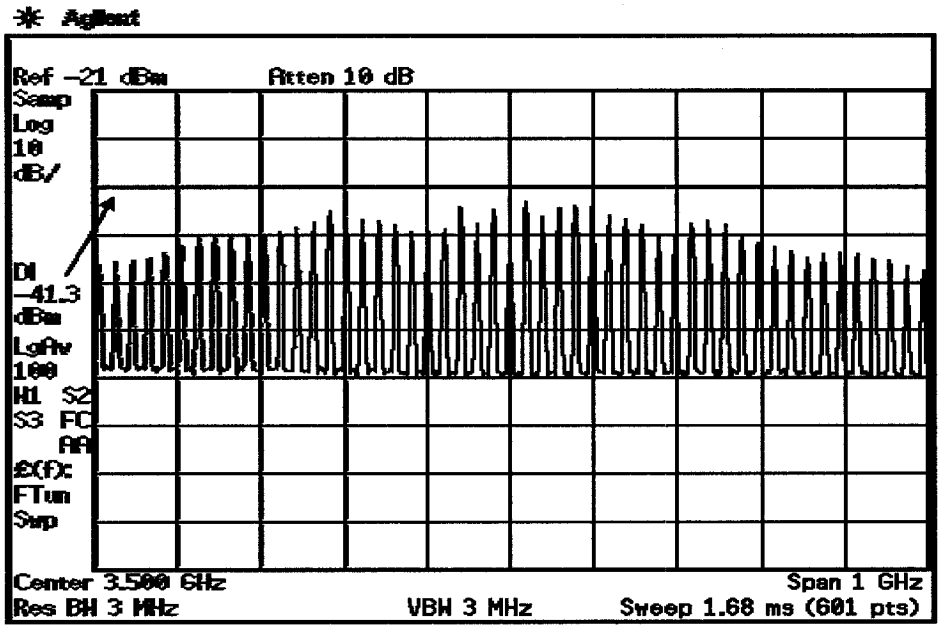

Fig. 2-6. Spectrum after filtering and upconversion.

CHAPTER 3 UWB SIX-PORT MODULATOR

Six-port circuits have been used for direct conversion receivers using sinusoidal signals for binary phase shift keying (BPSK), quadrature phase shift keying (QPSK), and quadrature amplitude modulation (QAM) schemes [12]-[15], [18]. In a six-port direct conversion receiver, the complex ratio of the input signals at port 1 and 2 can be determined by the power values at the remaining four outputs (ports 3 to 6). On the other hand, when the four outputs of a six-port circuit (Fig. 3-1) are terminated with certain loads, the six-port circuit can be used to realize direct phase modulation.

3.1 Architecture Description

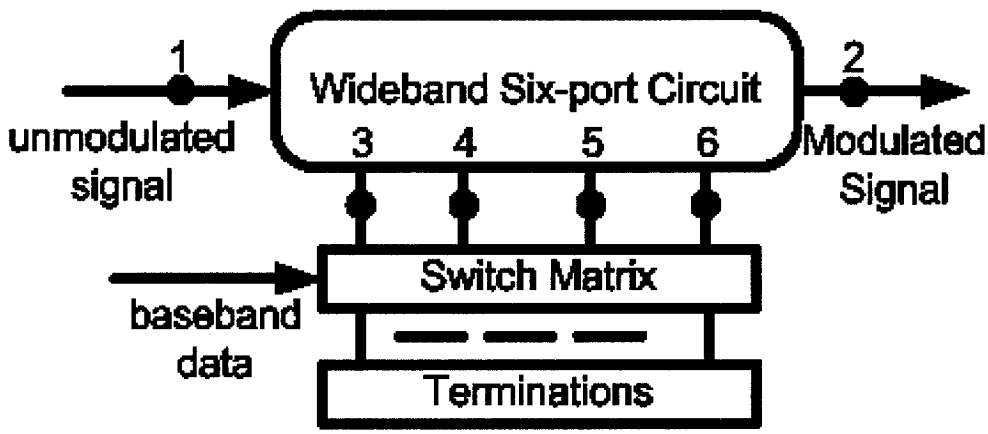

Fig. 3-1. Six-port based direct modulator architecture.

Fig. 3-1 shows the diagram of the six-port based direct modulator. It consists of a six-port circuit, a switch matrix, open terminations, and short terminations. The six-port circuit made of passive components is shown in Fig. 3-2. It is composed of one power divider and three hybrid couplers. The power divider has no phase difference between its

two output ports. Each hybrid coupler provides output signals with equal power and 90° phase difference.

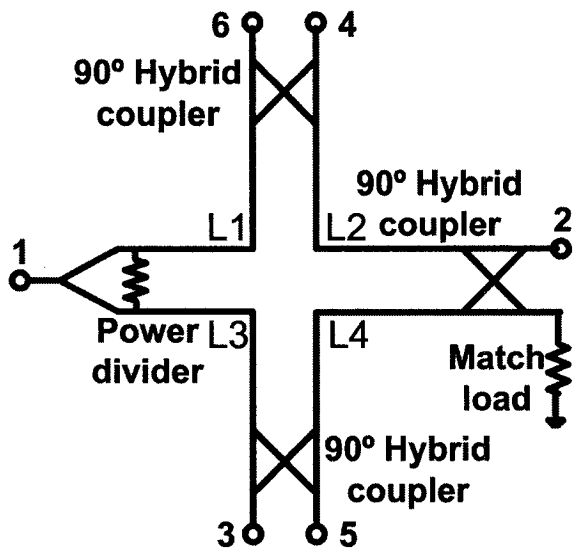

Fig. 3-2. Schematic of the six-port circuit (L1–L4 represent lengths of four connection transmission lines).

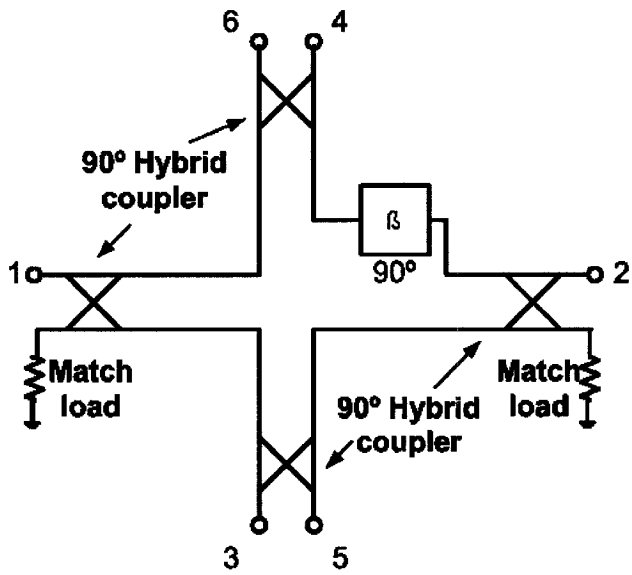

Fig. 3-3. Schematic of the six-port circuit using four hybrid couplers.

A different approach to create a six-port is illustrated in Fig. 3-3 and consists of four 90°-hybrid couplers and a 90° phase shifter. The phase shifter can simply be a length of transmission line providing a 90° phase shift at the center frequency. The schematic shown in Fig. 3-2 was adopted for the modulator because it facilitates the six-port circuit design and fabrication by avoiding the phase shifter design.

The six-port direct modulator operates as follows: port 1 is fed with an unmodulated signal, which is transferred to ports 3 to 6 through the different branches of the six-port circuit. Ports 3 to 6 are connected to open or short terminations by a switch matrix controlled by the baseband data to transmit. The reflected signals are then summed at port 2, which is the output of the modulated signal.

If the input signal is a sinusoidal signal, the output signal acquires different phases depending on the terminations applied at ports 3 to 6. Compared with the six-port modulator for sinusoidal signals, the essential differences when the six-port modulator operates with non-sinusoidal signals lie in the linear phase response over the wide band and uniform spectral phase modulation over the channel bandwidth. That is, if the input signal is a wideband signal, the phase spectrum of the entire signal must be uniformly modulated at any frequency in the operating channel with a 90° phase difference between successive modulation states.

The six-port circuit can be fabricated using several fabrication methods such as monolithic microwave integrated circuit (MMIC), substrate integrated waveguide (SIW), and metamaterial structure, etc. Using suitable fabrication technologies, the modulator can be scaled dimensionally to potentially operate from RF to millimetre

wave frequency ranges.

For quadrature phase shift keying (QPSK) modulation, only two types of terminations, open and short, are necessary. The direct modulation architecture can be extended to realize M-ary phase shift keying (M-PSK) by using more intermediary terminations having for instance 45° phase change aside from only short and open terminations. Thus, the output signal can attain more phase states in relation to the input signal.

This direct six-port modulator can be used to modulate either a single carrier signal or non-sinusoidal (pulse) signal according to the operating bandwidth of the six-port modulator. Based on previous six-port technology, it is believed that the entire 3.1 GHz to 10.6 GHz UWB band can be covered with one or two integrated circuit chips.

3.2 Modulation means and derivation of the transfer function

In this work, a novel modulation scheme, called phase spectrum modulation, is proposed to modulate an impulse UWB signal in binary or quaternary. The modulation function of a six-port modulator was first derived using a single carrier signal. Then the result is extended to phase spectrum modulation of impulse UWB signals.

The phase modulation function is described using a transfer function between port 1 and 2. The transfer functions under different termination configurations at port 3 to 6 are derived as follows.

As a component of the six-port circuit, the Wilkinson power divider shown in Fig. 3-4 can be described with the S-parameter in (3.1).

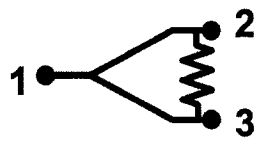

Fig. 3-4. Diagram of a Wilkinson power divider.

$$S=\frac{1}{\sqrt{2}}\begin{bmatrix}0 & -j & -j\\ -j & 0 & 0\\ -j & 0 & 0\end{bmatrix} \tag{3.1}$$

The other component of the six-port circuit, the 90° hybrid coupler shown in Fig. 3-5, can be described using the S-parameter in (3.2).

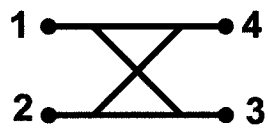

Fig. 3-5. Diagram of a 90° hybrid coupler.

$$S=\frac{1}{\sqrt{2}}\begin{bmatrix}0 & 0 & -j & 1\\ 0 & 0 & 1 & -j\\ -j & 1 & 0 & 0\\ 1 & -j & 0 & 0\end{bmatrix} \tag{3.2}$$

According to the structure of the six-port circuit shown in Fig. 3-2 and the above S-parameters, the transfer function between port 1 and port 2 of the modulator can be derived and expressed as follows:

$$H_i(f_c)=0.707\times e^{-j(\phi_1+3\phi_2+2\theta+45^\circ+i\cdot 90^\circ)},\quad i=0,1,2,3 \tag{3.3}$$

where ϕ_1 is the phase change of a power divider branch, ϕ_2 is the phase change of a hybrid coupler branch, θ is the phase change of a transmission line, i represents the

i^{th} configuration of four different termination configurations. For a single carrier at frequency f_c, phase values are constant. The value of $(\phi_1 + 3\phi_2 + 2\theta)$ is the unwanted total phase change of the components and the transmission lines. It can be designed to be a discrete multiple of 360° in order to eliminate the phase variation of modulated signal.

When the reference signal is a wideband signal, the constant phase in (3.3) at each frequency changes linearly with frequencies. It can be described using a linear function in (3.4).

$$\phi(f) = K \cdot f \tag{3.4}$$

where $\phi(f)$ represents the ideal linear phase response over frequency of the modulator, K is a constant which depends on the components of the modulator, and f represent frequency points within the desired bandwidth, e.g., 3–4 GHz of the operating bandwidth of the test bench.

From eq. (3.3) and (3.4), it can be seen that the phase difference between modulation states is satisfied at any frequency, while the constant K is only dependent on the circuit itself. Therefore, the phase plots under the four modulation states are linear with frequency and parallel with a 90° phase difference between successive modulation states at any frequency in the operating channel. The transfer function at four modulation states with wideband signal, such as an impulse UWB, is expressed by:

$$H_i(f) = 0.707 \times e^{-j\left[\phi(f)+i\cdot 90^\circ\right]}, \quad i = 0,1,2,3 \tag{3.5}$$

where i represents the i^{th} state of the four different modulation states for quadrature phase spectrum modulation.

When we observe the constellation diagram of a phase shift keying carrier signal, we observe discrete points at different phase angles. However, for a phase spectrum modulated impulse-UWB signal, the constellation will be concentrated within a single circle (actually several superposed circles). The circle covers phase points linearly changed for different frequencies of a UWB signal.

For each modulation state, the criteria on choice of short and open terminations are given in Table 1.

Table 1 Criteria on choice of short and open terminations for bit pairs.

Modulation state (i)	Port 3	Port 4	Port 5	Port 6	ΔΦ	I	Q
0	O	O	O	O	0°	0	0
1	O	S	O	S	90°	0	1
2	S	O	S	O	180°	1	0
3	S	S	S	S	270°	1	1

O: Open S: Short

3.3 Simulation of six-port modulator

3.3.1 Implementation of simulation model

A six-port simulation model was developed using Matlab-Simulink [34], [40]. Employing the S-parameters of each component of the six-port circuit, the mathematical relationships between the two input and four output ports are implemented using the Simulink model editor. The model simulating an ideal six-port circuit is shown in Fig. 3-6.

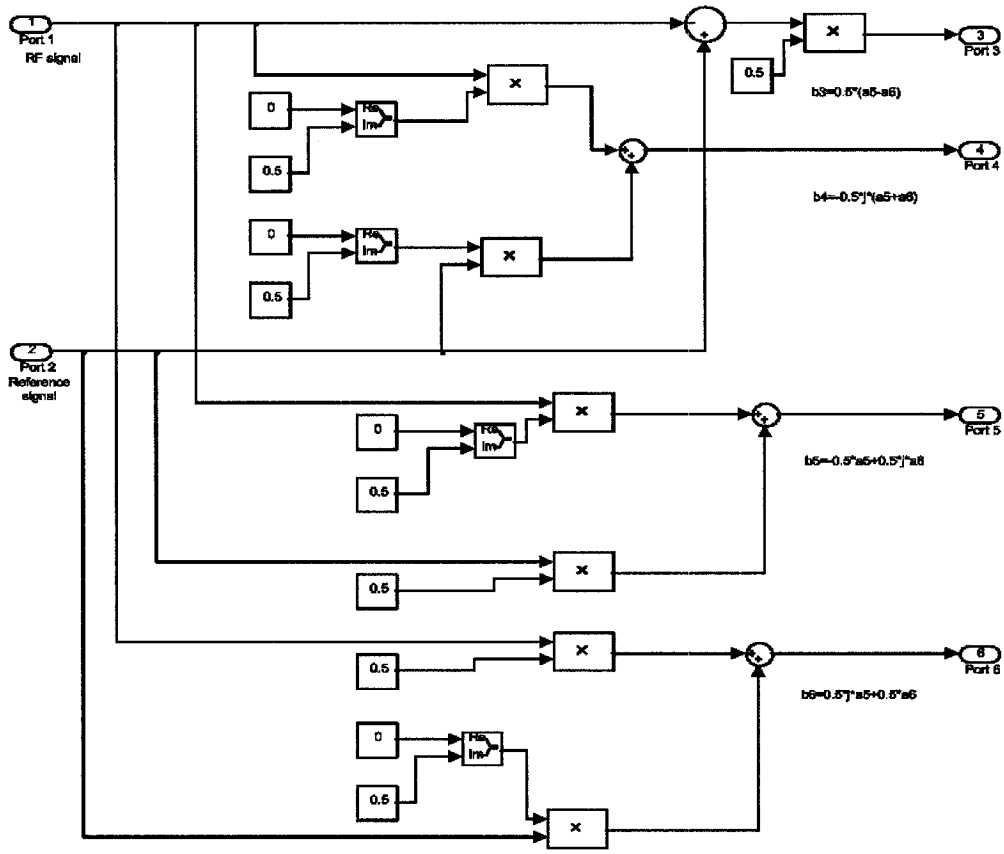

Fig. 3-6. A six-port simulation model in Simulink.

Using complex numbers for the six-port simulation model is straightforward because an S-parameter at a frequency point is a vector including both amplitude and phase. Those complex numbers do not include the variable of frequency. Thus the simulation model is frequency-independent. This also infers that phasor representation of a signal must be used to implement a system simulation based on this model. For an M-ary phase shift keying signal, its phasor representation can be written in (3.6), using Euler's theorem [41].

$$s(t) = \mathrm{Re}\left\{ \sqrt{\frac{2E}{T}} e^{j\omega_0 t} e^{j\phi_i(t)} \right\} \qquad \begin{matrix} 0 \le t \le T \\ i = 1,\ldots,M \end{matrix} \tag{3.6}$$

where the phase term, $\phi_i(t)$, will have M discrete values, typically given by

$$\phi_i(t) = \frac{2\pi}{M} \quad i = 1,\ldots,M \tag{3.7}$$

The parameter E is the symbol energy, T is the symbol time duration. The carrier angular frequency is ω_0. When both the modulated signal and the carrier signal (reference signal) in such a complex notation are fed into the six-port model, the constantly rotating aspect of the unmodulated carrier will be removed. The model will calculate only the information-bearing phasor. The above Simulink model is useful for analyzing six-port based transceivers at a system level. Signal processing algorithms for six-port based system can be easily tested in Simulink by using the above six-port model.

Furthermore, a six-port model in Advanced Design System (ADS) [43] was developed for facilitating the design, fabrication, and verification of six-port circuits. In this model (Fig. 3-7), each component (power divider and hybrid couplers) is simulated using measured S-parameter data. Measured S-parameter data can be read directly using data access component (DAC) [43]. The reconstruction of the intermediate values ($\hat{x}(f)$) between two successive frequency points are interpolated using linear interpolation method [44] described in (3.8).

$$\hat{x}(f) = x(n \cdot \Delta f) + \frac{x(n \cdot \Delta f) - x(n \cdot \Delta f - \Delta f)}{\Delta f}(f - n \cdot \Delta f) \qquad (3.8)$$
$$n \cdot \Delta f \le f < (n+1) \cdot \Delta f$$

where f is the frequency, Δf is the frequency space between two successive frequency points. Because S-parameter is complex, its magnitude and angle are interpolated separately. For a 3-port device, such as a power divider, its practical model based on measured S-parameter data can be implemented using three data access components as

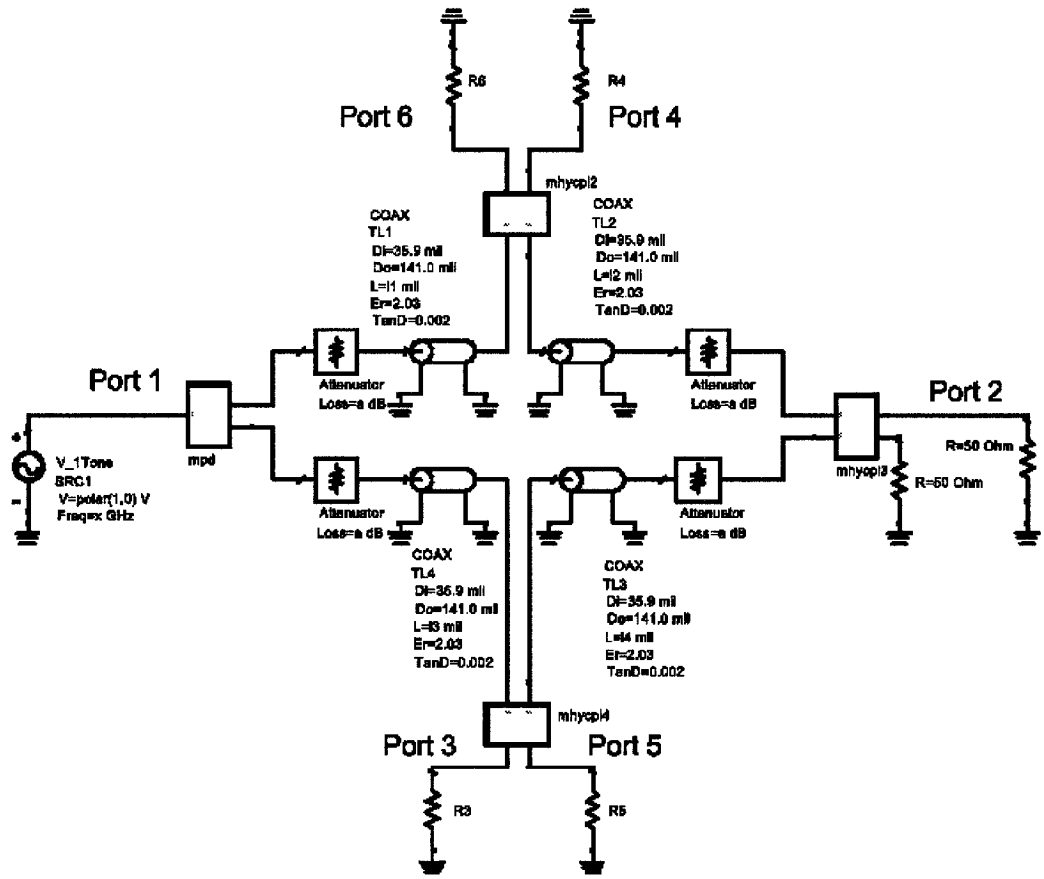

Fig. 3-7. A six-port simulation model in ADS.

shown in Fig. 3-8. Three sets of 2-port S-parameter data are obtained by changing port connection of the power divider. A practical model of a hybrid coupler (4-port device)

can be implemented using the similar method.

Four sections of transmission lines are simulated using a coaxial line model. The inner diameter, outer diameter, and dielectric constant in the coaxial line model are set to the practical value of the selected coaxial cable. The coaxial line model can also be replaced with a data access component using the measured S-parameter of the selected coaxial cable.

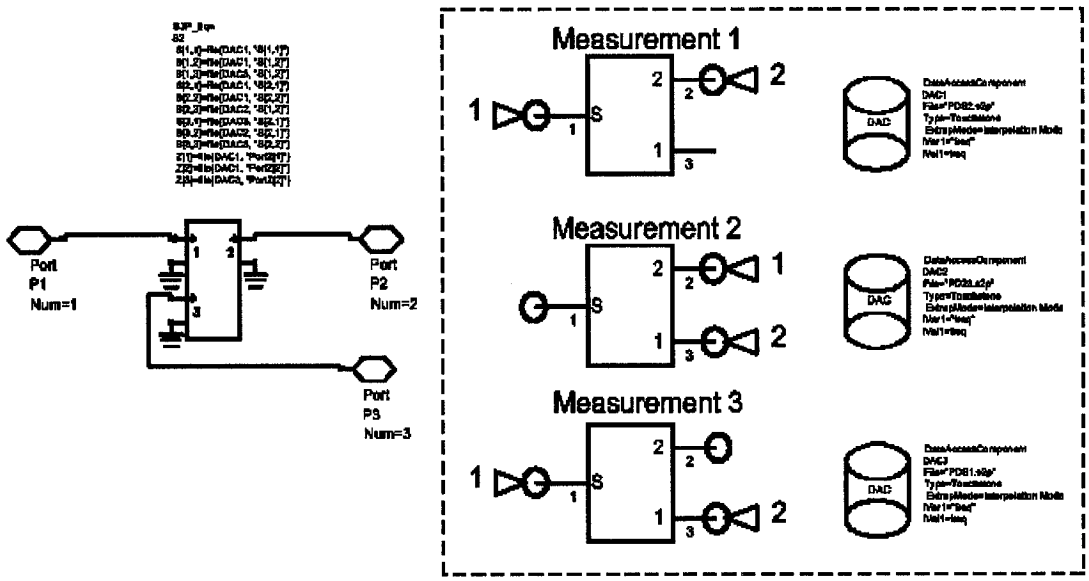

Fig. 3-8. Creating a 3-port dataset from three 2-port measured data.

3.3.2 Simulation results

An ideal six-port modulator was first simulated with a single carrier. In the simulation shown in Fig. 3-7, a six-port circuit model was implemented based on the schematic of Fig. 3-2. The power divider and hybrid couplers were simulated using ideal S-parameters. Under different termination configurations, the output waveforms of the various QPSK modulation states were obtained and are shown in . Based on the phase difference between each modulated signal, it can be seen that the results agree with eq. (3.3).

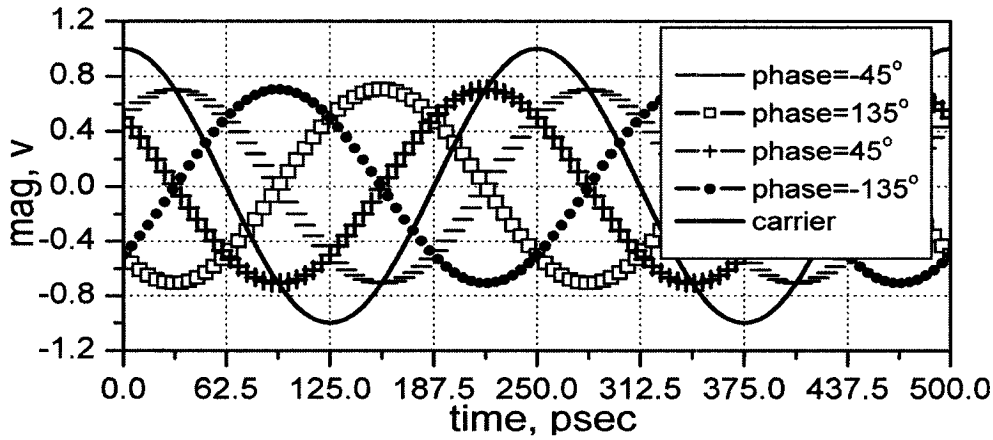

Fig. 3-9. Simulation results of a single carrier signal and QPSK modulated signals.

A more realistic simulation in ADS was performed using the measured S-parameters of the commercial power divider and hybrid couplers in order to study the effect of phase and amplitude imbalances. The commercial power divider and hybrid couplers used in the test bench have a typical amplitude imbalance of ±0.30dB and phase imbalance of ±3°, as stated by the manufacturer [45], [46]. An IQ impairment analysis

was done by sweeping the amplitude imbalance between -0.3 dB to 0.3 dB and the phase imbalance between -3° to 3°. The simulation results show the phase difference ranges from -11.3° to +11.4° and the amplitude difference ranges from 0.3dB to 2.3dB for the QPSK modulated signals. The impaired IQ constellation points are presented in Fig. 3-10 and compared with the ideal points.

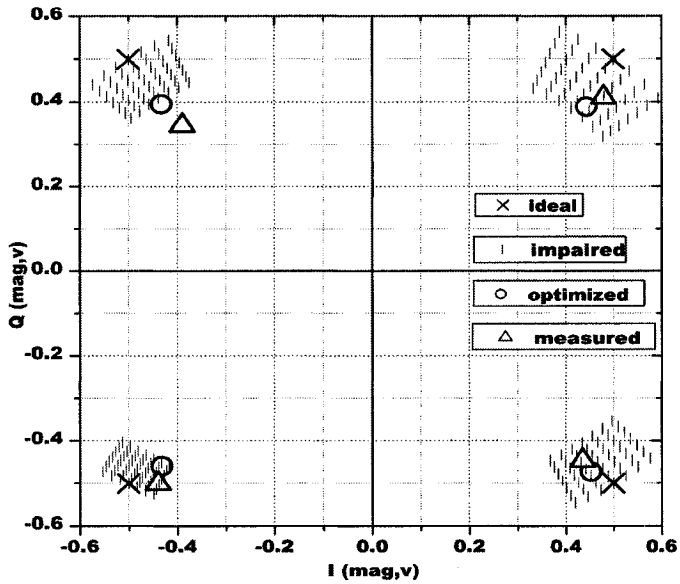

Fig. 3-10. Comparison of IQ constellations obtained with single carrier.

An error vector analysis is also done to further quantify the modulator performance in terms of magnitude and phase errors. With both magnitude and phase values associated, error-vector-magnitude (EVM) is effective for analyzing or troubleshooting the effect of phase and amplitude imbalance existing in a six-port modulator. The figure of merit, error-vector-magnitude, is the unsigned scalar distance between the end point of a reference phasor and the actual or measured phasor [42]. EVM is defined in (3.9) as a percentage of the peak signal level, usually defined by the constellation's corner stage

(Fig. 3-11).

$$Error\ vector\ magnitude = \frac{average\ error\ magnitude}{peak\ signal\ magnitude} \times 100\% \qquad (3.9)$$

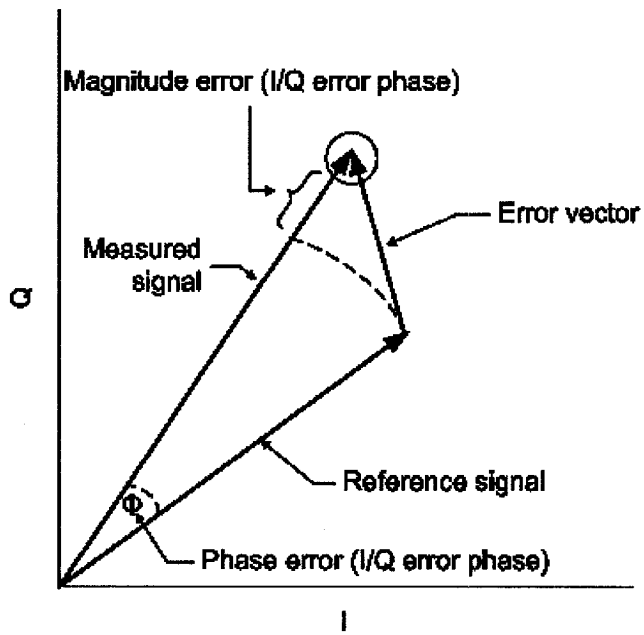

Fig. 3-11. Error vector magnitude.

The commercial hybrid coupler used in the test bench set up has a maximum amplitude imbalance of ±0.20dB and phase imbalance of ±3 degrees. The error vector magnitude analysis is done by sweeping the amplitude imbalance between -0.2dB to 0.2 dB and the phase imbalance between -3° to 3°. The combined effect of amplitude and phase imbalance is simulated and presented in Fig. 3-12. The EVM is as low as 14.5% which indicates that this modulator can achieve acceptable phase modulation accuracy. The minimum EVM requirement for transmit modulation is 17.5% defined in the 3rd generation partnership project (3GPP) technical specifications [35].

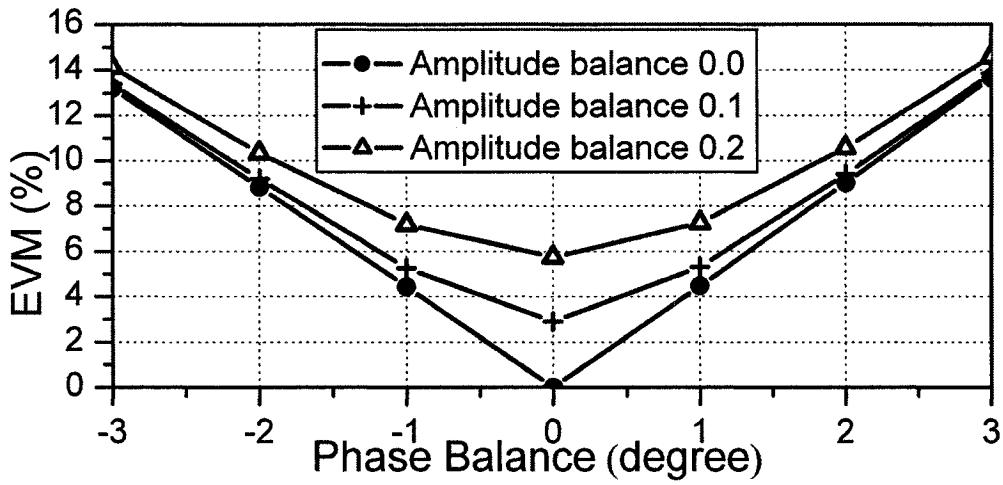

Fig. 3-12. Combined effect of amplitude and phase imbalance at 3.5 GHz.

In order to further reduce the contribution to EVM by the phase and amplitude imbalance, an optimal design method is adopted. To overcome the IQ impairment, an optimization process was used according to eq. (3.3). The lengths of four connecting cables are specified as parameters to be optimized under the goal of minimizing both the phase error and amplitude error. During the optimization process two different search methods, gradient and random, were used for better accuracy. The modulator design was modified using the optimal lengths and simulated again. The optimized IQ constellation is compared with ideal and impaired points in Fig. 3-10. Phase difference from 0.7° to 3.8° and amplitude difference from 0.4dB to1.63dB were achieved at 4.0 GHz carrier frequency, an improved result compared to the IQ impairment analysis. Note that the contribution to the IQ impairment by the phase and amplitude imbalance can also be reduced by calibration algorithms used in receiver processing [36].

The six-port modulator working in an ultra wide band mode was also simulated by sweeping frequency over the desired bandwidth (3 to 4 GHz). The simulation results are

compared with the measurement results presented in section 3.4.

3.4 Experimental Results

The six-port modulator, shown in Fig. 3-13, is composed of one power divider, three hybrid couplers, switches, and Open/Short terminations. It was designed and fabricated using commercial components. The characteristics of each component between 3-4 GHz are the following. The power divider has a phase imbalance of 4° and amplitude imbalance of 0.6 dB [45]. The insertion loss, is typically 0.5 dB, while the isolation between two output ports is typically 22 dB [45]. As for the hybrid couplers, they

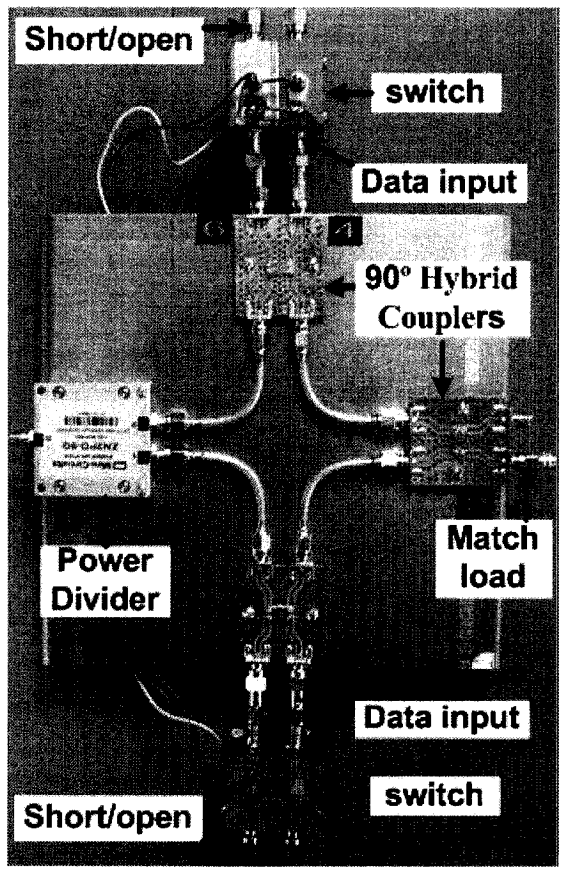

Fig. 3-13. A six-port modulator fabricated with commercial components.

exhibit a phase imbalance of 4° and amplitude imbalance of 0.2 dB. Their insertion loss is maximally 0.2 dB, while the minimum isolation is 22 dB [46].

The switches have a typical switching time of 20 ns which corresponds to a symbol rate of 50 Mega symbol per second (Msps). The insertion loss is maximally 1.5 dB, while the minimum isolation is 38 dB [47].

Finally, the lengths of coaxial transmission lines were obtained using the previously described optimizing method. The coaxial transmission lines were fabricated using truncated optimal lengths within a manufacturing tolerance of 0.1 inch.

3.4.1 S-parameter measurement of six-port modulator

The goal of the S-parameter measurement is to characterize the fabricated six-port modulator and to estimate its operational bandwidth.

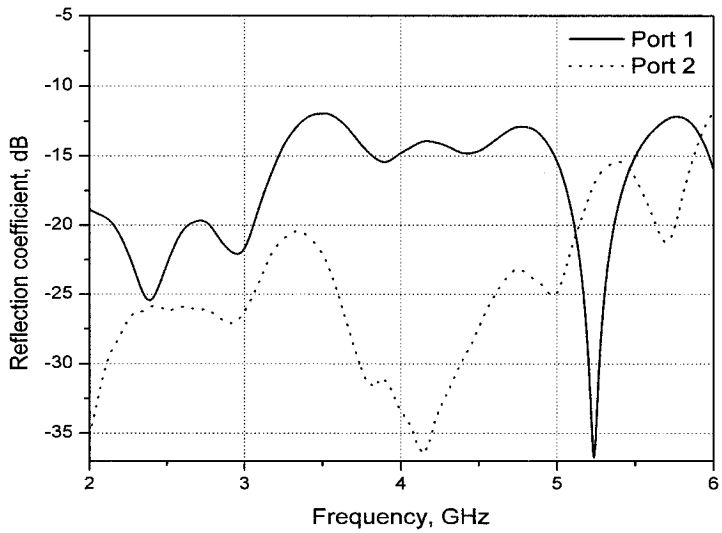

Fig. 3-14. Measured reflection coefficients at port 1 (input) and port 2 (output) of the six-port modulator.

Fig. 3-14 shows the measured S11 (input reflection coefficient) and S22 (output reflection coefficient) of the fabricated six-port modulator. The reflection coefficient of port 1 is below -12 dB over the bandwidth, which is acceptable, while the reflection of port 2 is below -20 dB over the bandwidth indicating a better match. Fig. 3-15 shows the measured forward transmission coefficients between the input and output ports of the six-port modulator at four modulation states. The variation observed is within 1 dB to -3 dB of the theoretical value of -3 dB over the bandwidth. This is due to the length variance of the fabricated cables and can be mitigated by signal processing at the receiver. Fig. 3-16 shows the forward transmission coefficients measured between port 1

and four termination ports (ports 3 to 6). Within the bandwidth of interest (3–4 GHz), the four forward transmission coefficients are comparable to the theoretical value of -6 dB, with a variation between 0 dB and -1 dB.

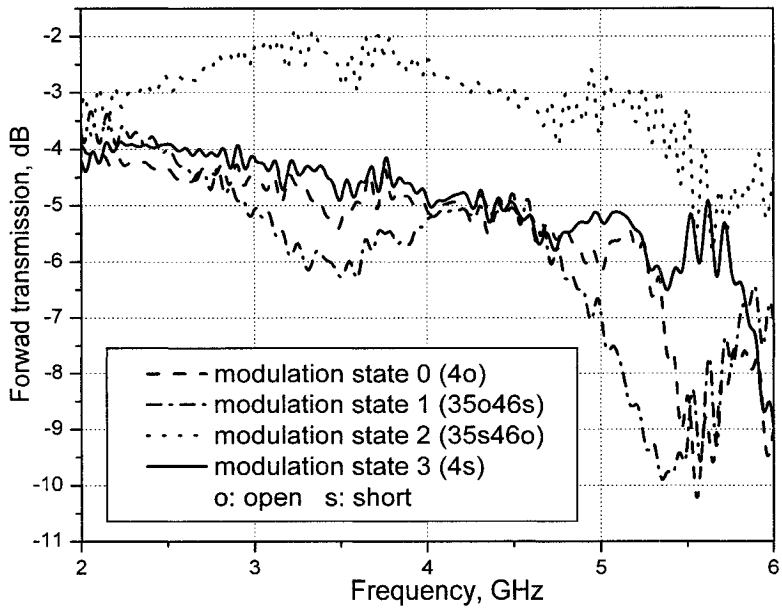

Fig. 3-15. Measured forward transmission coefficient between port 1(input) and port 2 (output port) of the six-port modulator at four modulation states.

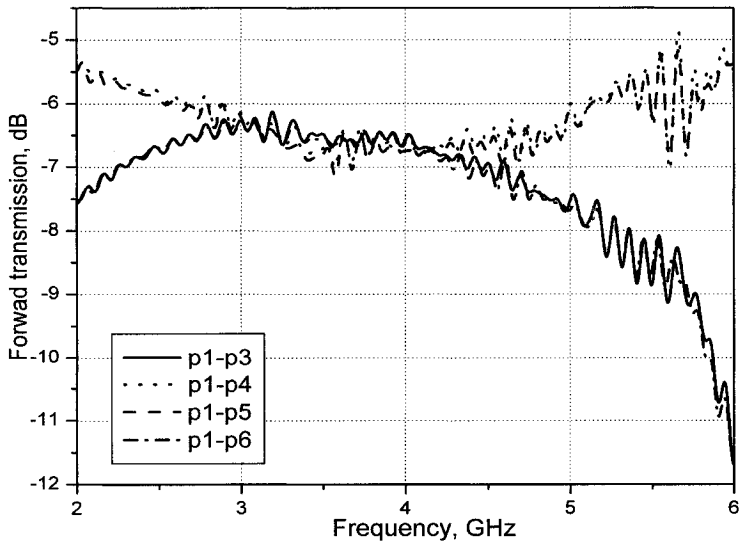

Fig. 3-16. Measured forward transmissions between the input port and the termination ports (3–6) of the six-port modulator.

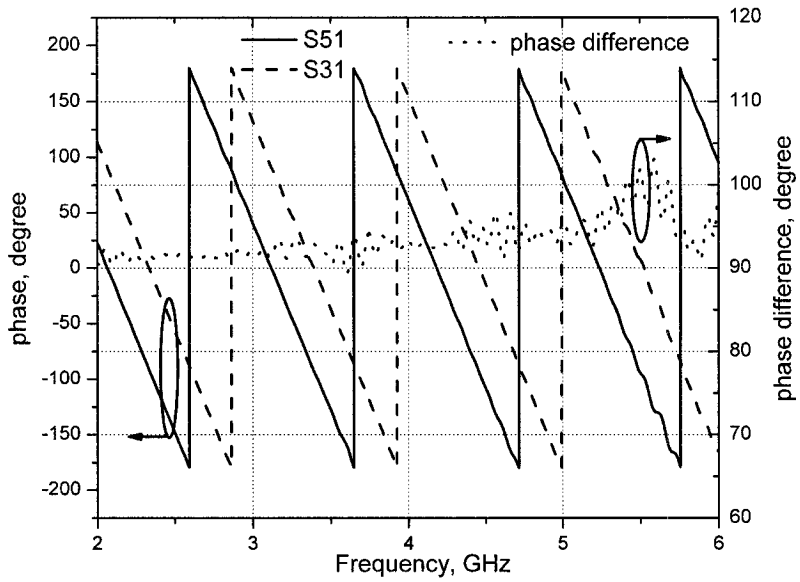

Fig. 3-17. Measured phase of forward transmissions between the input port and the termination ports (3 and 5) of the six-port modulator.

Fig. 3-17 shows the phase of the forward transmission coefficients measured between port 1 and two termination ports (port 3 and 5). The phase difference between S31 and S51 is also plotted. The measured phase difference is comparable to the theoretical value of 90°, with a variation of ±2° over the interested bandwidth (3–4 GHz). Fig. 3-18 shows the phase of the forward transmission coefficients measured between port 1 and the other two termination ports (port 4 and 6). The phase difference between S41 and S61 is also plotted. The measured phase difference is also comparable to the theoretical value of 90° with a variation ±2° over the interested bandwidth (3–4 GHz).

Fig. 3-19 shows forward transmission coefficients measured between four termination ports (port 3 to 6) and port 2. Within the interested bandwidth (3–4 GHz), the four forward transmission coefficients are also comparable to the theoretical value -6 dB, with a variation between 0 and -1 dB. Fig. 3-20 shows the phase of the forward transmission coefficients measured between two termination ports (port 3 and 5) and port 2. The phase difference between S32 and S52 is also plotted. The measured phase difference is comparable to the theoretical value of 90°, with a variation of ±2° over the interested bandwidth (3–4 GHz). Fig. 3-21 shows the phase of the forward transmission coefficients measured between the other two termination ports (port 4 and 6) and port 2. The phase difference between S42 and S62 is also plotted. The measured phase difference is comparable to the theoretical value of 90°, with a variation of ±2° over the interested bandwidth (3–4 GHz).

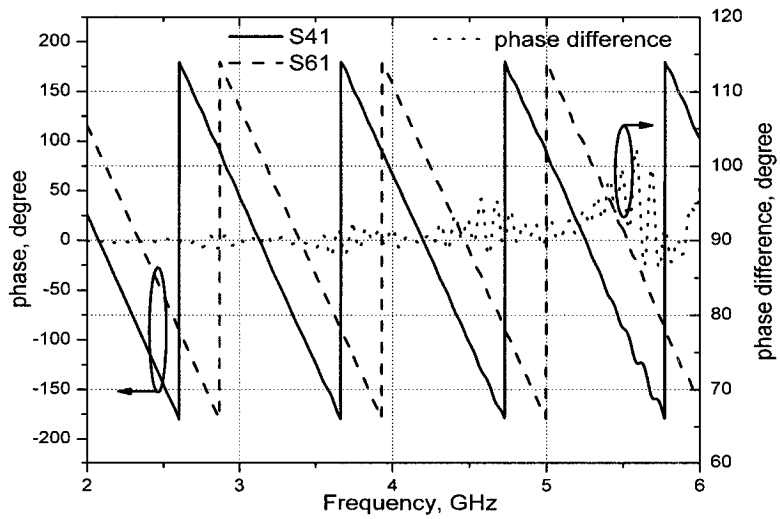

Fig. 3-18. Measured phase of forward transmissions between input port and termination ports (4 and 6) of the six-port modulator.

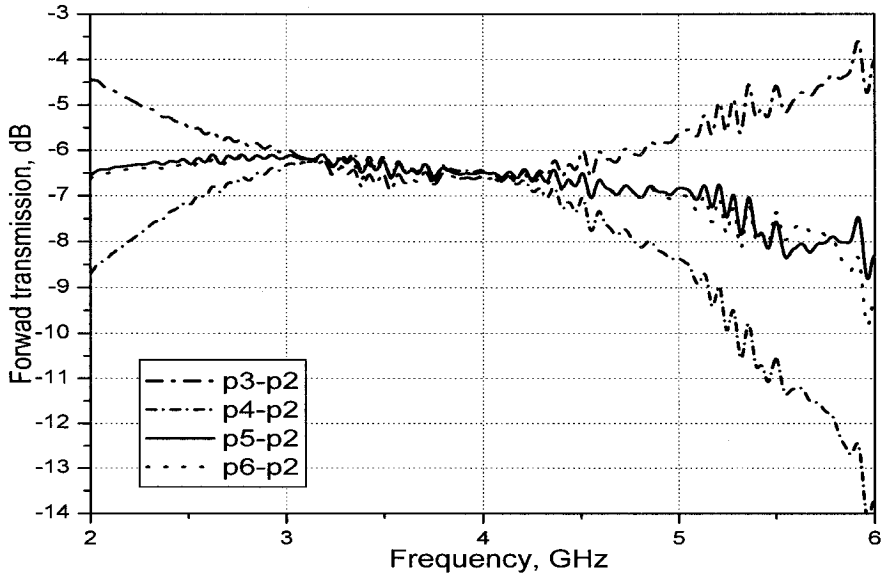

Fig. 3-19. Measured forward transmissions between termination ports (3 – 6) and output (port 2) of the six-port modulator.

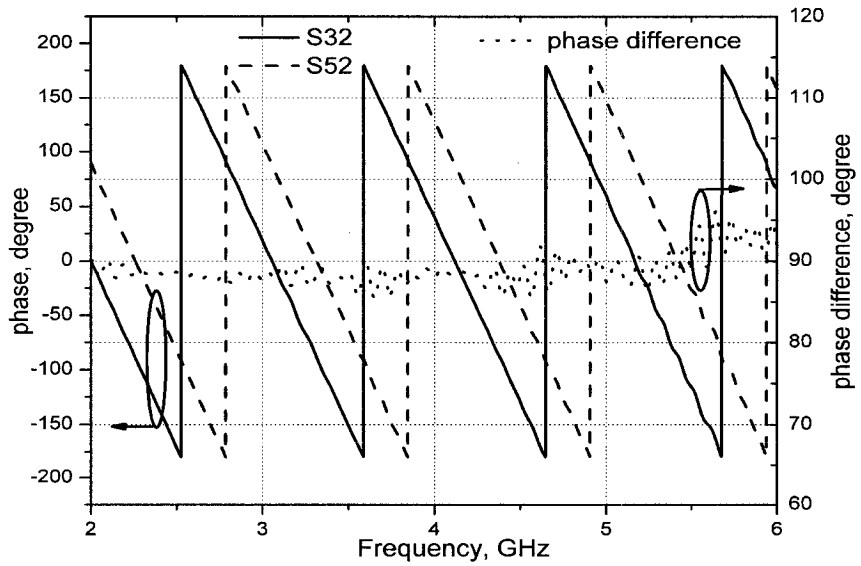

Fig. 3-20. Measured phase of forward transmissions between termination ports (3 and 5) and output (port 2) of the six-port modulator.

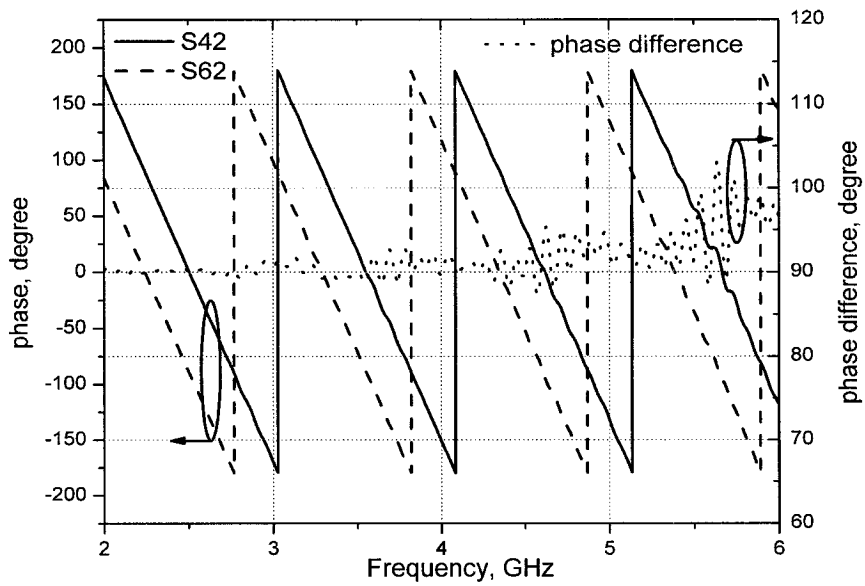

Fig. 3-21. Measured phase of forward transmissions between termination ports (4 and 6) and output (port 2) of the six-port modulator.

3.4.2 Modulation measurement results with single-frequency sinusoidal signal

Different combinations of connectorized coaxial shorts and opens were applied to ports 3 to 6. The modulated signal constellation is compared with simulated and ideal points shown in Fig. 3-10. A phase difference from 0.8° to 4.5° and an amplitude difference from 0.5 dB to 2.7 dB were achieved. This result shows close correlation with the previous optimized result using exact cable lengths.

For real-life characterization of the modulator, a second measurement, with commercial microwave switches and a digital data generator, was also undertaken. The data generator provides two rectangular pseudo random sequences. One sequence is for in-phase (I) channel and the other is for quadrature (Q) channel. These modulating

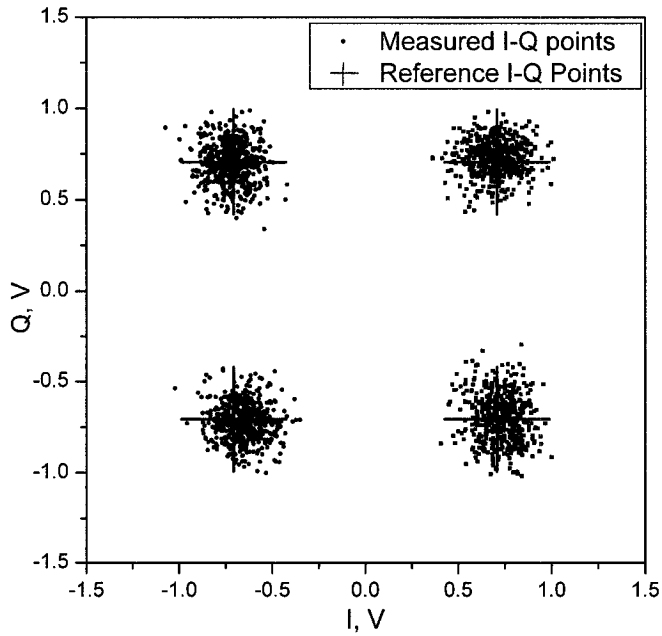

Fig. 3-22. Measured constellation of modulated signal having carrier frequency of 3.5 GHz and rectangular modulating signals of 10 Msps.

sequences were used to switch opens and shorts onto ports 3-6 using commercial microwave switches. Each sequence is at a symbol rate of 10 Msps. Thus a data rate of 20 Mbps was achieved using this modulator. The data rate was limited by the available equipment (digital data generator), thus higher data rates can be theoretically achieved. Fig. 3-22 shows the measured normalized constellation of the modulated signal using a vector signal analyzer (Agilent VSA89600). The carrier signal had a frequency of 3.5 GHz and a signal to noise ratio of 12 dB. The measured EVM was 10.3% rms, where rms indicates the square root of the sum of the squares of the normalized EVM values measured at each symbol time. The definition of EVM is given in equation (4.9).

3.4.3 Modulation measurement results with non-sinusoidal signal

By sweeping frequencies over the operating channel (3–4 GHz) of the wideband signal, S-parameter measurements were carried out between ports 1 and 2. Different combinations of connectorized coaxial shorts and opens were manually applied to ports 3 to 6 as indicated in Table 1.

The measured S21 data under four modulation states was used to plot the phase spectrum. The phase plots under four modulation states are linear with frequency and parallel with a 90° phase difference between successive modulation states at any frequency in the operating channel. Fig. 3-23 shows the measured and simulated phase response between ports 1 and port 2 of the modulator at any frequency between 3GHz and 4GHz for modulation states 0, 1, 2, and 3. Both simulation and measurement results shown in Fig. 3-23 are in agreement with (3.5). Fig. 3-24 shows the result obtained for binary phase spectrum modulation.

The six-port direct modulator can be used either for single carrier phase modulation or pulse signal phase spectrum modulation as long as the circuit is linear in phase in the desired bandwidth.

Compared with a heterodyne modulator which requires two IF mixers, in-phase and quadrature-phase carriers and an RF upconversion section, this direct phase modulator eliminates the need for IF modulation and RF upconversion, Consequently, due to the passiveness of six-port technology, the modulator intrinsically has the advantages of reduced circuit complexity, increased signal integrity, and low power consumption. Extendibility to M-ary phase shift modulation is also possible because the architecture allows a variety of terminations to be applied to its ports 3–6.

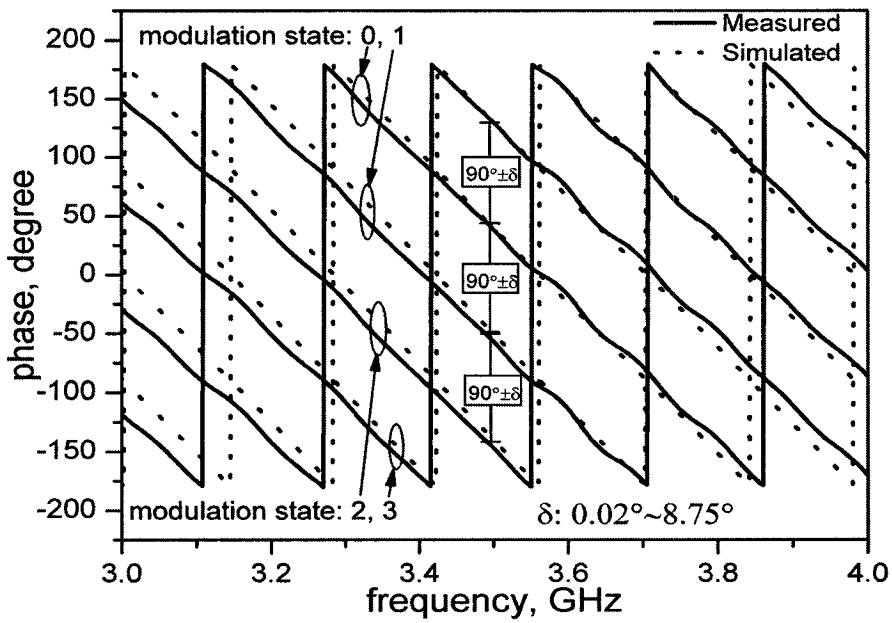

Fig. 3-23. QPSM simulated and measured phase response between port 1 and port 2 of modulator between 3 GHz and 4 GHz.

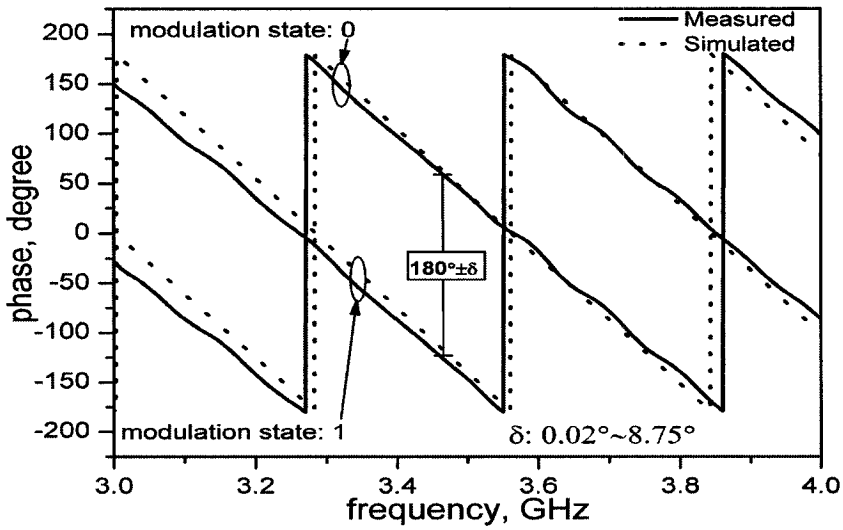

Fig. 3-24. BPSM simulated and measured phase response between port 1 and port 2 of modulator between 3 GHz and 4 GHz.

CHAPTER 4 UWB SIX-PORT DEMODULATOR

4.1 Architecture Description

The six-port demodulator shown in Fig. 4-1 is composed of a six-port circuit using the same structure (Fig. 3-2.) as the modulator. This quasi-symmetry between the modulator and demodulator circuits makes design and fabrication easier. Ports 1 and 2 are fed respectively with the reference signal and the unknown signal to be demodulated. Four output signals are simultaneously available at ports 3 to 6, which are connected to power detectors. The power detectors are composed of zero-biased Schottky diodes. Output signals from the power detectors are then used for demodulation either by analog or digital methods.

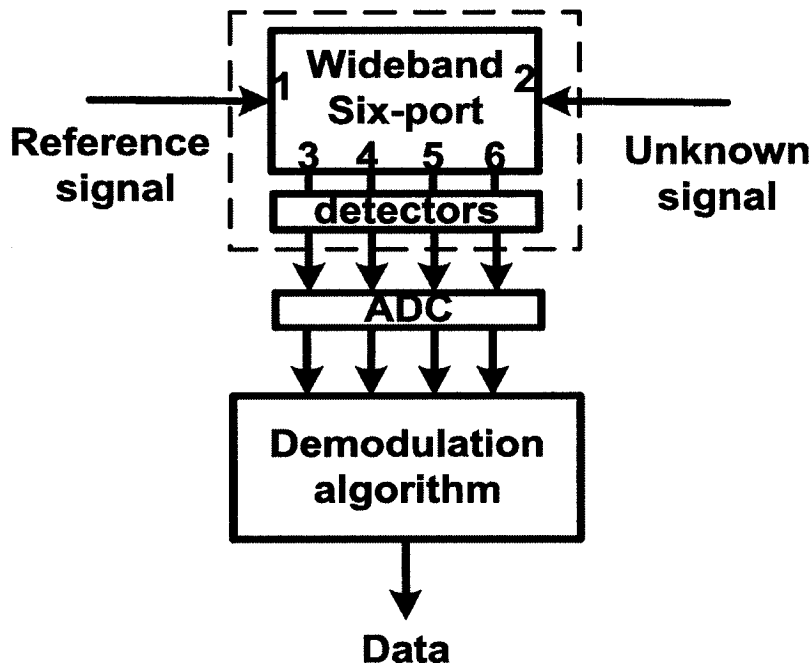

Fig. 4-1. Diagram of a six-port demodulator.

4.2 Analysis of demodulation method

4.2.1 Six-port output signals

Let a_1 be the reference signal at port 1 of the six-port circuit, and expressed in a phasor form:

$$a_1 = Ae^{j\theta_1} \tag{4.1}$$

Let a_2 be the unknown signal at port 2, and expressed in a phasor form:

$$a_2 = Ae^{j\theta_2} \tag{4.2}$$

The two signals are assumed to have the same amplitude A and angular frequency ω. The angular frequency ω is omitted in the phasor expressions.

According to the structure of the six-port circuit and the S-parameters of a power divider and a hybrid coupler (eq. 3.1 and 3.2), the four output signals are given by:

$$\begin{aligned} b_3 &= -0.5 \cdot j \cdot (a_2 - a_1) \\ b_4 &= 0.5 \cdot (a_2 + ja_1) \\ b_5 &= 0.5 \cdot j(a_2 + a_1) \\ b_6 &= -0.5 \cdot j \cdot (a_2 - ja_1) \end{aligned} \tag{4.3}$$

where b_3, b_4, b_5, and b_6 represent the output signals at ports 3–6 respectively.

4.2.2 Analysis of power detectors

The six-port modulator adopts four zero-biased Schottky diodes as power detectors. The $I-V$ characteristic curve of a diode is given by

$$I(V) = I_S(e^{V/nV_T} - 1) \tag{4.4}$$

where:

$V_T = KT/q$ ($V_T = 25mV$ at $T = 293° K$)

I_S = Diode saturation current

n = Ideality factor ($1 \le n \le 2$), which depends on the material and physical structure of the diode. For a Schottky diode, $n = 1.2$.

Without any loss of accuracy for most of our analyses and discussions, a Taylor series expansion [37] of (4.4) can be approximated with the three-term for small signals (i.e., $v/nV_T << 1$). The small-signal approximation can be expressed as:

$$I(v) = I_0 + i \tag{4.5}$$

where

$$i = vG_d + 1/2(v^2 G_d') + ... \tag{4.6}$$

and where G_d is the dynamic conductance of the diode (the inverse of the junction resistance), I_0 is a DC bias current. When an RF signal having a frequency ω_0 and amplitude A given by

$$a(t) = A\cos(\omega_0 t) \tag{4.7}$$

is applied to the diode, its total current is composed of a DC bias (I_0) and an AC current From (4.5) and (4.6), the diode current is given by:

$$I = I_0 + i' \tag{4.8}$$

where

$$i' = G_d A\cos(\omega_0 t) + 1/2\left[G_d' A^2 \cos^2(\omega_0 t)\right] \tag{4.9}$$

Using the identity:

$$\cos^2(\omega_0 t) = \left[1+\cos(2\omega_0 t)\right]/2,$$

we can write (4.9) as:

$$i' = A^2 G_d'/4 + AG_d \cos(\omega_0 t) + A^2 G_d' \cos(2\omega_0 t)/4 \tag{4.10}$$

Because zero-biased Schottky diodes are used, i.e., $I_0 = 0$, the total DC current is given by:

$$I_{DC} = A^2 G_d'/4 \tag{4.11}$$

Equation (4.11) shows that the output DC current of the diode is proportional to A^2, which is the input RF power. The output RF signals of frequency ω_0 and other higher harmonics are filtered out using a simple low-pass filter. Under this condition, the detector is said to operate in the square-law region. Thus, based on the analysis of power detectors, the DC current at the output of the four Schottky power detectors of the six-port demodulator is proportional to the power at the output of the four signals (b_3, b_4, b_5, and b_6) at ports 3–6 respectively.

As an example, the power of b_3 is calculated as follows.

$$|b_3| = |-0.5 \cdot j \cdot (a_2 - a_1)| = 0.5|a_2 - a_1| = 0.5\left|Ae^{j\theta_2} - Ae^{j\theta_1}\right|$$

$$= 0.5A|(\cos\theta_2 + j\sin\theta_2) - (\cos\theta_1 + j\sin\theta_1)|$$

$$= 0.5A|(\cos\theta_2 - \cos\theta_1) + j(\sin\theta_2 - \sin\theta_1)|$$

$$= 0.5A\sqrt{(\cos\theta_2 - \cos\theta_1)^2 + (\sin\theta_2 - \sin\theta_1)^2}$$

$$= 0.5A\sqrt{\cos^2\theta_2 - 2\cos\theta_2\cos\theta_1 + \cos^2\theta_1 + \sin^2\theta_2 - 2\sin\theta_2\sin\theta_1 + \sin^2\theta_1}$$

$$= 0.5A\sqrt{2 - 2\cos\theta_2\cos\theta_1 - 2\sin\theta_2\sin\theta_1}$$

$$= 0.5A\sqrt{2 - 2(\cos\theta_2\cos\theta_1 + \sin\theta_2\sin\theta_1)}$$

$$= 0.5A\sqrt{2 - 2\cos(\theta_2 - \theta_1)} = \frac{A}{\sqrt{2}}\sqrt{1 - \cos(\theta_2 - \theta_1)} \tag{4.12}$$

Using the magnitude of b_3 in (4.12) and assuming the unit resistance, the power of b_3 is obtained in (4.13):

$$|b_3|^2 = 0.5A^2|1 - \cos\Delta\theta| \tag{4.13}$$

where $\Delta\theta = \theta_2 - \theta_1$.

Then the power detector output signal from port 3 can be expressed in (4.14) after normalizing by A^2.

$$s_3 = 0.5|1 - \cos\Delta\theta| \tag{4.14}$$

Similar results can be obtained for the detector output signals from ports 4, 5, and 6. Equation (4.15) shows the four detector output signals for ports 3 to 6.

$$
\begin{aligned}
s_3 &= 0.5\left|\cos\Delta\theta - 1\right| \\
s_4 &= 0.5\left|-\sin\Delta\theta + 1\right| \\
s_5 &= 0.5\left|\cos\Delta\theta + 1\right| \\
s_6 &= 0.5\left|\sin\Delta\theta + 1\right|
\end{aligned}
\tag{4.15}
$$

Because the phasor form is used during the derivation, equation (4.15) is satisfied when the reference and the unknown signal have the same frequency. For a pulse signal, equation (4.15) is valid because the pulse signal can be decomposed into its frequency components.

The output signals versus phase difference are plotted in Fig. 4-2. For a certain phase difference between the reference and the unknown signals, four output signals have different amplitude which will be used for implementing the demodulation algorithm. As an example, when the phase difference between the reference signal and the unknown signal is $\pi/2$, s_4 has a minimum amplitude and s_6 has a maximum amplitude.

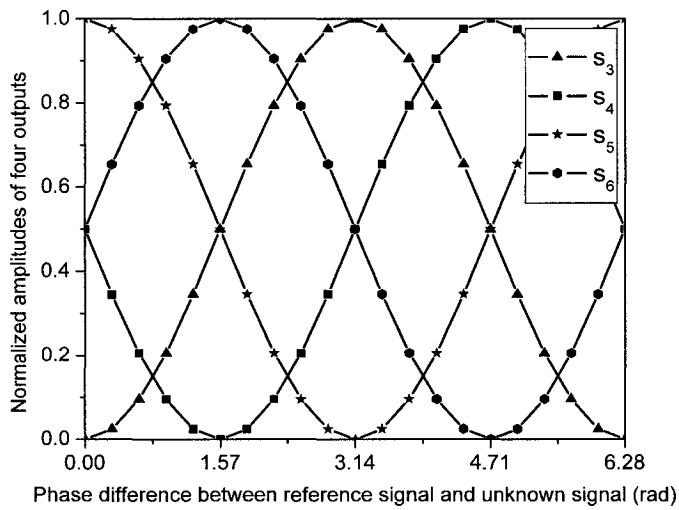

Fig. 4-2. Normalized output signals (at port 3–6) versus phase difference.

At ports 3 and 5, the output signal amplitudes have median values (between minimum and maximum amplitudes).

For a pulse signal modulated using the phase spectrum modulation (BPSM or QPSM) scheme (mentioned in chapter 3), a fixed phase change at each frequency point is maintained. Thus, the ampltidue profile shown in Fig. 4-2 is also valid.

4.3 Simulation of six-port demodulator

The six-port circuit for the demodulator was simulated using the ideal six-port model shown in Fig. 3-6. Based on the above analysis of a power detector, an ideal power detector is modeled using a square law block. A complete six-port demodulator model was implemented in Simulink and is shown in Fig. 4-3.

In the simulation, the ideal rectangular pulse signal has a repetition period of 6.4 ns and width of 320 ps. When the rectangular pulse train is fed into the demodulator model, the four output signals generate pulsed amplitude profiles which vary according to the phase spectrum difference. For a certain phase difference, each output signal has a pulsed voltage which occurs only at the pulse duration.

Fig. 4-4 show the simulated output signals at ports 3–6 for modulation state 0. At this modulation state, the phase difference $\Delta\theta$ at each frequency is equal to 0°. Hence, s_3 has minimum amplitude and s_5 has maximum amplitude. At ports 4 and 6, output signal amplitudes have median values. The simulation result agrees with the derivation result in (4.15).

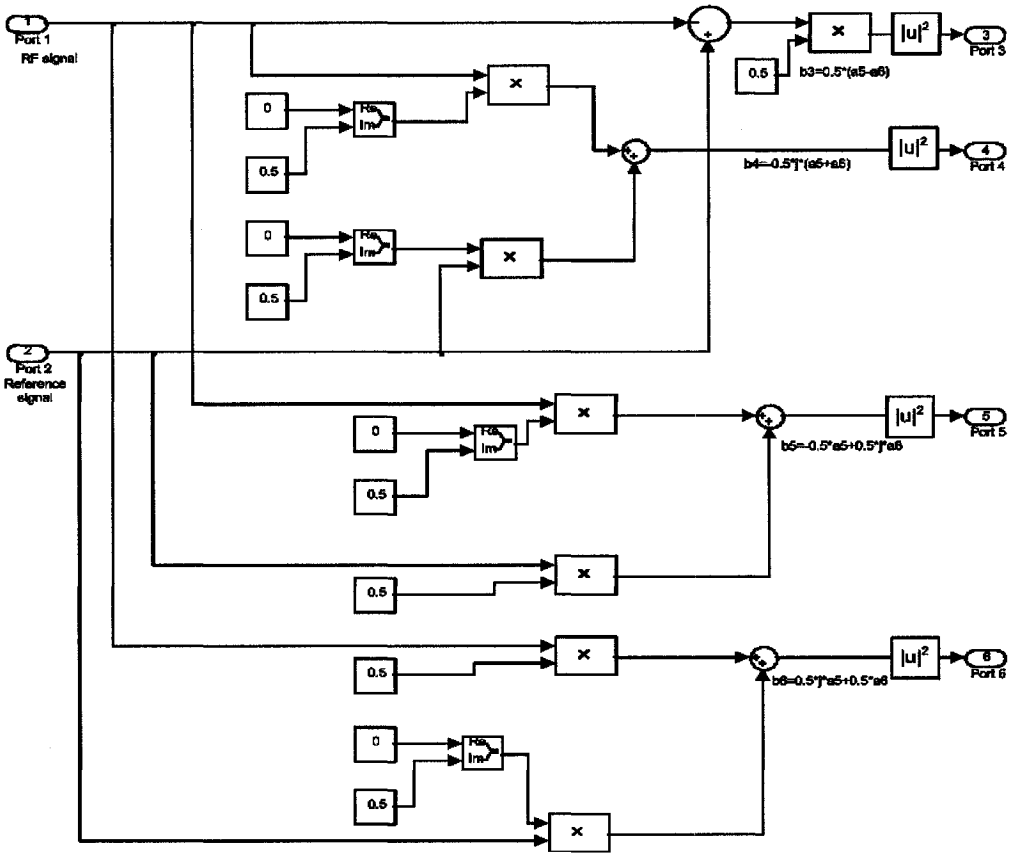

Fig. 4-3. An ideal six-port demodulator model in Simulink.

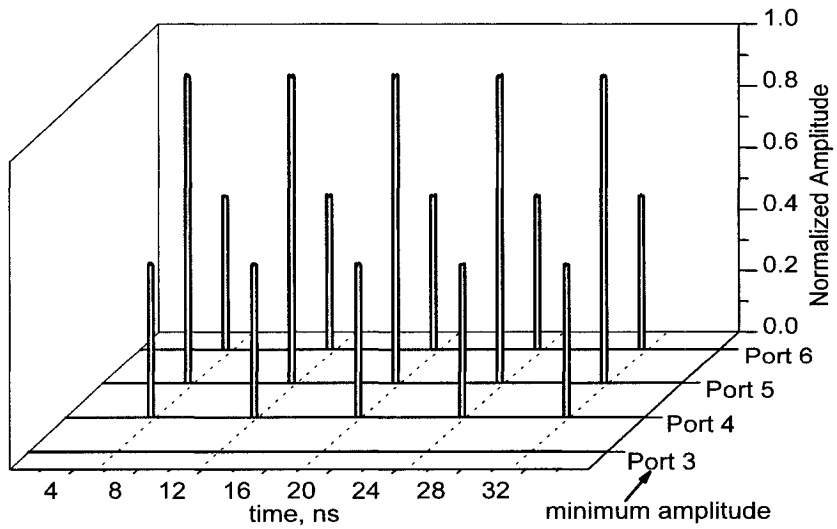

Fig. 4-4. Signals simulated at ports 3 to 6 of the demodulator for modulation state 0.

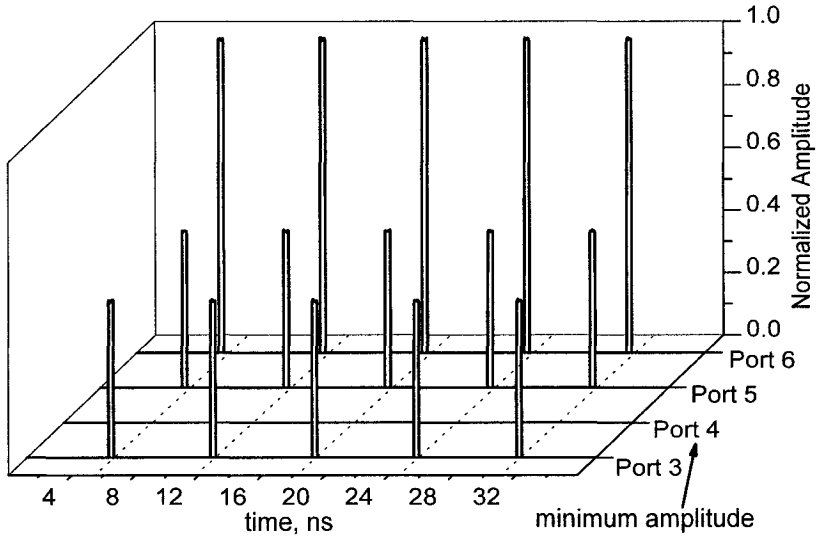

Fig. 4-5. Signals simulated at ports 3 to 6 of the demodulator for modulation state 1.

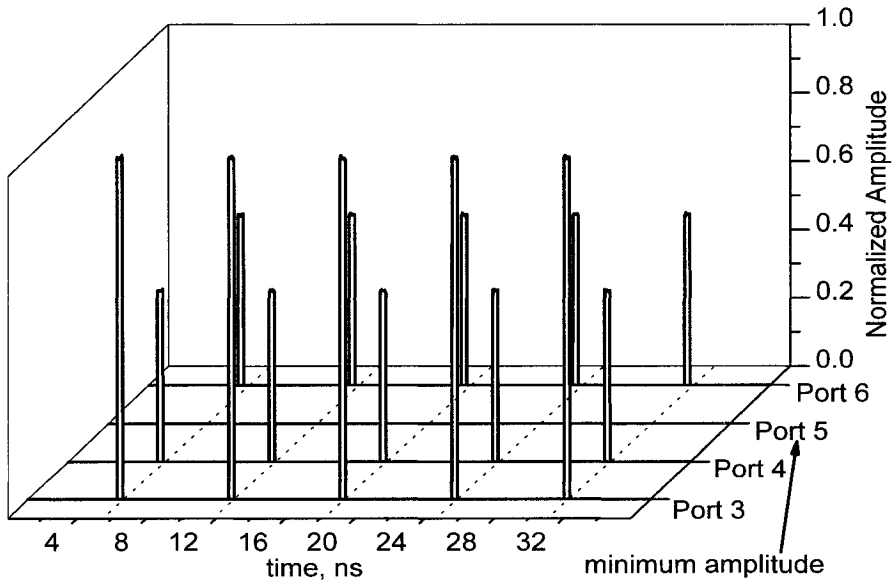

Fig. 4-6. Signals simulated at ports 3 to 6 of the demodulator for modulation state 2.

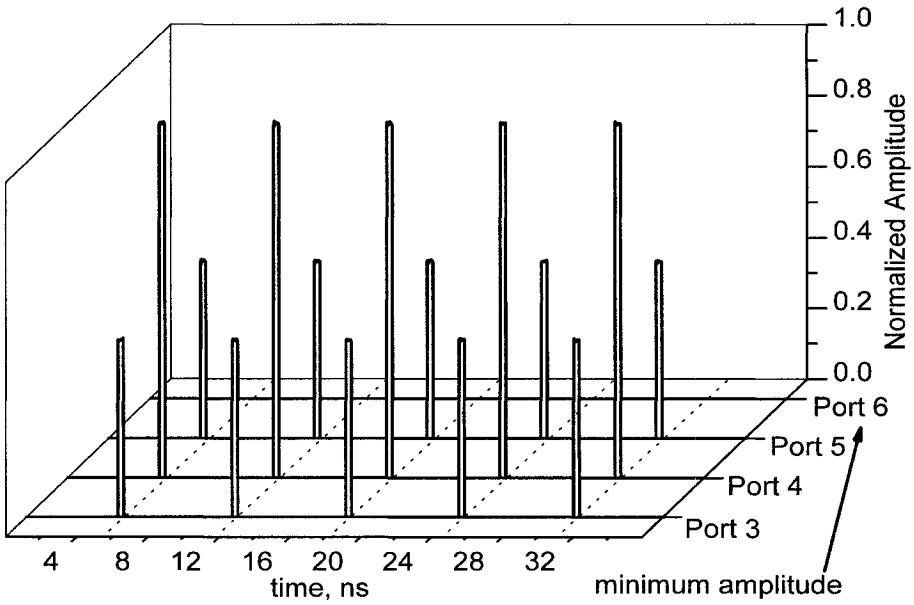

Fig. 4-7. Signals simulated at ports 3 to 6 of the demodulator for modulation state 3.

Results for the other three modulation states were also obtained and shown in Fig. 4-5 to Fig. 4-7 respectively

It is readily seen that s_4 is minimum when the modulation state is 1, s_5 is minimum when the modulation state is 2, and s_6 is minimum when the modulation state is 3. Hence, during a symbol period, all terms in (4.15) have non-zero pulse amplitudes except for one term (corresponding to the modulation state) which has zero pulse amplitude.

4.4 Measurement of six-port demodulator

A six-port demodulator, shown in Fig. 4-8, was designed and fabricated using commercial components (one power divider, three hybrid couplers, and four power

detectors). The power divider has a typical phase and amplitude imbalance 4° and 0.6 dB, respectively [45]. The attenuation resulting from inserting this power divider, i.e. insertion loss, is typically 0.5 dB. The isolation between two output ports is typically 22 dB [45]. The hybrid couplers have a typical phase and amplitude imbalance of 4° and 0.2 dB, respectively. The insertion loss is maximally 0.2 dB. The minimum isolation is 22 dB [46]. The power detector has a low level sensitivity of 0.5 mV, a frequency range between 10 MHz and 12.4 GHz, and a frequency response flatness ±0.3 dB [48].

4.4.1 S-parameter measurement of six-port demodulator

The purpose of S-parameter measurement is to evaluate the six-port demodulator from the perspective of hardware and estimate the effective bandwidth of the six-port modulator.

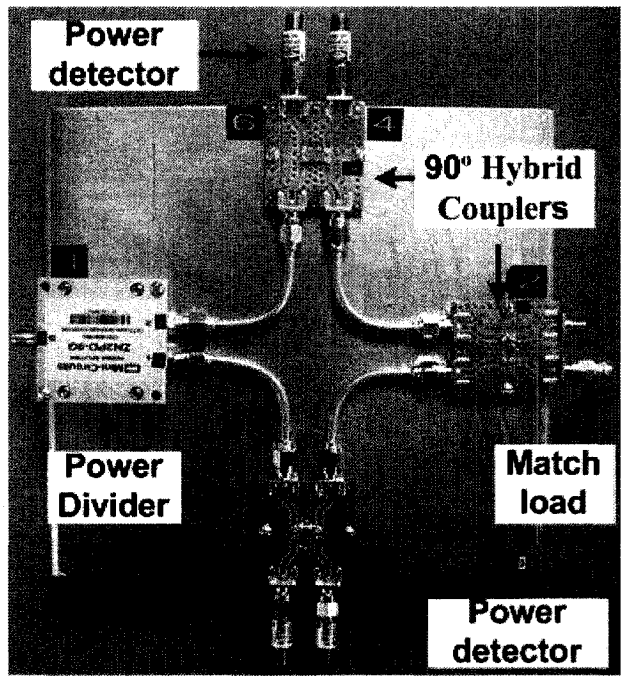

Fig. 4-8. A six-port demodulator fabricated with commercial components.

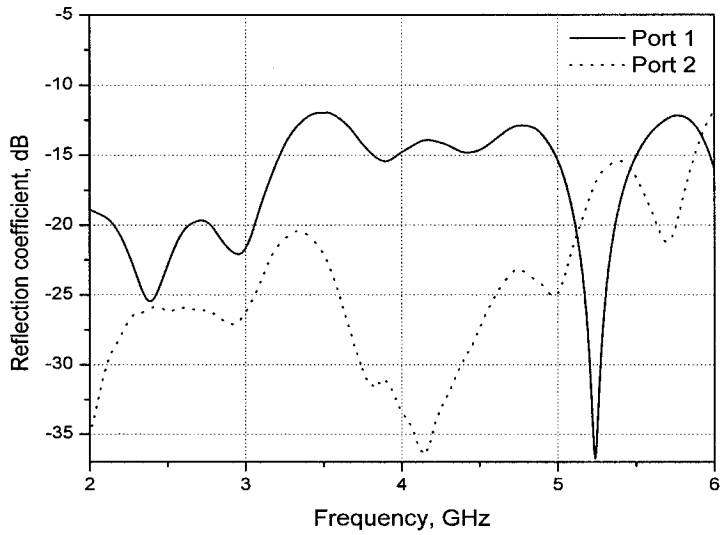

Fig. 4-9. Measured reflection coefficients at input port 1 and input port 2 of the six-port demodulator.

Fig. 4-9 shows measured S11 (input reflection coefficient) and S22 (output reflection coefficient) of the fabricated six-port demodulator. The reflection coefficient of port 1 is below -12 dB over the bandwidth, which is acceptable. The reflection of port 2 is below -20 dB over the bandwidth indicating a more perfect match. When six-port is used as a demodulator, port 1 and 2 are used as input ports of reference signal and received signal respectively. Fig. 4-10 shows the measured isolation between the input port and the output port of the six-port demodulator, which reveals expected high isolation.

To estimate the effective bandwidth of the six-port demodulator, S-parameter measurements were carried out between input ports (1 and 2) and output ports (3 to 6). Fig. 4-11 shows the forward transmission coefficients measured between port 1 and four output ports (3 – 6). Within the interested bandwidth (3 – 4 GHz), the four forward transmission coefficients are in agreement with the theoretical value of -6 dB, with a

variation between 0 and -1 dB.

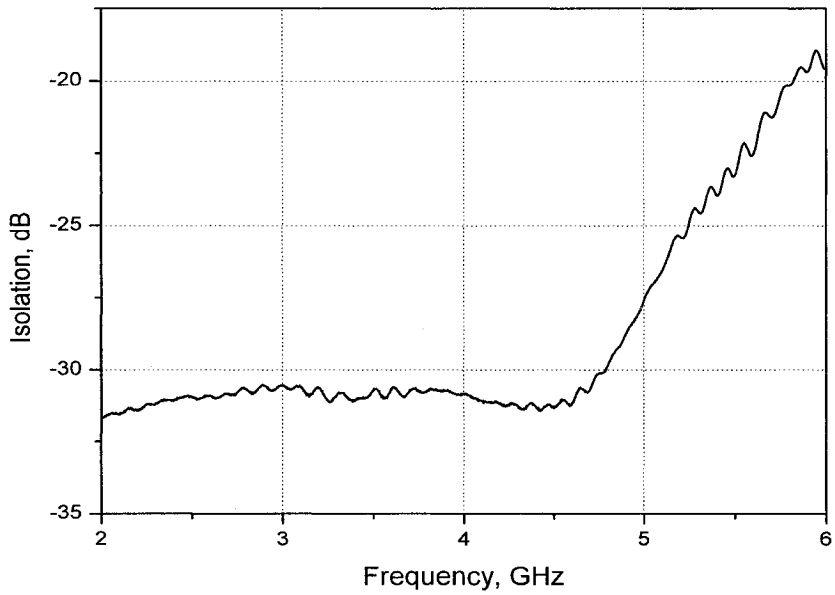

Fig. 4-10. Measured isolation between input port 1 and input port 2 of the six-port demodulator.

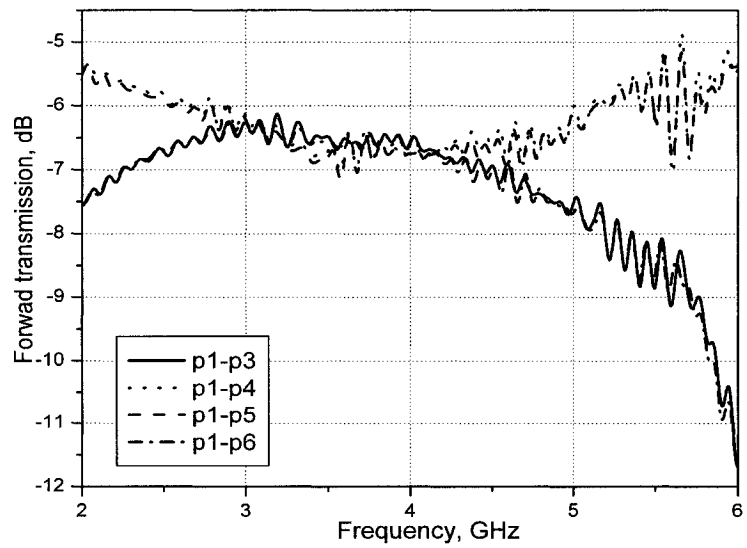

Fig. 4-11. Measured forward transmissions between input port 1 and output ports of the six-port demodulator.

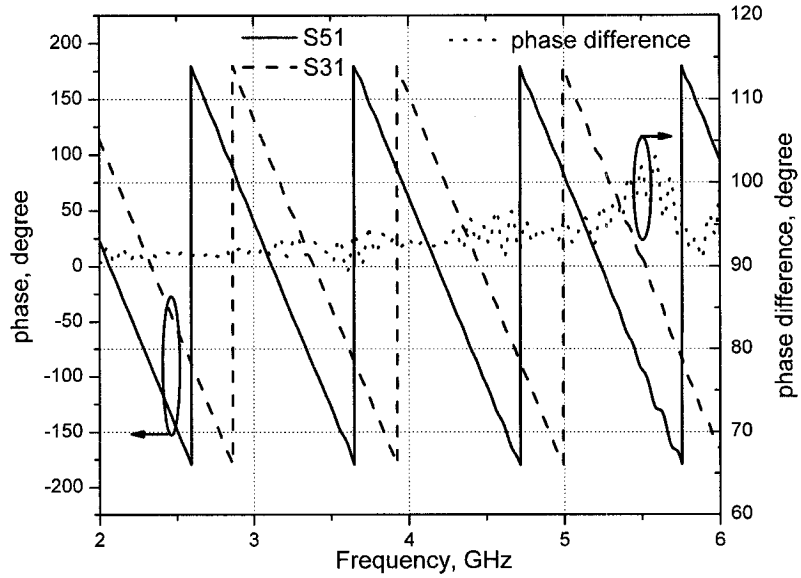

Fig. 4-12. Measured phase of forward transmissions between input port 1 and output ports (3 and 5) of the six-port demodulator.

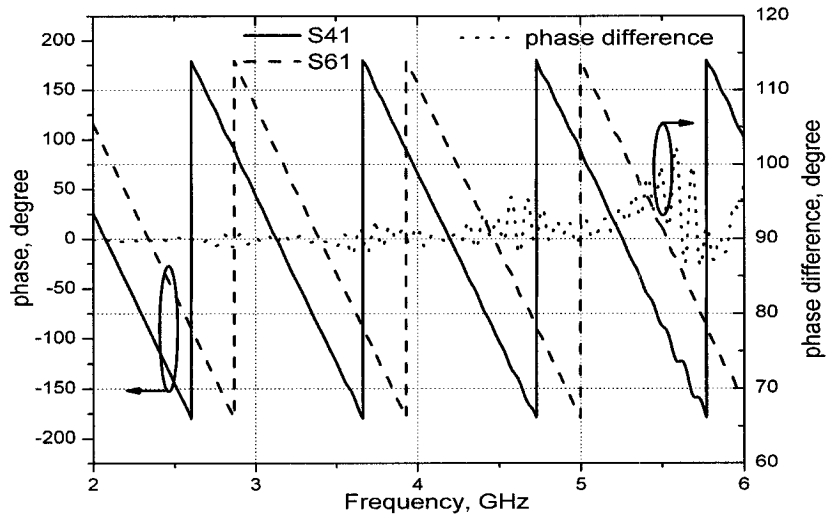

Fig. 4-13. Measured phase of forward transmissions between input port 1 and output ports (4 and 6) of the six-port demodulator.

Fig. 4-12 shows the phase of the forward transmission coefficients measured between port 1 and two output ports (ports 3 and 5). The phase difference between S31 and S51 is also plotted. The measured phase difference is in agreement with the theoretical value of 90°, with a variation of ±2° over the interested bandwidth (3–4 GHz). Figure 5.13 shows the phase of the forward transmission coefficients measured between port 1 and the other two output ports (ports 4 and 6). The phase difference between S41 and S61 is also plotted. The measured phase difference is in agreement with the theoretical value of 90°, with a variation of ±2° over the bandwidth of interest (3–4 GHz).

Fig. 4-14 shows the forward transmission coefficients measured between input port 2 and four output ports (3 to 6). Within the bandwidth of interest (3–4 GHz), the four

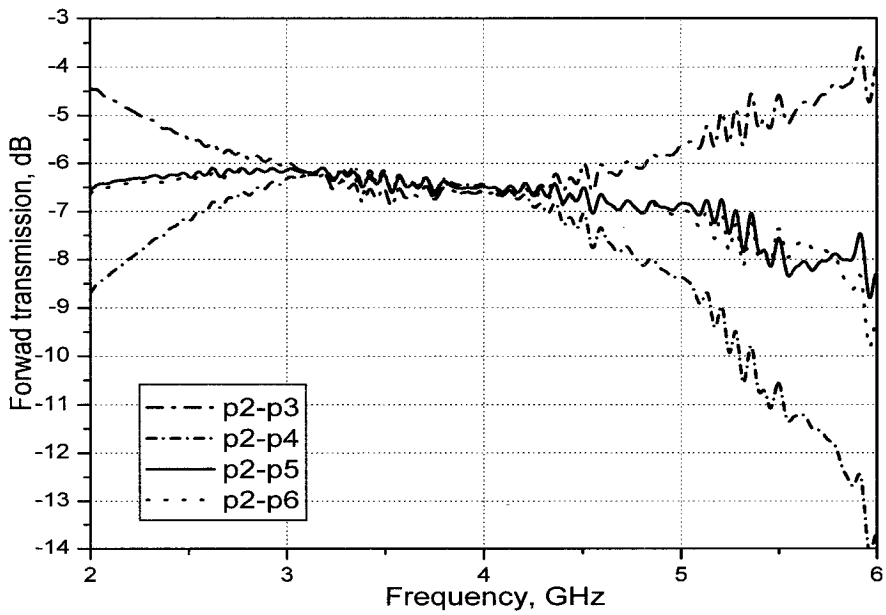

Fig. 4-14. Measured forward transmissions between input port 2 and output ports (3 – 6) of the six-port demodulator.

forward transmission coefficients are in agreement with the theoretical value of -6 dB, with a variation between 0 and -1 dB. Fig. 4-15 shows the phase of the forward transmission coefficients measured between input port 2 and two output ports (port 3 and 5). The phase difference between S32 and S52 is also plotted. The measured phase difference is in agreement with the theoretical value of 90°, with a variation of ±2° over the interested bandwidth (3–4 GHz). Fig. 4-16 shows the phase of the forward transmission coefficients measured between input port 2 and the other two output ports (port 4 and 6). The phase difference between S42 and S62 is also plotted. The measured phase difference is in agreement with the theoretical value of 90°, with a variation of ±2° over the bandwidth of interest (3–4 GHz).

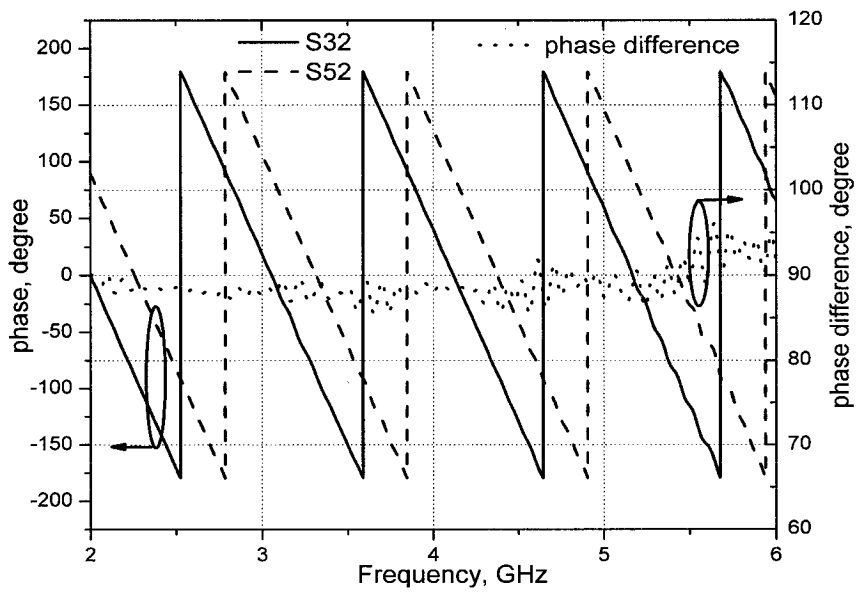

Fig. 4-15. Measured phase of forward transmissions between input port 2 and output ports (3 and 5) of the six-port demodulator.

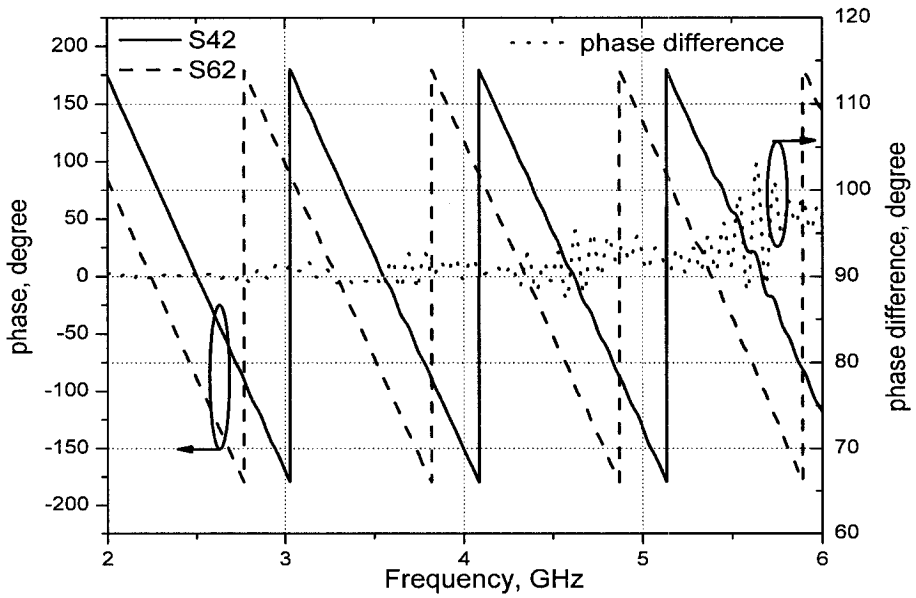

Fig. 4-16. Measured phase of forward transmissions between input port 2 and output ports (4 and 6) of the six-port demodulator.

4.4.2 Functional measurement of six-port demodulator

Measurements of output signals under four modulation states have been done using the six-port demodulator circuit and available instruments. In this measurement, the available pulse generator provides a pulse signal with 50 ns repetition period and 2 ns pulse width. Fig. 4-17 shows the measurement of output signals at port 3 to 6 for modulation state 1. The minimum pulse amplitude of this modulation state is readily seen at port 4, including additive noise. It agrees with the derivation in (4.15) and simulation results in Fig. 4-5. Results for the other three modulation states were also obtained and are similar.

Based on the above analysis and verification (simulation and experiments) of six-port

demodulation function, the demodulation can be done by comparing the amplitudes of output signals and selecting the minimal value. The symbol decision is then converted into corresponding bit pairs.

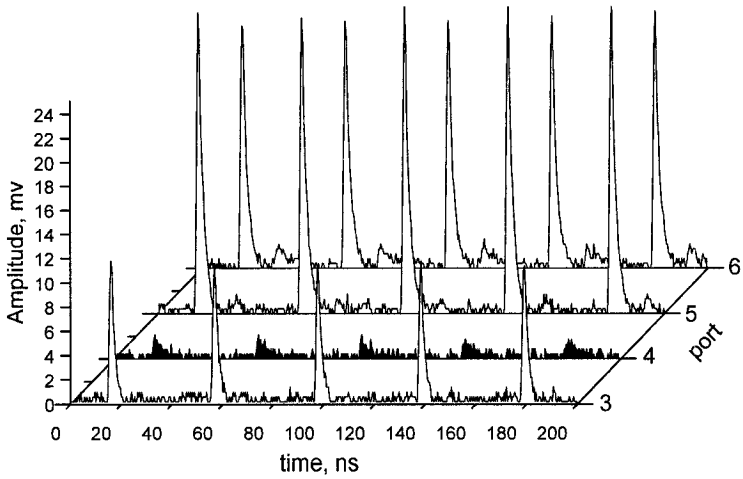

Fig. 4-17. Signals measured at ports 3 to 6 of demodulator for modulation state 1.

4.5 Implementation of demodulation algorithm

Based on the above results, demodulation algorithms were implemented on a field-programmable gate-array (FPGA) DSP platform. Fig. 4-18 illustrates the basic functions of the demodulation algorithm for a binary phase modulated signal. The output signals at

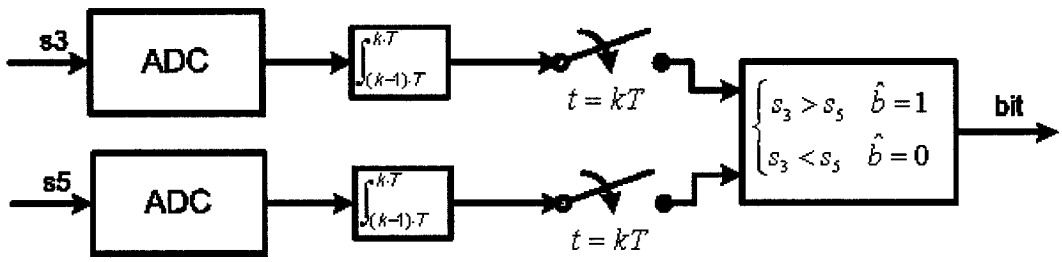

Fig. 4-18. Illustration of demodulation algorithm for a binary phase modulated signal.

ports 3 and 5 are sampled by analog-to-digital converters. The samples are integrated over the pulse repetition period (T). At clock times $t = kT$, a comparison of the accumulator outputs is done and a bit decision is given. If $s_3 > s_5$, a decision of bit 1 is made; otherwise, bit 0 is made. For a binary phase modulated signal, signal outputs from ports 3 and 5 are sufficient for demodulation. Output signals at ports 4 and 6 can be used for time-of-flight estimation using six-port circuits [49].

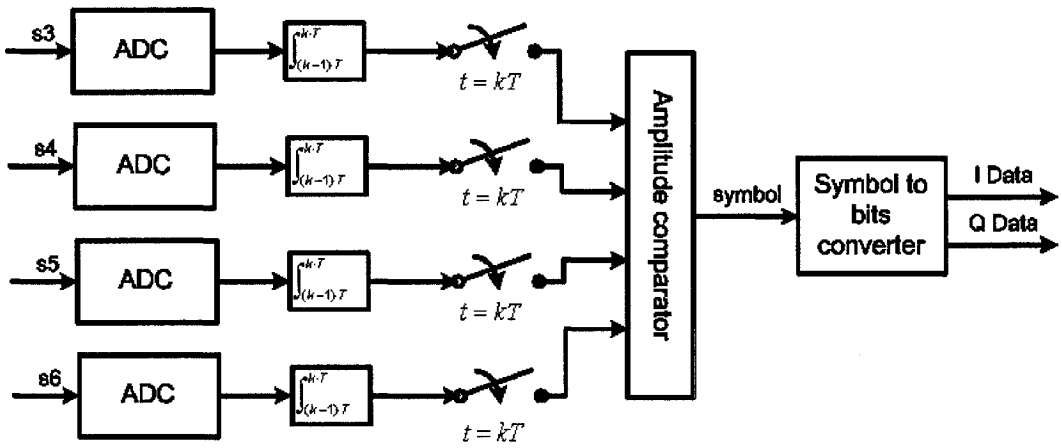

Fig. 4-19. Illustration of demodulation algorithm for quaternary phase modulated signal.

Fig. 4-19 illustrates the basic functions of the demodulation algorithm of a quaternary phase modulated signal. Four output signals are sampled by analog-to-digital converters. Then samples are integrated over the pulse repetition period (T). At clock times $t = kT$, a comparison of accumulator outputs is done and the port with minimum amplitude is chosen. If the amplitude of s_3 is minimum, symbol (0) is given. The remaining symbols (1, 2, and 3) can be deduced by analogy. Symbol (1) corresponds to the minimum amplitude present at port 4. Symbol (2) corresponds to the minimum amplitude present at port 5. Symbol (3) corresponds to the minimum amplitude present at port 6. Each

symbol is then mapped to binary data and separated into I and Q channel. The symbol to bits converter can be realized according to the truth table (Table 2).

Table 2 Truth table of symbol to bits converter.

Inputs				outputs	
D_0	D_1	D_2	D_3	I	Q
1	0	0	0	0	0
0	1	0	0	0	1
0	0	1	0	1	0
0	0	0	1	1	1

The converter can be implemented with OR gates whose inputs are determined directly from the truth table. Output I is equal to 1 when the input digit is 1 at D_2 or D_3. Output Q is equal to 1 when the input digit is 1 at D_1 or D_3. These conditions can be expressed by the output Boolean functions (5.16). And the bit converter can be implemented with two OR gates [50].

$$\begin{aligned} I &= D_2 + D_3 \\ Q &= D_1 + D_3 \end{aligned} \tag{4.16}$$

Based on the above results, demodulation algorithms were implemented on a field-programmable gate-arrays (FPGAs) DSP platform. The FPGA DSP platform includes analog-to-digital converters, digital I/O interface, and a Stratix EP1S80 FPGAs device [51]. The Stratix EP1S80 FPGAs device is in density of 79,040 logic elements (LEs). Each LE contains a four-input look-up-table (LUT), which is a function generator that can implement any function of four variables. In addition, each LE contains a programmable register and a carry chain with carry select capability. A single LE also supports dynamic single bit addition or subtraction mode [52]. The DSP blocks in the

Stratix devices run at 333 MHz to provide data throughput performance of 2.67 giga multiply-accumulate (GMAC) operations per second per DSP block. The FPGA device (EP1S80) on the platform includes 22 DSP blocks which can provide a combined throughput of up to 58.6 GMAC per second [52].

The above algorithms were first built using graphical-based design-entry methods. The design was then converted to a device programming image by the assembler of the development tool (Quartus II [53]) so that the FPGA device can be configured with the

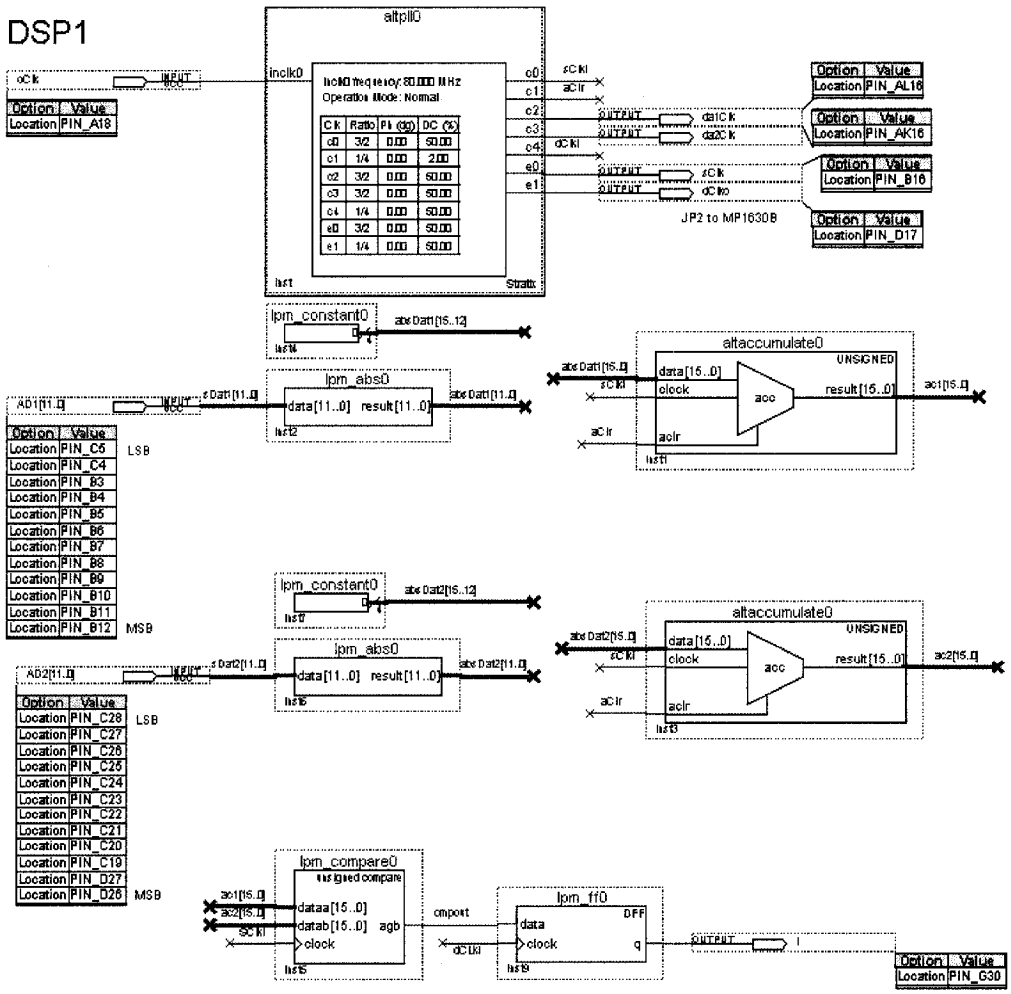

Fig. 4-20. FPGA implementation of demodulation algorithm.

desired algorithm. As an example, Fig. 4-20 shows part of the design schematic of the demodulation algorithm.

Along with the above algorithms, baseband clock management is necessary for symbol synchronization. The involved clock signals, shown in Fig. 4-21, include analog-to-digital converter (ADC) sampling clock, symbol clock, an external clock signal synchronizing the data generator, a trigger signal synchronizing pulse generator, and internal clock signals of FPGA device. These clock signals having different frequencies are derived from a single clock source of 80 MHz oscillator on the DSP platform. Using

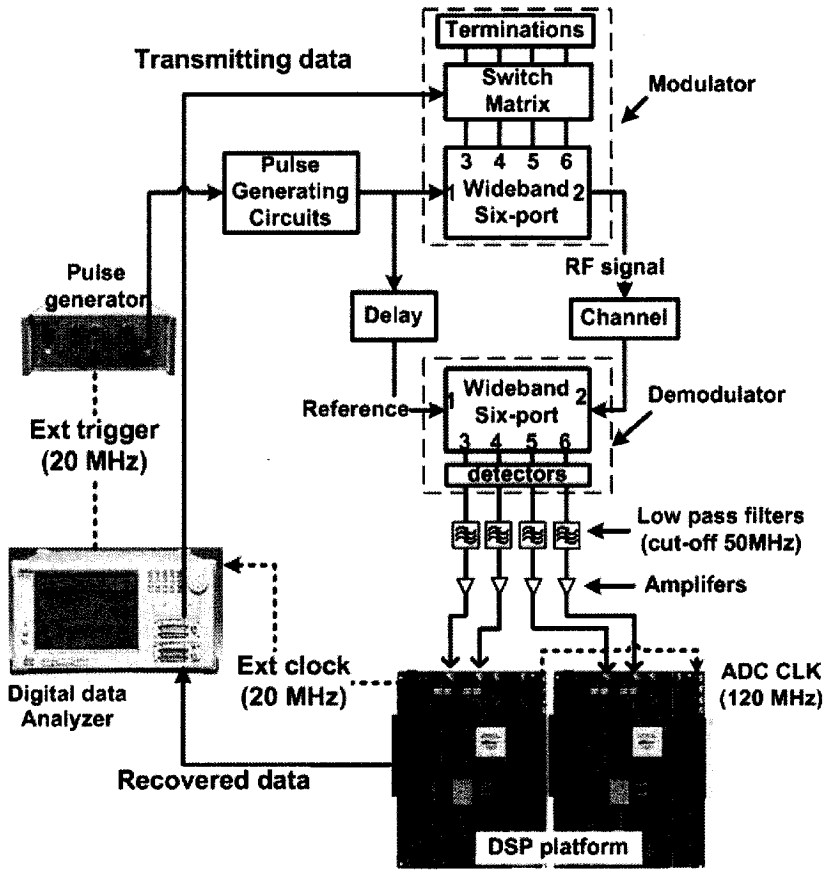

Fig. 4-21. Baseband clock management design.

the phase-locked loops (PLL) functionality built in the FPGA devices, clock signals having a desired frequency are synthesized at the PLL ports using scaling factors. The detailed clock design can also be found in Fig. 4-20.

The algorithms were tested using the test bench. The amplitude comparison for binary phase modulated signal is readily seen in Fig. 4-22 where the recovered bits output from the DSP platform are compared with the transmitted bits. As we can see, the transmitted bits are correctly recovered with a certain delay. The adoption of FPGA digital signal processor in the proposed UWB platform is for the purpose of increasing the flexibility of the system and adapting it to software defined radio (SDR) needs. In addition, using design-ready intellectual property (IP) functions provided with the DSP platform significantly shortens the implementation time.

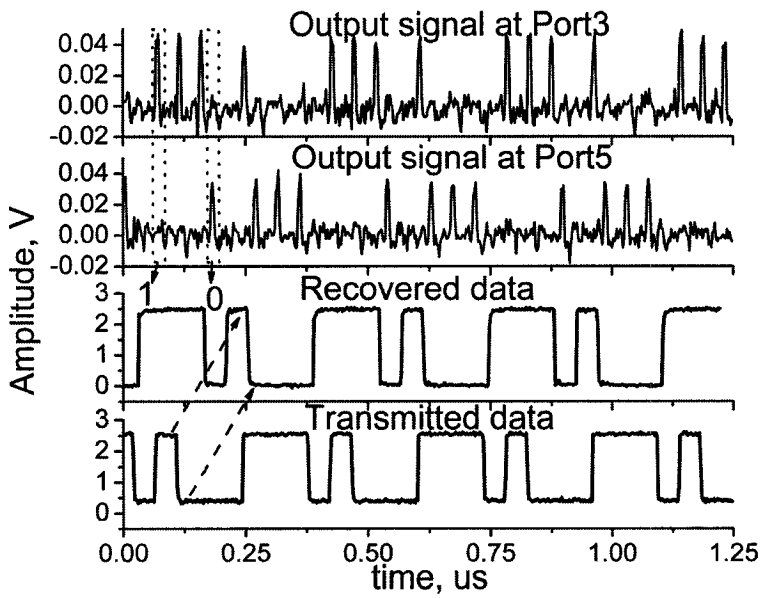

Fig. 4-22. Measured waveforms at ports 3 and 5 and comparison of recovered data with transmitted data.

CHAPTER 5 SYSTEM PERFORMANCE STUDY

5.1 System performance over AWGN channel

In this section, the performance of the proposed UWB system is studied to characterize the bit error probability (P_e). The relation between the bit energy to noise power density ratio (E_b/N_0) and P_e using phase spectrum modulation is derived using the following hypothesis.

The first hypothesis is that each pulse is confined within a pulse duration time and the duration time is finite. The inter symbol interference (ISI) from the same transmission is absent. We consider a multi-path-free channel over which no replicas of pulses are present. A single user is considered thus multi-user interference due to pulse transmitted from other users is ignored. Also, a perfect synchronization between transmitter and receiver is assumed.

The simulation and measurement results are also compared with theoretical calculation. A link budget using this six-port based UWB radio is analyzed for a point-to-point link.

5.1.1 Pulse signal and symbol energy

An expression of a pulse train is usually obtained considering a pulse symmetric at $t = 0$ [54]. However, we will use an expression for a periodic pulse (with a delay $t_0 \neq 0$) sequence. The expression is more meaningful for studying the actual phase spectrum which makes more sense for phase spectrum modulation. Also, this is a

common case for practical pulse generators. In this UWB system, we consider a periodic sequence of rectangular pulses $x(t)$ upconverted to a carrier frequency f_c. The periodic pulse train can be expressed by:

$$\begin{aligned} x(t) &= \sum_{n=-\infty}^{\infty} A_p \cdot rect\left[(t - nT - t_0)/\tau\right] \\ &= \left\{A_p \cdot rect[(t - t_0)/\tau]\right\} * \delta_T(t) \end{aligned} \tag{5.1}$$

where $rect(x)$ is the normalized rectangular function expressed in (5.2)

$$rect(x) = \begin{cases} 1 & |x| < 1/2 \\ 0 & |x| > 1/2 \end{cases} \tag{5.2}$$

and $\delta_T(t)$ is a periodic sequence of delta-functions expressed in (5.3).

$$\delta_T(t) = \sum_{n=-\infty}^{\infty} \delta(t - nT) \tag{5.3}$$

The amplitude and width of the rectangular pulse signal are represented by A_p and τ respectively, while the pulse repetition period is T. Each pulse is centered at a particular position $t_0 \neq 0$ relative to nT, where n is an integer number.

In the pulse generation circuit of the test bench, a mixer is used to upconvert the spectrum of rectangular pulse to the frequency range between 3.10 GHz and 10.6 GHz. Since a mixer can be mathematically expressed as a multiplier [55], the output signal of the pulse generating circuit can be expressed in (6.4)

$$s(t) = x(t) \times A_c \cos(\omega_c t) \tag{5.4}$$

where A_c is amplitude of carrier signal and $\omega_c = 2\pi f_c$ is the angular frequency of the

carrier signal.

For a phase spectrum modulation UWB system, a frequency domain analysis is appropriate for the pulse signal used for transmission. With the above definitions in the time domain and the Fourier Transform theorems, the amplitude and phase spectrum of the transmitted pulse signal can be obtained as follows:

$$S(f)=\frac{1}{2}A_c\left[X\left(f-f_c\right)+X\left(f+f_c\right)\right] \tag{5.5}$$

$$X(f)=\ \mathrm{F}\{\mathrm{x(t)}\}=F\left\{A_p\cdot rect[(t-t_0)/\tau]\right\}\times F\left\{\delta_T(t)\right\} \tag{5.6}$$

Using the results in [56],

$$\begin{aligned} F\left\{A_p\cdot rect[(t-t_0)/\tau]\right\} &= A_p\tau\cdot sinc(\tau f)e^{-j2\pi t_0 f} \\ F\left\{\delta_T(t)\right\} &= \frac{1}{T}\sum_{n=-\infty}^{\infty}\delta(f-n/T) \end{aligned} \tag{5.7}$$

where the *sinc* function is defined as follows:

$$sinc(x)=\frac{sin(\pi x)}{\pi x} \tag{5.8}$$

The exponential form of $X(f)$ can be obtained

$$\begin{aligned} X(f) &= A_p\tau\cdot sinc(\tau f)e^{-j2\pi t_0 f}\times\frac{1}{T}\sum_{n=-\infty}^{\infty}\delta(f-n/T) \\ &= \frac{A_p\tau}{T}\sum_{n=-\infty}^{\infty}sinc(\tau f)e^{-j2\pi t_0 f}\delta(f-n/T) \end{aligned} \tag{5.9}$$

Hence, the amplitude and phase spectra of $X(f)$ can be expressed as follows:

$$\begin{cases} |X(f)| = \dfrac{A_p \tau}{T} |sinc(\tau f)|, & \text{when } f = n/T \\ |X(f)| = 0, & \text{otherwise} \end{cases} \tag{5.10}$$

$$\varphi_X(f) = \begin{cases} -2\pi t_0 f & \text{for } sinc(\tau f) > 0 \\ -2\pi t_0 f \pm \pi & \text{for } sinc(\tau f) < 0 \end{cases} \tag{5.11}$$

The amplitude and phase spectra of $S(f)$ can be obtained by shifting $X(f)$ with f_c.

Fig. 5-1 and Fig. 5-2 show the amplitude and phase spectra of $S(f)$ respectively.

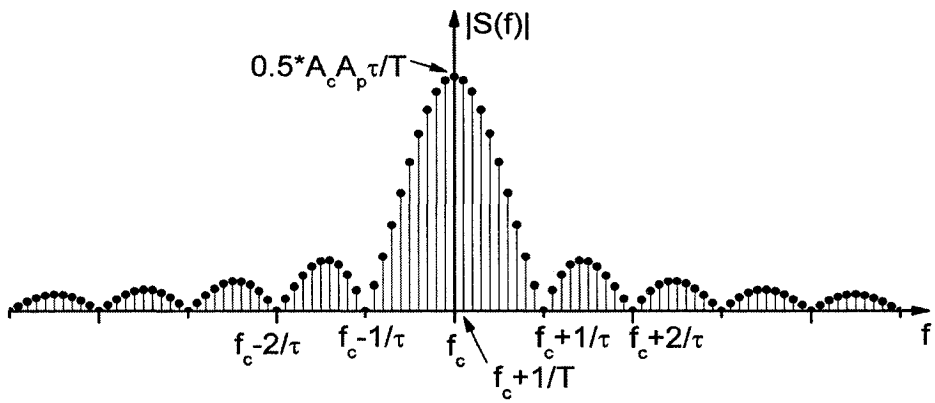

Fig. 5-1. Amplitude spectra of pulse signal s(t).

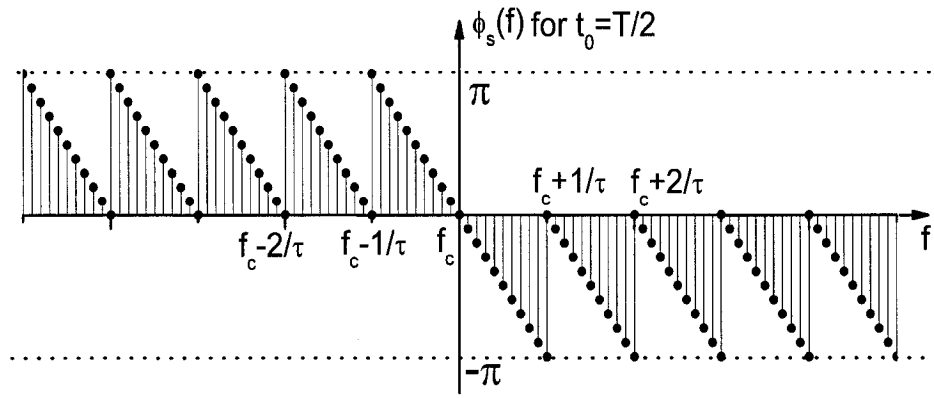

Fig. 5-2. Phase spectra of pulse signal s(t).

The amplitude spectrum of $S(f)$ is invariant with respect to any time delay. The only effect of a time delay (t_0) is to add a constant term to the phase spectrum that varies linearly with frequency.

For quaternary phase modulated signal, the phase spectra can be expressed in (5.12)

$$\varphi_{s,QPSM}(f)=\begin{cases} -2\pi t_0 f + i\cdot 90^\circ & for\ \sin c(\tau f)>0 \\ -2\pi t_0 f \pm \pi + i\cdot 90^\circ & for\ \sin c(\tau f)<0 \end{cases} \qquad (5.12)$$
$$i=0,1,2,3$$

For binary phase modulated signal, the phase spectra can be expressed in (5.13)

$$\varphi_{s,BPSM}(f)=\begin{cases} -2\pi t_0 f + i\cdot 180^\circ & for\ \sin c(\tau f)>0 \\ -2\pi t_0 f \pm \pi + i\cdot 180^\circ & for\ \sin c(\tau f)<0 \end{cases} \qquad (5.13)$$
$$i=0,1$$

In MIR UWB transmission, each pulse represents one symbol and the transmission happens only over the pulse duration (τ), i.e., the pulse width. The symbol energy (E_s) can be computed by multiplying the pulse duration time (τ) with the peak power. For a pulsed signal, the peak power is the rate at which energy is delivered during each pulse [57]. The peak power in MIR system is calculated by integrating the power spectral density ($|S(f)|^2$) over the bandwidth used for transmission. To comply with the FCC unilateral mask limit, $2|S(f)|^2$ is used for the computing in (5.14).

$$E_s=\tau\cdot 2\int_{f_L}^{f_H}|S(f)|^2\,df \qquad (5.14)$$

where f_L and f_H are the lowest and highest frequencies of interest.

5.1.2 Noise source - Additive white Gaussian noise

Assume the only source at the receiver is additive white Gaussian noise (AWGN). The bilateral thermal noise power spectral density (PSD) $N_0/2$ expressed in Joule, i.e., W/Hz is given by [58]:

$$\frac{1}{2}N_0 = \frac{1}{2}k \cdot Temp_0 \cdot NF(f) \tag{5.15}$$

where $k = 1.38 \cdot 10^{-23} Joules/K$ is the Boltzman constant and $NF(f)$ is the noise figure of the receiver. It is assumed that the noise temperature of the receiving antenna is the standard room temperature $Temp_0 = 290K(or 17°C)$. Although the noise figure $NF(f)$ is frequency dependent, we will neglect this effect in the simulation.

5.1.3 Analysis of Pe vs. E_b/N_0 for phase spectrum modulation

Analyzing a frequency point of a signal modulated using QPSM is equivalent to QPSK modulation of a single carrier at the same frequency. Although the absolute phase varies with the frequency, the phase difference at a certain frequency is the same with respect to frequency during a symbol period. Also, the noise power spectral density is $N_0/2$ over the spectrum. Therefore we can use BER performance result in (5.15) of single carrier QPSK modulation [59] to evaluate the QPSM scheme.

$$\mathrm{P}_{e,QPSM} = Q\left(\sqrt{\frac{2E_b}{N_0}}\right) \tag{5.16}$$

where

$$Q(y) = \frac{2}{\sqrt{\pi}} \int_y^{\infty} e^{-x^2} dx$$

For quaternary phase spectrum, each pulse (or symbol) represents two bits. Therefore, the bit energy can be calculated using the result in (5.14) as follows:

$$E_{b,QPSM} = \frac{1}{2} E_s = \frac{1}{2} \cdot \tau \cdot 2 \int_{f_L}^{f_H} |S(f)|^2 \, df = \tau \cdot \int_{f_L}^{f_H} |S(f)|^2 \, df \qquad (5.17)$$

For binary phase spectrum modulation, bit error probability has the same expression as equation (5.16). Each pulse (or symbol) represent one bit. Therefore, bit energy is equal to symbol energy as in (5.14).

5.1.4 Link budget

Let us suppose that the signal propagates over a free-space propagation channel. Through link budget analysis, we can specify the transmitted power and the average signal to noise ratio required to achieve a given level of performance at some desired data rate. In a similar manner, given the allowed power, we can evaluate the maximum distance over which propagation can occur when a predetermined probability of error must be guaranteed at the receiver, at a given data rate.

Suppose we have a required performance level (P_e) at data rate R, using equation (5.16), we can find the required signal to noise ratio per bit $(E_b/N_0)_{req}$. The average power level (P_R) at receiver input can be found using equation (5.18).

$$\frac{P_R}{N} = \frac{R}{W} \left(\frac{E_b}{N_0} \right)_{req} \qquad (5.18)$$

where N is the total noise power over the considered bandwidth (W).

Assuming the gain of the transmit and receiving antenna are equal over the bandwidth of the UWB system, the required transmit power (P_T) can be calculated as:

$$P_T = P_R + L - G_R - G_T - G_{LNA} \ (dB) \tag{5.19}$$

where L is link loss in dB, G_{LNA} is the gain of low noise amplifier in receiver, G_R and G_T are the receiving and transmitting antenna gain, respectively.

The link loss for free space propagation is frequency-dependent and can be expressed in (5.20).

$$L(f) = \left(\frac{4\pi d}{\lambda}\right)^2 = \frac{(4\pi d)^2 f^2}{c^2} \tag{5.20}$$

where d is the distance of propagation, $\lambda = c/f$ is the wavelength.

Although a link loss for a UWB signal can be obtained by integrating equation 6.20 over the frequency bandwidth, the observation of wideband link loss in [60] shows narrowband models for link loss can be used to approximate the link loss for a UWB system with an error of only 1.5 dB. Thus, the link loss can be empirically calculated using the center frequency.

A UWB signal has an emission mask which determines the maximum allowed transmitted power. From the system design, G_{LNA}, G_T, G_R are all known. The coverage range in distance can be evaluated using equations (5.18 – 5.20) given a BER requirement at the receiver.

5.1.5 Comparison of performance results by theoretical calculation, simulation, and measurement (direct connection)

5.1.5.1 UWB system simulation

The whole multi(six)-port impulse UWB system was simulated using the Agilent Advance Design System (ADS). The simulation schematic (Fig. 5-3) includes pulse generator, modulator, demodulator, noise source, and clock synchronization.

The six-port modulator changes the phase of each frequency point with the same value during a symbol period in the phase spectrum modulation. Without losing accuracy of describing this behavior in simulation, the wideband six-port modulator is simulated using ideal wideband phase shifter model controlled by base band data. This ideal phase shifter provides an equal phase change for each frequency.

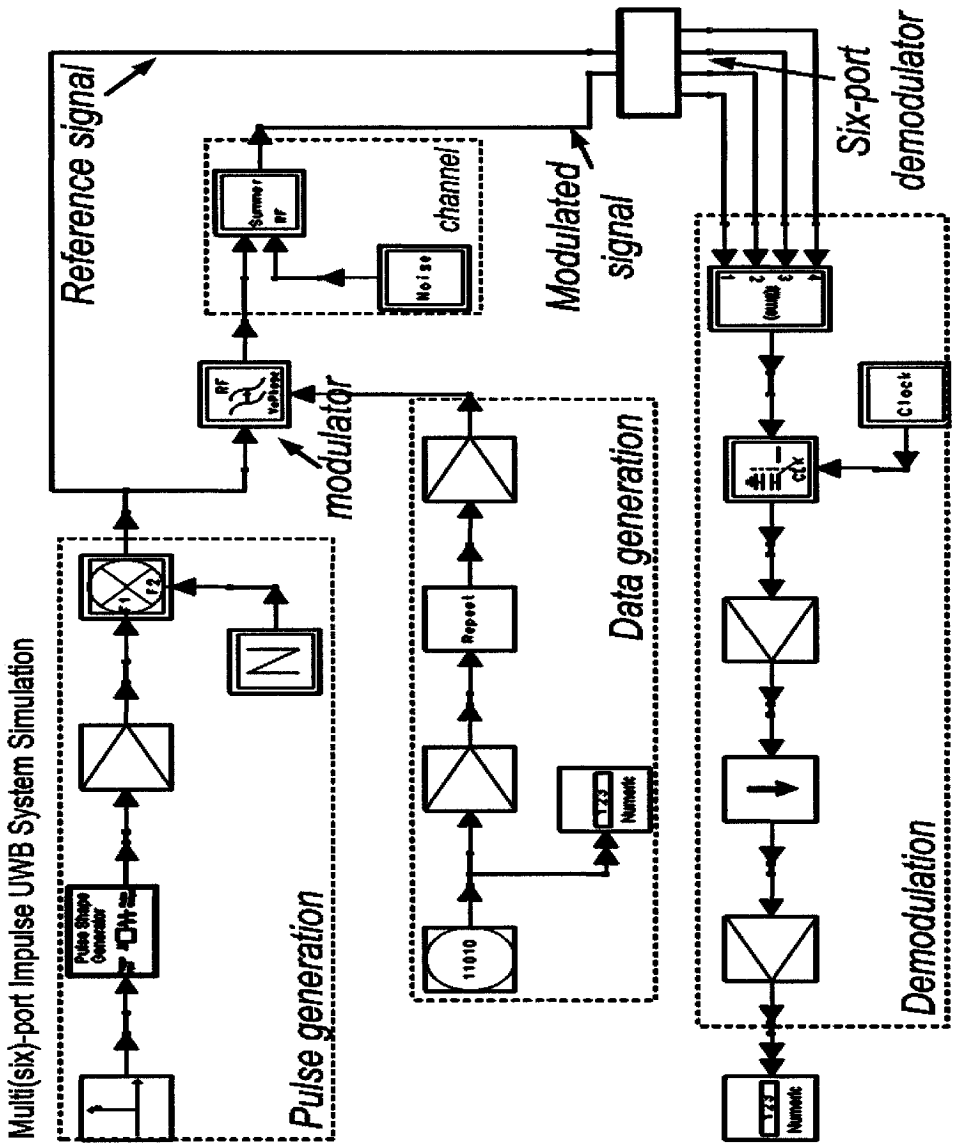

Fig. 5-3. Multi(six)-port Impulse UWB system simulation.

The six-port demodulator was implemented for this system simulation in ADS. The similar method as described in section 4.3 is used to develop this six-port demodulator

model shown in Fig. 5-4. The symbol detection function is simulated using a timed symbolic defined component [61]. This component generates a timed data output that is evaluated using a user defined expression. The detection method described in section 4.3 is defined in the component by specifying equations that relate four input voltages to the symbol output. The Baseband synchronization was also included.

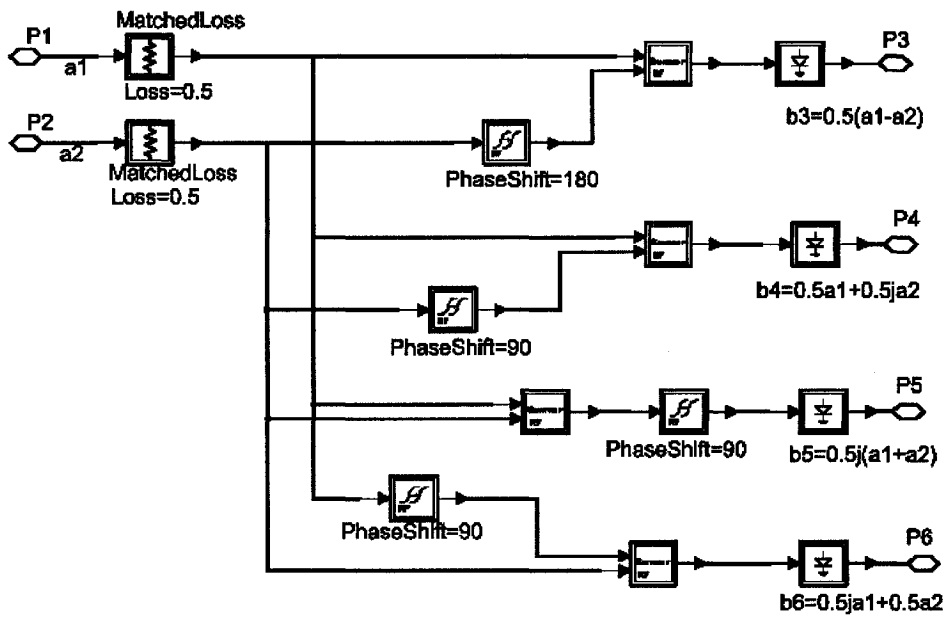

Fig. 5-4. Six-port demodulator model for data flow simulation.

Using the simulation controller - Timed synchronous data flow (TSDF) [62], the entire UWB system can be simulated integrating RF simulation with signal processing simulation. The system simulation is performed in discrete time steps. At each time step, the signals generated by all the sources are propagated through the system and the outputs are evaluated. The TSDF controller is used to control the flow of mixed numeric and timed signals for system-level analog/RF simulation. This time step specifies the time between each sample. In the UWB system simulation, one tenth of pulse width is

used as the time step.

For the system simulation using quaternary phase spectrum modulation, the bit error rate (BER) of the UWB system is obtained by comparing the output data stream to the input data stream. The input data stream in bit is first mapped to a symbol stream using binary mapping. The recovered symbol stream is then converted back to a bit stream for comparison. Typical hardware BER measurements are based on the exact number of bit-errors and the number of bits transmitted (Monte Carlo measurement) [63]. In the simulation, we used the Monte Carlo method to estimate the bit error rate (BER'). For the BER' result to be statistically significant, the number of bits required (N_{bits}) should typically be on the order of 10/BER (as a rule of thumb). For finite N_{bits} a reasonable uncertainty exists in a simulation result of BER'. The reliability of the BER estimation is usually qualified in terms of confidence intervals. Applying a normal approximation, a confidence level $(1-\alpha)$ can be expressed in (5.21) with a chosen d_α [64]. And the corresponding confidence interval (y_-, y_+) is given by (5.22) [64].

$$1-\alpha = \frac{1}{\sqrt{2\pi}} \int_{-d_\alpha}^{d_\alpha} e^{-t^2/2}\, dt = erf\left(\frac{d_\alpha}{\sqrt{2}}\right) \tag{5.21}$$

$$y_\pm = BER\left\{1 + \frac{d_\alpha^2}{2\eta}\left[1 \pm \sqrt{\frac{4\eta}{d_\alpha^2} + 1}\right]\right\} \tag{5.22}$$

where $erf(x)$ is error function defined by $erf(x) = \frac{2}{\sqrt{\pi}} \int_0^x e^{-t^2} dt$. η is a ratio of total bit number to expected BER ($\eta = N_{bits} / BER$). As an example, the confidence interval on a BER (1E-4) is plotted in Fig. 5-5 for a 95% confidence level, i.e., $(1-\alpha) = 95\%$. From Fig. 5-5, one can see a simulation with 10E4 total bits produce a 95% confidence interval of about (2*BER, 0.5*BER), i.e. a factor of about 2 on the BER. Therefore, some variation observed on the BER simulation results shown in Fig. 5-6 is reasonable.

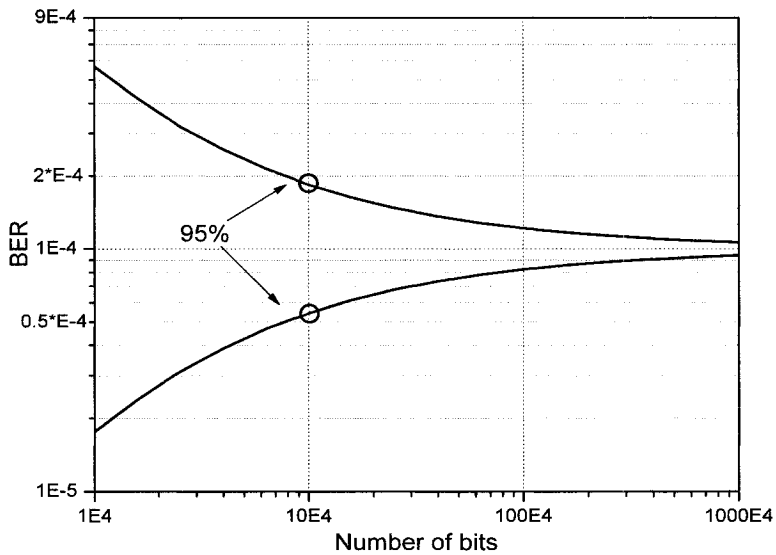

Fig. 5-5. The 95% Confidence interval on observed BER 1E-4.

To obtain the bit errors, the output bit stream is compared with a reference bit steam which is a delayed version of the input bit stream. The delay caused by the system can be determined by observing the plots of input and output streams in the data display. Then the synchronization required between the reference bit stream and the output bit stream is achieved by introducing the same amount using the delay component.

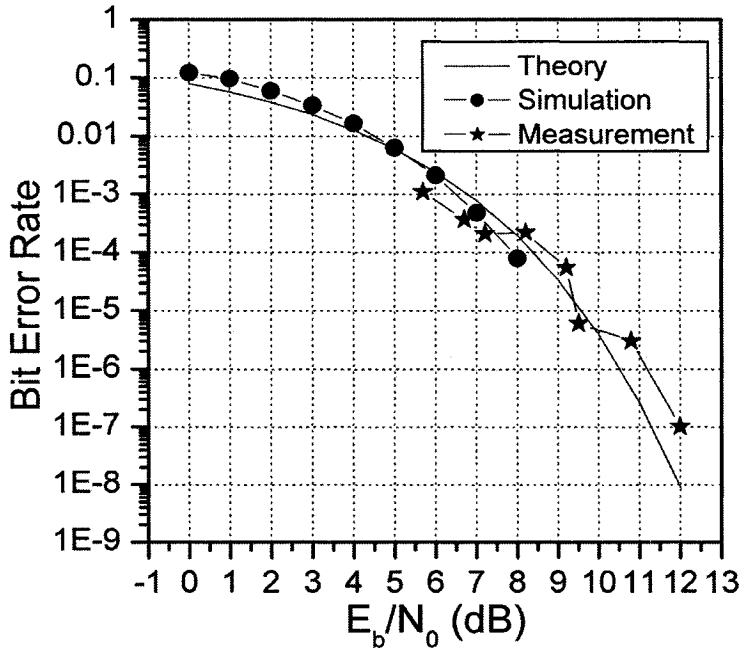

Fig. 5-6. Comparison of simulated, measured and theoretical BER for data rate of 20 Mbps.

5.1.5.2 UWB test bench measurement using direct cable connection

A proof-of-concept experiment has been realized on a test bench (Fig. 5-7) composed of the pulse generating circuit, six-port modulator, demodulator, and the FPGA programmable signal processing platform implementing the demodulation algorithm and synchronization control.

The up-converter operating at a center frequency of 3.5 GHz converts the pulse signal to a signal occupying 1GHz spectrum between 3-4 GHz. The full spectrum, fed into the wide band six-port modulator, is modulated through the switch matrix whose control inputs are connected to baseband data. The modulated and reference signals are fed into the six-port demodulator whose outputs provide different

signal profiles used for demodulation. The delay in the reference signal path is manually adjusted to match the receiving signal path delay. In future developments of the platform, this will be accomplished using synchronization algorithms. The output signals are sampled and processed by the DSP platform performing the demodulation algorithms. The amplitude comparison is readily seen, as shown in Fig. 4-22, where the recovered bits are compared with the transmitted bits. Assuming an AWGN channel, the bit error rate of test bench has been simulated and measured at a data rate of 20 Mbps. The BER results shown in Fig. 5-6 are compared with theoretical values according to [38]. It shows the close agreement with some variations, typically ranging from 0.3×10^{-4} to 1.1×10^{-4} at 8dB of E_b/N_0 .

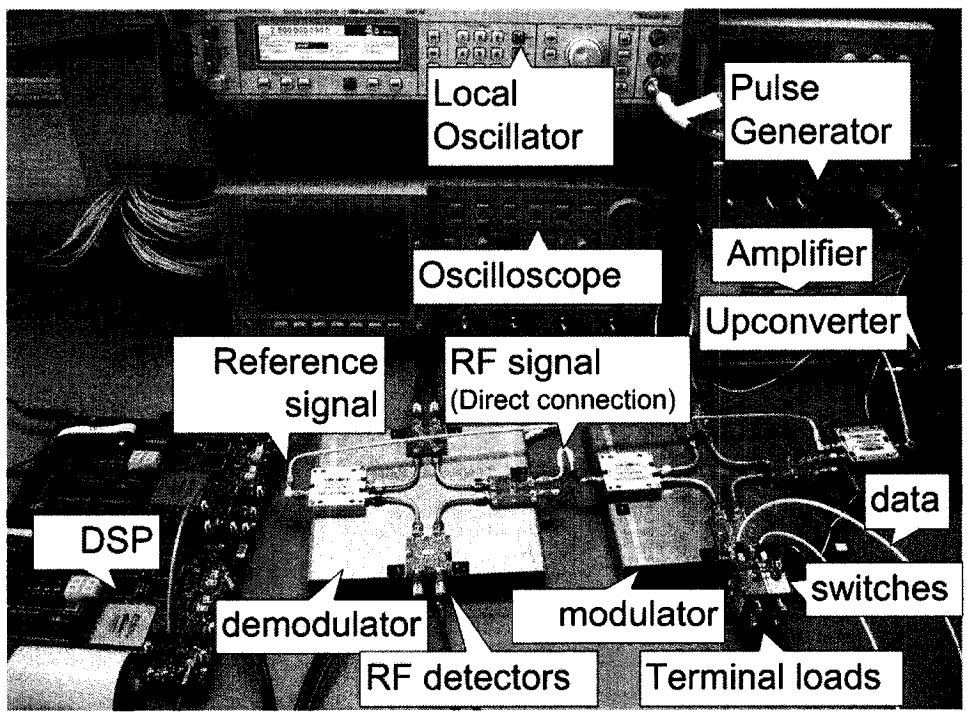

Fig. 5-7. Mulit(six)-port impulse UWB test bench (3–4GHz) (direct connection).

5.2 Measurement using UWB antennas

The antenna selected for the proposed UWB system of this work must meet several requirements including consistent behavior (pattern, gain, matching, and low or no dispersion) across the operational band [65], easy integration with six-port based UWB front-end, and low-cost. Particularly, an antenna with linear phase response over the bandwidth is desired for transmitting a phase spectrum modulation signal..

For the measurement over a point-to-point wireless link, we adopted planar semicircular wedge UWB antennas with co-planar waveguide (CPW) feed [66]. It has the advantage of ultra-wide band operation, omnidirectionality, ease of fabrication and low-cost. The characteristics of the used antennas including matching, radiation pattern, and detail geometry can be found in [66].

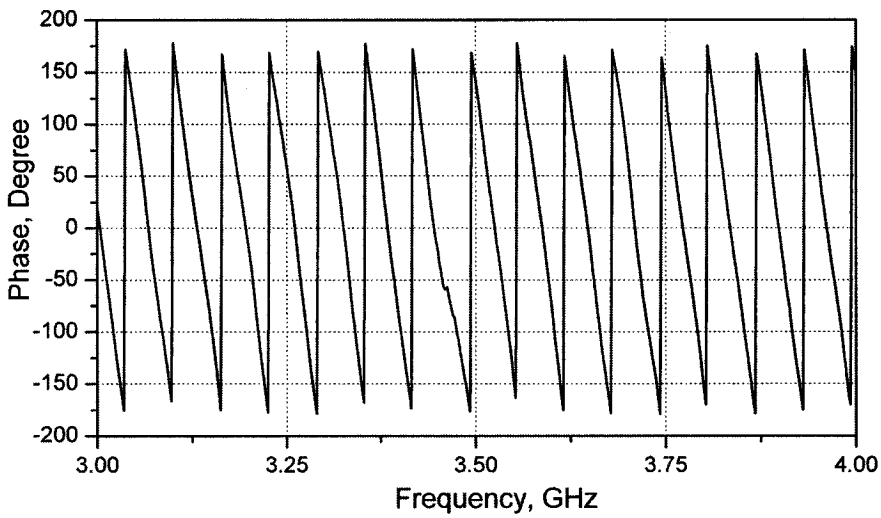

Fig. 5-8. Measured phase response of the wireless link using UWB antennas.

As a focus of this work, the phase linearity is examined by measuring forward transmission between the input port of the transmit antenna and the output port of the

receive antenna. Two antennas were fixed on a same level with a distance of 40 cm. Fig. 5-8 shows the phase response of the measured forward transmission. The phase response is linear over the frequency range, validating the design procedure.

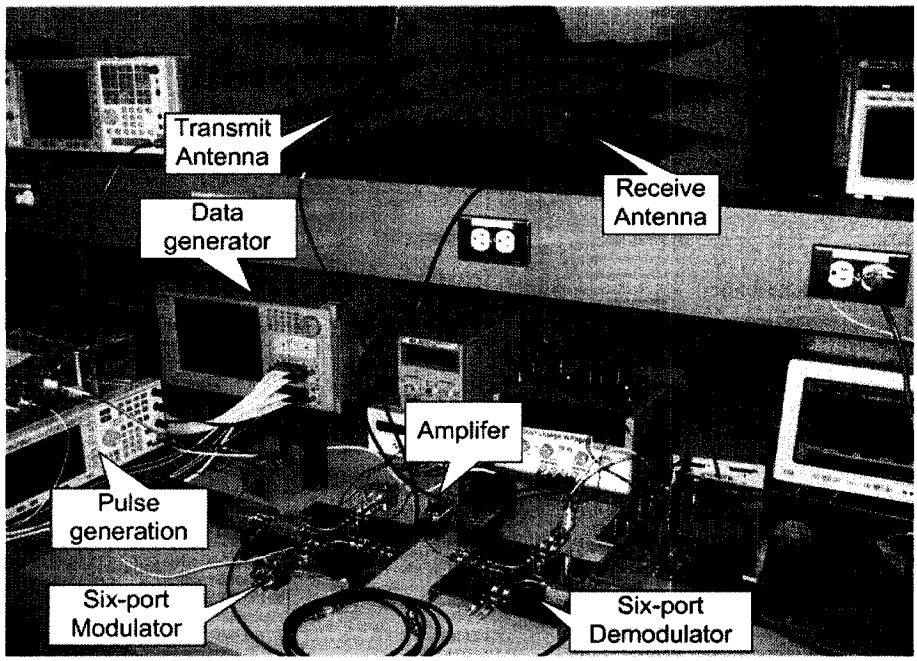

Fig. 5-9. Mulit(six)-port impulse UWB test bench (3–4GHz) (point-to-point wireless link).

A UWB test bench using wireless link (Fig. 5-9) was implemented by replacing the direct cable connection with the UWB antennas. An amplifier is connected at the receive antenna terminal to compensate the link loss. A system measurement was done using the test bench and UWB antennas. The measured BER results shown in Fig. 5-10 are compared with theoretical, simulation and measurement results using direct connection. The close agreement among these results once again strengthens the proposed UWB system function over an AWGN channel using both wired and wireless link.

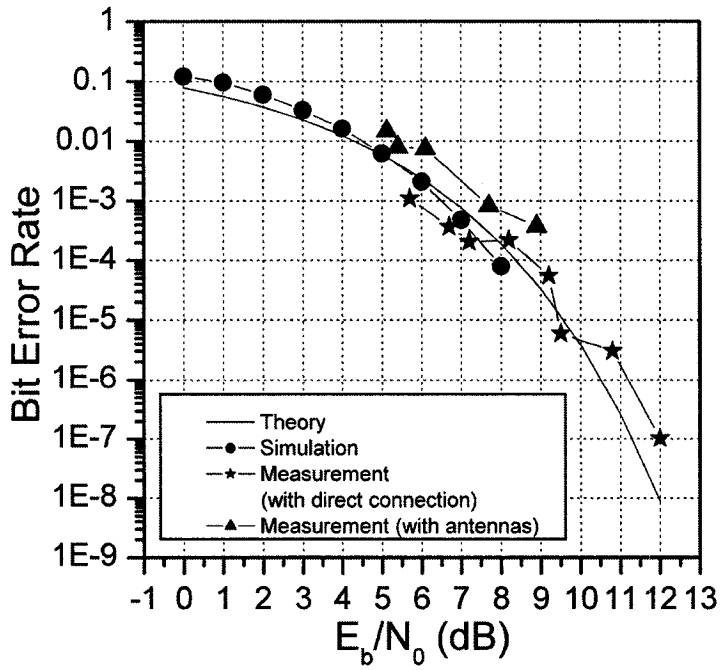

Fig. 5-10. BER result using point-to-point wireless link and comparison.

5.3 Synchronization method

One of the practical issues considered when implementing the UWB test bench is synchronization. In order to demodulate the received signal, the received pulse signal and a reference signal are coherently processed in six-port demodulator. It requires that a reference signal must be synchronized to the received signal using a certain method. During above simulation and experimental study of the multi-port UWB system, the reference signal is derived from the transmitted pulse signal using a power divider. A certain length of transmission line is inserted into the reference signal path to match the receiving signal path delay. In future developments of the platform, this synchronization will be accomplished using an algorithm based on the six-port output signals. An investigation has been done on the output signal of six-port demodulator under non-synchronization situations, i.e., an arbitrary delay exists between the reference signal and

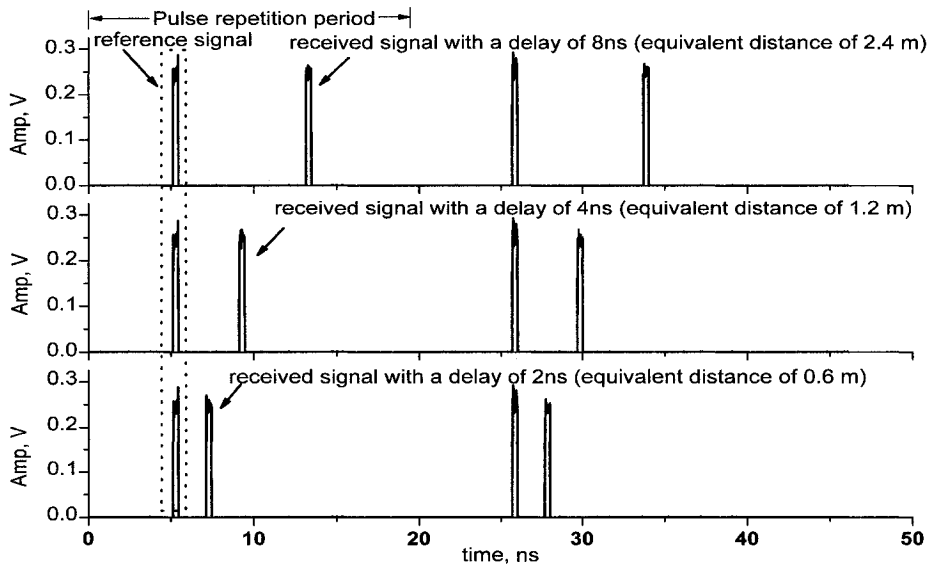

Fig. 5-11. Simulated output signals for three different delays.

the received signal. The purpose is to find the delay by observing the signals at the six-port demodulator outputs.

System simulation has been carried out with practical parameters over an additive white Gaussian noise (AWGN) channel. A pulse signal occupying a frequency band from 3.1 to 6.2 GHz is used for simulation. Its fractional bandwidth is 0.67. The width of each pulse is 320 ps which is equivalent to a space resolution of 0.6 cm. The pulse repetition period is 20.48 ns. The simulation focuses on the time delay and doesn't include the power decay factor. Fig. 5-11 shows the output signals for three different delays between reference signal and received signal. Within a pulse repetition period, the output signal is a waveform with two pulses. The simulation results show that the time difference between two pulses is equivalent to the propagation delay between the reference pulse and the received pulse. The propagation delay can be easily converted to a free space distance between transmitter and receiver. Since the output signal can be regarded as a pattern for a certain delay, a pattern recognition algorithm [67] was used to estimate delay values.

A proof-of-concept experiment was done to verify this function. In the experiment, two input ports of a six-port demodulator are fed respectively with a reference signal and a delayed received signal. Six-port output signals are measured when the delay in the receive path is changed using three different cables with lengths of 6, 11, and 14 feet, respectively. Fig. 5-12 shows this set up. It is readily seen in Fig. 5-13 that within a pulse repetition period, the measured time difference between two voltage peaks is equivalent to the length of cable. This equivalence can be verified using equation (5.23).

$$delay = \frac{l}{(c/\sqrt{\varepsilon_r})} \tag{5.23}$$

where l is the length of cable, $c = 3.0 \cdot 10^8\ m/s$ is the speed of light in free space,

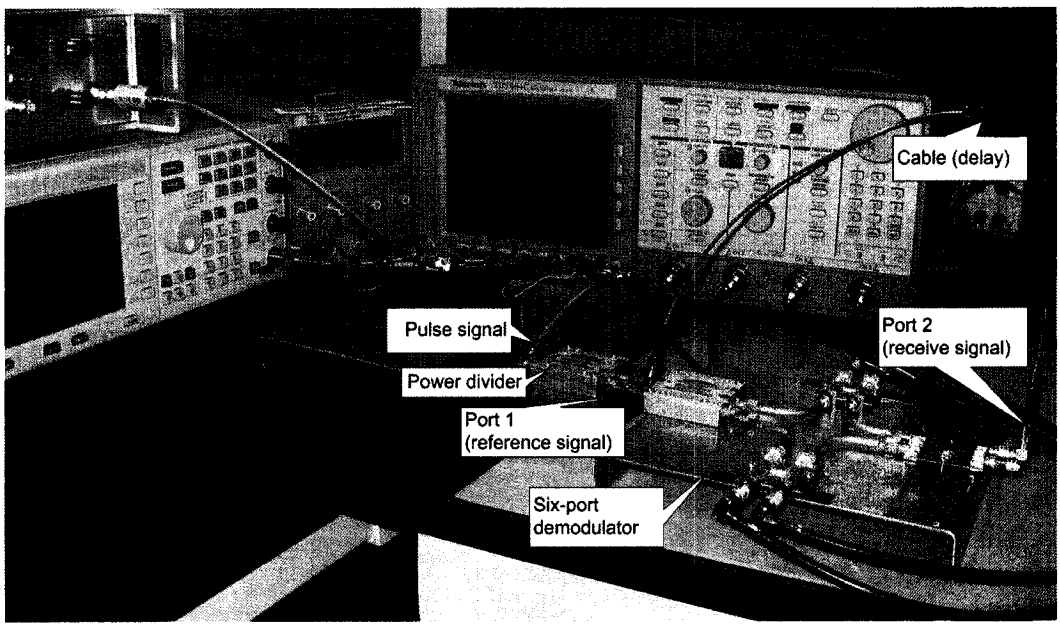

Fig. 5-12. Experimental set up for delay estimation using six-port output signals.

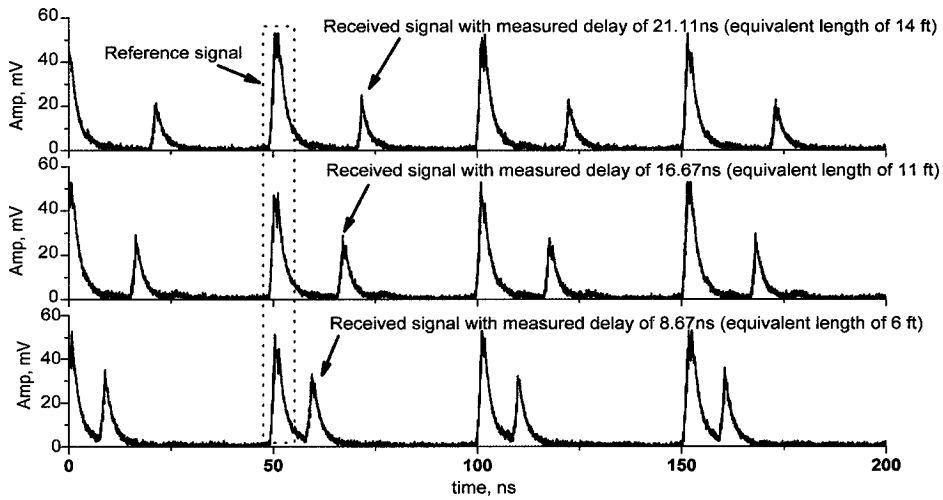

Fig. 5-13. Measured signals at Port 3 for three different delays.

$\varepsilon_r = 2.03$ is the known dielectric constant of the material of used cables. The small deviation caused by connectors between cables is neglected.

Based on the above results, a synchronization algorithm can be developed to facilitate the generation at receiver of a reference pulse acquiring and synchronizing to the transmitted signal. The algorithm based on recognition of six-port output signal pattern may provide a unique solution for this multi(six)-port UWB system.

5.4 Factors affecting system performance

System performance can degrade from the ideal performance including constraints such as additive noise, multipath interference, channel interference, and implementation of the transceiver, etc. This section qualitatively discusses some of the influences with the experimental results.

5.4.1 Hardware limitations

A 3-dB forward transmission loss exists in a six-port modulator due to the losses introduced by 3 dB power divider and hybrid couplers in the six-port circuit.

The phase and amplitude of modulated signals is affected by phase and amplitude imbalance from the power divider and hybrid couplers. This phase and amplitude imbalance is deterministic and can be minimized by the design method of six-port circuits described in chapter 3.

The data rate of the six-port modulator is limited by the switching time. In the modulator, the baseband data controls switches. A data stream can not be faster than the response of a switch.

The sensitivity of six-port receiver is limited by the sensitivity of power detectors. To

comply with FCC average power limit ($P_{\max}^{+}(f) = -41.3\ dBm/MHz$) in the considered test bench, the maximum allowed total power $P_{\max}$ for the pulse signal occupying frequencies between $f_L = 3.0\ GHz$ and $f_H = 4.0\ GHz$ can be calculated as follows:

$$\begin{aligned} P_{\max}|_{dBm} &= 10\log_{10}\left(\int_{3.0\cdot10^3}^{4.0\cdot10^3} P_{\max}^{+}(f)df\right) \\ &= -41.3 + 10\log_{10}\left(\frac{4.0\cdot10^3 - 3.0\cdot10^3}{1}\right) \\ &= -11.3\ dBm \end{aligned} \tag{5.24}$$

The power detector adopted in the test bench has low level sensitivity of 0.5 mV, which corresponds to -53 dBm in a 50-Ohm system. Considering the 3 dB power divider, the six-port demodulator can accept a maximum link attenuation of about 39 dB. In case that the attenuation is beyond the limit, a low noise amplifier is necessary at the receiver.

5.4.2 Multi-path effects

There exist multiple paths from a transmitter to a receiver due to physical effects of reflection, absorption, diffraction, and scattering by objects in-between the transmitter and the receiver [68]. Due to the different path lengths, a transmitted UWB pulse signal will arrive at the receiver as the sum of several pulses with different delays and strengths (related to path length and conditions).

A potential benefit of UWB radio transmission is fine time resolution leading to elimination of frequency fading problem in multipath environment. As for a transmitted ideal impulse signal, the received paths are isolated and independent of one another, and

therefore impulses arriving from different paths do not interact with each other. The powers from different paths add algebraically. However, for a narrowband system the received power is the result of the phasor summation of several vectors corresponding to different paths. Therefore the received signal fluctuates in power and fades deeply at particular locations.

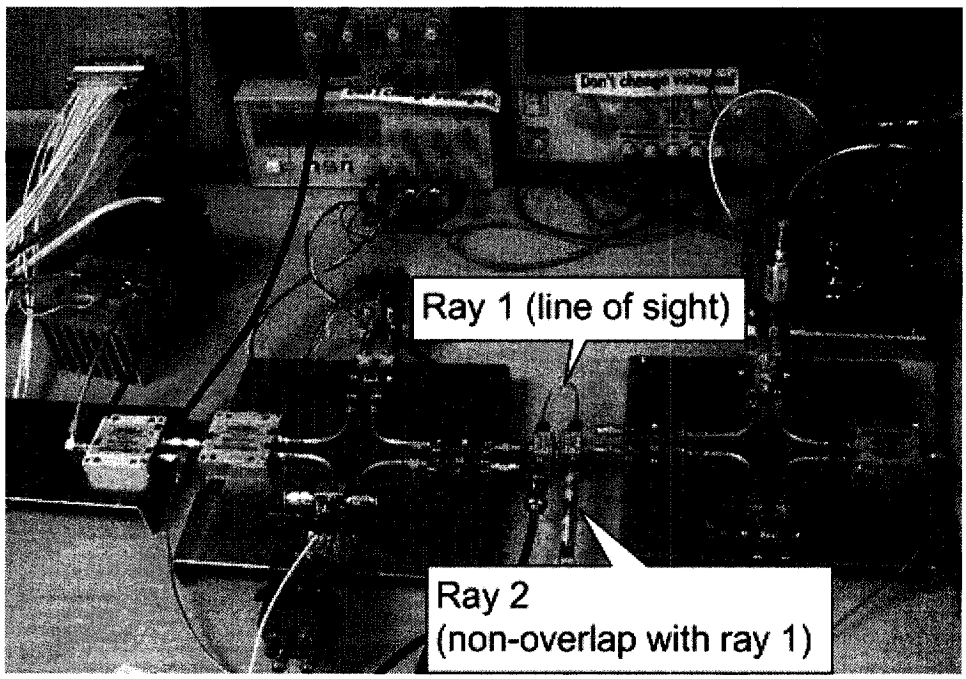

Fig. 5-14. Experimental setup for MIR UWB measurement in a two-path channel.

In the MIR UWB test bench, a pulse signal with 2-ns width is used. If pulses from multipaths arrive within one pulse width they will interfere, while if they are separated by at least one pulse width they will not interfere. Thus the required distance between multipaths to avoid interference is 60 cm. The separation distance required between multipaths can be decreased by decreasing pulse width.

If pulses do not overlap, multipath pulse signals are resolvable at receiver. It is feasible to demodulate a signal based on the strongest resolvable path. Other paths can be filtered out in the time domain. Alternatively, a RAKE receiver can be used to accumulate the energy of resolvable strongest paths [69].

A non-overlap two-path channel was considered in the experiment. The experimental two-path channel was set up using power dividers, one attenuator, and two different lengths of cables (Fig. 5-14). It has a power delay profile shown in Fig. 5-15. The measured time difference and the power difference between these two paths are 17.27ns and 14.4 dB respectively.

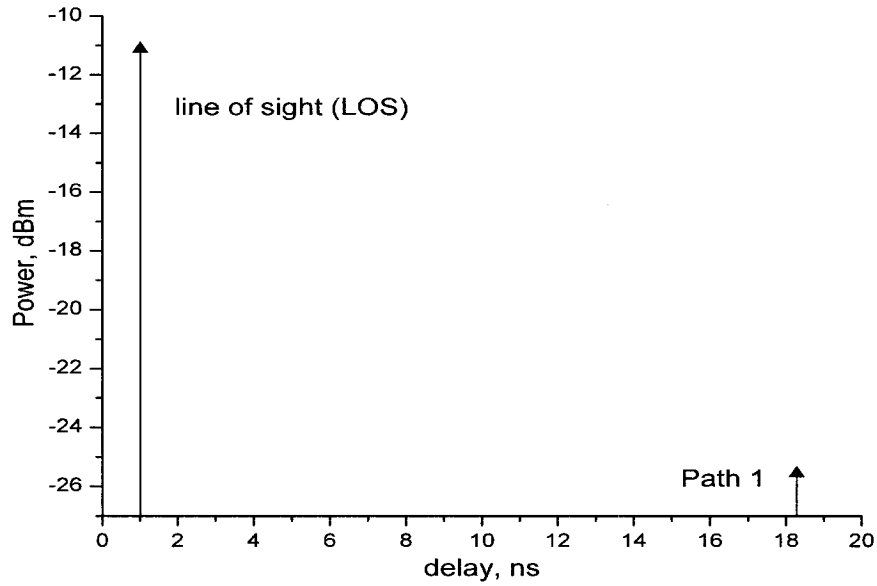

Fig. 5-15. Power delay profile of the experimental two-path channel.

The baseband processing selects the strongest line-of-sight signal for demodulation and simply filters out the other path by timing control. The measured BER performance is shown in Fig. 5-16. It proves the mutlipath immunity of MIR UWB bench under a certain condition. However, more sophisticated algorithms can be developed for operating the MIR in practical multipath channels. The observed performance degradation is due to the attenuation introduced by the power divider (3 dB) in the two-path setup.

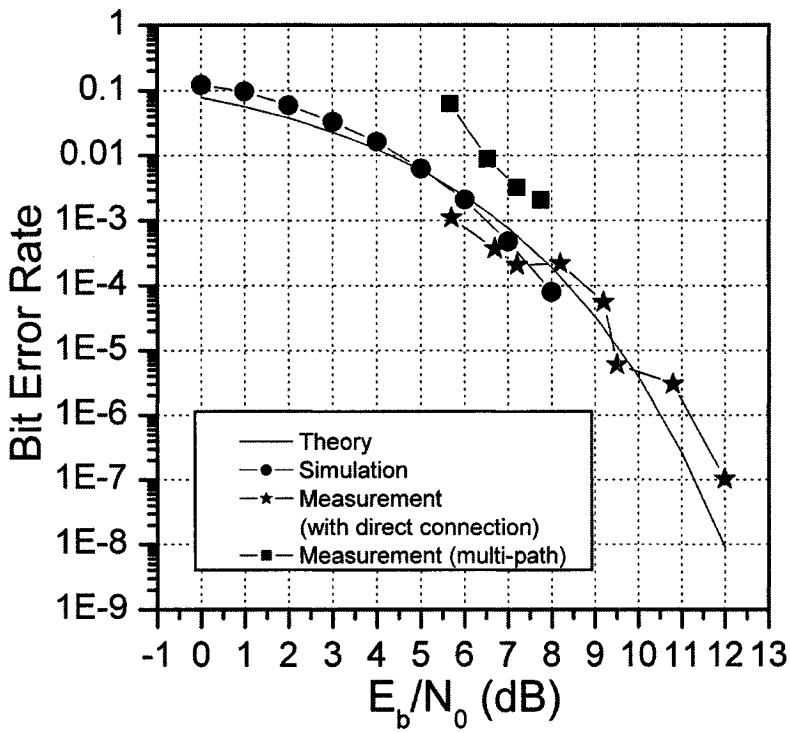

Fig. 5-16. BER of MIR test bench over a two-path channel.

5.4.3 Impact of narrow band interference on MIR UWB

The MIR UWB system uses a wide bandwidth to transmit information. A narrow band signal within the occupied UWB bandwidth will act as interferers to the UWB system. Performance degradation will depend upon the number and distribution of the narrow band signal, the relative powers, and the type of modulation used.

The following experiment considered a single narrow band signal which is a QPSK modulated signal occupying 1.2 MHz bandwidth. The carrier signal is located at the center of the UWB signal spectrum. This interferer and UWB signal were fed into the receiver using a power combiner. Starting at a reference performance point, the power level of the narrow band signal was increased from -30 dBm to 0 dBm. The UWB signal was unchanged. The measurement results in Fig. 5-17 observed performance degradation caused by the narrowband interferer.

In a practical environment, if the frequency of the narrow band interferer is known by e.g. a spectrum measurement, several techniques can be used to suppress the interferer. A hardware solution is to adopt dual-band six-port circuits based on metamaterial composite right/left handed (CRLH) transmission lines [70]. It is conceptually equivalent to integrate a single wideband six-port and a notch filter into one compact circuit. Also, the transmit pulse signal can be shaped in terms of pulse width and repetition period to avoid the interference [71].

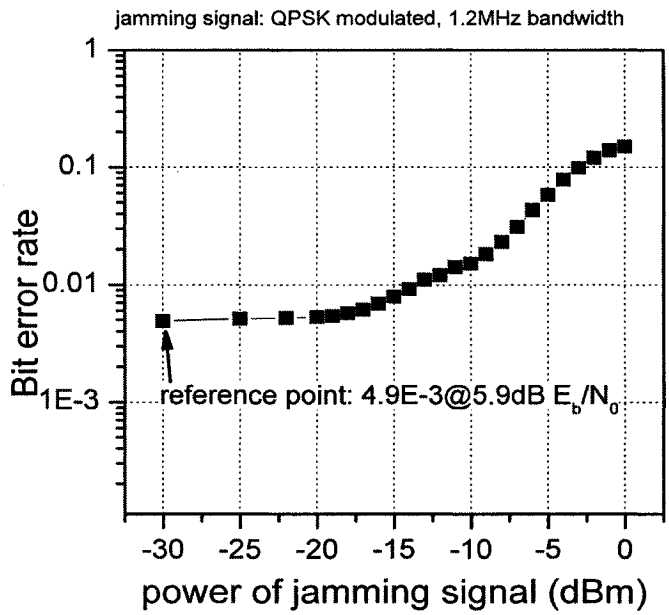

Fig. 5-17. Impact of jamming signal.

5.4.4 Coexistence with narrowband radio

The FCC has restricted the maximum power emitted by the UWB systems to be a power spectral density of -41.3 dBm/MHz. A narrow band radio, e.g. IEEE 802.11a standard, has a power spectral density of 4 dBm/MHz for the band of 5.25-5.35 GHz [72]. A typical UWB pulse signal has a spectrum approximately flat over a narrow bandwidth. Consequently, the effect of the UWB signal is to raise the noise floor of the narrow band systems that utilize the same spectrum.

An experiment was done to show the effect of UWB signal on a narrow band QPSK signal. Fig. 5-18 shows spectrums of both narrow band signal and UWB signal over the bandwidth 3.0 – 4.0 GHz. For the narrow band signal, the effective noise level is the level of UWB signal. This effect of the UWB signal on the narrow band radio is observed by measuring constellations of narrow band radio. Three constellations (Fig. 5-19 – Fig. 5-21) were obtained at typical values of C/I_{UWB} - 20 dB, 11 dB, and 5 dB. C/I_{UWB} denotes the ratio of narrow band carrier power to the UWB interference power at the same frequency. Performance degradation can be visually observed from Fig. 5-19 to Fig. 5-21. The figure of merit (EVM) shows the degradation quantitatively. The rms average is the square root of the sum of the squares of the normalized EVM values measured at each symbol time [73]. The definition of EVM can be found in equation (3.9).

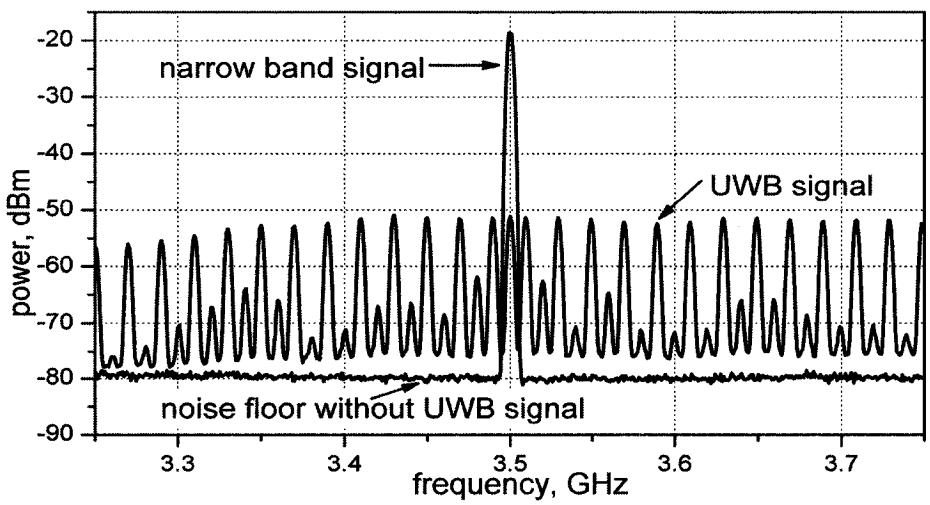

Fig. 5-18. Spectrums of narrow band signal and UWB signal.

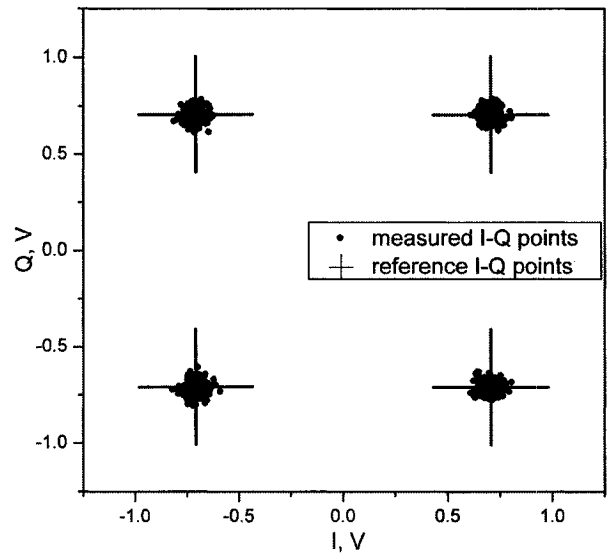

Fig. 5-19. Normalized I-Q constellation C/I_{UWB} = 20dB, EVM = 4.51 % rms.

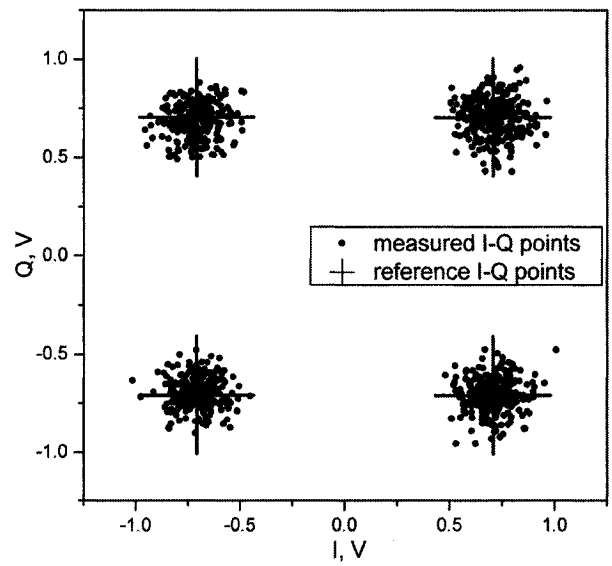

Fig. 5-20.Normalized I-Q constellation C/I_{UWB} = 11dB, EVM = 12.6 % rms.

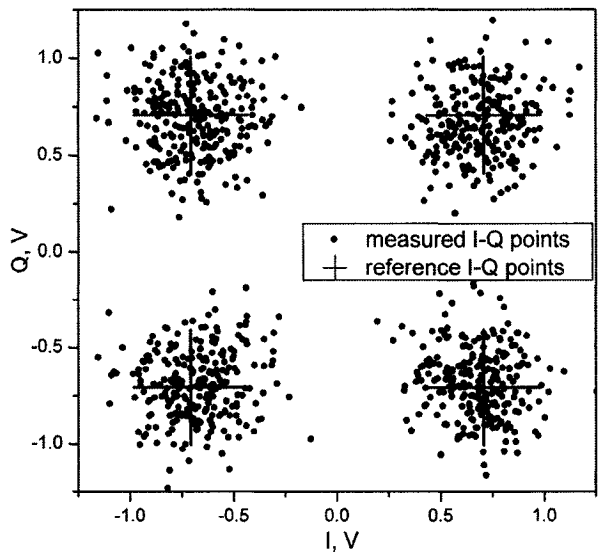

Fig. 5-21. Normalized I-Q constellation $C/I_{UWB} = 5$ dB, EVM = 25.2 % rms.

5.5 Comparison with other UWB systems

In this section, the proposed MIR UWB system is compared with other UWB systems from a more qualitative viewpoint.

- For transceiver architectures, other UWB systems usually include a circuit controlling timing or shape (depends on modulation scheme) at the transmitter end and a correlation circuit at the receiver end. The MIR UWB adopts a quasi-symmetric transceiver architecture (using six-port circuits for both modulation and demodulation).
- For modulation schemes, common choices of modulation scheme in existing

Impulse-UWB system include pulse position modulation (PPM), pulse amplitude modulation (PAM), and pulse shape modulation. In the MIR UWB system, the proposed phase spectrum modulation scheme encodes the information in phase spectrum of a pulse signal over a single wideband channel. In previous modulation methods, data information is conveyed either in position, amplitude or shape of a pulse but do not use wideband single channel phase spectrum modulation. Considering one of the leading proposal for UWB standards, a direct-sequence UWB system spreads one bit into multiple pulses using a pseudo random (PR) code. And one of the modulation schemes (PAM, PSM, or on-off keying) is superposed on each of these PR coded multiple pulses [74].

- A common UWB receiver is based on a correlation circuit which consists of a multiplier and an integrator [75]. The single output from the correlation circuit is then used for bit detection. In a MIR UWB bench, the wide band six-port demodulator equivalently realizes the correlation function. Its four output signals facilitate subsequent signal processing. The complexity of having more outputs can be traded off by realizing both UWB communication and positioning functions on a single hardware [76].

CHAPTER 6 CONCLUSIONS AND FUTURE WORKS

A multi(six)-port impulse radio for UWB communications has been proposed and studied. The multi(six)-port radio validates full channel (3-4 GHz) novel phase spectrum modulation scheme using a six-port modulator and demodulator circuits. The implemented MIR UWB test bench was measured with direct connection, point-to-point wireless link, and a two-ray channel. System performance results were obtained by simulations and experiments. They are in close agreement with the theoretical reference. On the other hand, factors degrading system performance were investigated. The MIR UWB is also able to coexist with existing radio system although it raises the noise floor to a certain extent. A brief comparison with other UWB systems was also given.

Major contributions are summarized as follows:

- The six-port concept has been applied to UWB.
- Novel phase spectrum modulation and demodulation algorithms have been proposed and validated using simulations and experimental results.
- An optimum method was proposed for six-port design.
- The MIR UWB performance over wireless link, simplified multipath channel, and coexistence with standard narrow band radio, was experimentally characterized.

Proposals for future work on the MIR UWB prototype include:

- Design of integrated circuit which integrates UWB antennas, six-port modulator, and demodulator on a single chip.

- Develop a synchronization algorithm for MIR.
- Investigate the capability of accommodating both impulse-UWB and multi-band UWB standards on the same MIR hardware configuration.
- Study the capability of realizing both UWB communication and positioning functions using a single MIR hardware.

References

[1] Wentzloff, D.D., Blazquez, R., Lee, F.S., Ginsburg, B.P., Powell, J., Chandrakasan, A.P. (2005). System Design Considerations for Ultra-Wideband Communication. IEEE Communications Magazine, 43 , 8, 114-121.

[2] Romme, J., Siemons, J., Durisi, G. (2003). A Method for the Detection of the Narrowband Interferer. 2003 IWUWBS workshop, Oulu, Finland, [online]. Available: http://www.whyless.org/public/wp5_publications.htm.

[3] Ohhikata, Y., Kobayashi, T. (2005). Proposal for an MB-OFDM UWB System Simultaneously Undertaking Ranging and Communications. 2005 IEEE International Conference on Ultra-Wideband, 604-608.

[4] Fontana, R.J. (2004). Recent System Applications of Short-Pulse Ultra-Wideband (UWB) Technology. IEEE Transactions on Microwave Theory and Techniques, 52, 9, 2087-2104.

[5] Oppermann, I., Hämäläinen, M., Iinatti, J. *UWB Theory and Applications*. Chichester, England : Wiley, 2004, 5.

[6] Federal Communications Commision (2002). First report and Order in the matter of revision of the commsion's rules regarding ultrawideband transmission systems.

[7] Nekoogar, F. *Ultra-wideband communications fundamentals and applications*. Upper Saddle River, NJ : Prentice Hall PTR, 2006, ch.4.1.

[8] Da Silva, J.A.N., De Campos, M.L.R. (2003). Performance Comparison of Binary and Quaternary UWB Modulation Schemes. IEEE Global Telecommunications Conference, 2, 789-793.

[9] Pahlavan, K., Levesque, A.H. *Wireless information networks*. Hoboken, N.J. : Wiley-Interscience, 2005, 596.

[10] Di Benedetto, M.-G., Giancola, G. *Understanding ultra wide band radio fundamentals*. Upper Saddle River, N.J. : Prentice Hall PTR, 2004,1-3.

[11] Engen, G.F. (1997). A (Historical) Review of the Six-Port Measurement Technique. IEEE Transactions on Microwave Theory and Techniques, 45, 12, 2414-2417.

[12] Li, J., Bosisio, R.G., Wu, K. (1995). Computer and Measurement Simulation of a New Digital Receiver. IEEE Transactions on Microwave Theory and Techniques, 43, 12, 2766-2772.

[13] Luy, J.-F., Mueller, T., Mack, T., Terzis, A. (2004). Configurable RF Receiver Architectures. IEEE Microwave Magazine, 5, 1, 75-82.

[14] Tatu, S.O., Moldovan, E., Brehm, G., Wu, K., Bosisio, R.G. (2002). Ka-Band Direct Digital Receiver. IEEE Transactions on Microwave Theory and Techniques, 50, 11, 2436-2442.

[15] Xiong, X.Z., Fusco, V.F. (2003). Wideband 0.9 GHz to 5 GHz Six-Port and Its Application As Digital Modulation Receiver. IEE Proceedings - Microwaves, Antennas and Propagation, 150, 4, 301-307.

[16] Hentschel, T. (2005). The Six-Port As a Communications Receiver. IEEE Transactions on Microwave Theory and Techniques, 53, 3, 1039-1047.

[17] Laskar, J., Matinpour, B., Chakraborty, S. *Modern Receiver Front-Ends Systems, Circuits, and Integration*. Hoboken, N.J. : Wiley-Interscience, 2004.

[18] Xu, X., Bosisio, R.G., Wu, K. (2006). Analysis and Implementation of Six-Port Software-Defined Radio Receiver Platform. IEEE Transactions on Microwave Theory and Techniques, 54, 7, 2937-2943.

[19] Zhao, Y., Viereck, C., Frigon, J.F., Bosisio, R.G., Wu, K. (2005). Direct Quadrature Phase Shift Keying Modulator Using Six-Port Technology. Electronics Letters, 41, 21, 1180-1181.

[20] Jackson, B.R., Saavedra, C.E. (2004). 2.4 GHz Direct-Digital Binary Phase Shift Keying Modulator Using MEMS Switch. Electronics Letters, 40, 24, 1539-1541.

[21] Jokanovic, B., Stojanovic, S., Peric, M. (2001). Direct QPSK Modulator for Point-to-Point Radio Link at 23 GHz. 5th International Conference on Telecommunications in Modern Satellite, Cable and Broadcasting Service, 1, 217-220.

[22] Moldovan, E., Tatu, S.-O., Gaman, T., Wu, K., Bosisio, R.G. (2004). A New 94-GHz Six-Port Collision-Avoidance Radar Sensor. IEEE Transactions on Microwave Theory and Techniques, 52, 3, 751-759.

[23] Gutierrez Miguelez, C., Huyart, B., Bergeault, E., Jallet, L.P. (2000). A New Automobile Radar Based on the Six-Port Phase/Frequency. IEEE Transactions on Vehicular Technology, 49, 4, 1416-1423.

[24] Xu, X., Bosisio, R.G., Wu, K. (2005). A New Six-Port Junction Based on Substrate Integrated Waveguide Technology. IEEE Transactions on Microwave Theory and Techniques, 53, 7, 2267-2273.

[25] Deslandes, D., Wu, K. (2001). Integrated Microstrip and Rectangular Waveguide in Planar Form. Microwave and Wireless Components Letters, 11, 2, 68-70.

[26] Nguyen, H.V., Caloz, C. (2006). Metamaterial-Based Dual-Band Six-Port Front-End for Direct Digital QPSK Transceiver. IEEE Mediterranean Electrotechnical Conference, 363-366.

[27] Caminiti, F.. (2005). Progetto e Realizzazione Di Antenne Per Sistemi UWB. Laurea Thesis, Univ. of Pavia.

[28] Xu, X., Tatu, S.O., Moldovan, E., Bosisio, R.G., Wu, K. (2002). Analysis of FDSS Ultra-Wideband Six-Port Receiver. IEEE Radio and Wireless Conference, 87-90.

[29] Huyart, B., Bergeault, E., Geneves, G., Jallet, L.P. (1999). Design and Measurement Results of a Six-Port Network Analyzer in the 1-18GHz Frequency Band. Annales des Telecommunications, 46, 7-8, 443-451.

[30] Siwiak, K., McKeown, D. *Ultra-wideband radio technology*. Chichester, England : Wiley, 2004, 60-62.

[31] Taylor, J.D. *Ultra-wideband radar technology*. Boca Raton, FL.: CRC Press, 2001, chapter 10.

[32] Xu, X., Bosisio, R.G., Wu, K. (2005). A New Six-Port Junction Based on Substrate Integrated Waveguide Technology. IEEE Transactions on Microwave Theory and Techniques, 53, 7, 2267-2273.

[33] Nguyen, H.V., Caloz, C. (2006). Metamaterial-Based Dual-Band Six-Port Front-End for Direct Digital QPSK Transceiver. IEEE Mediterranean Electrotechnical Conference, 363-366.

[34] Lyshevski, S.E. *Engineering and scientific computations using MATLAB.* Hoboken : Wiley-Interscience, 2003, 172-173.

[35] 3-Genaration Partner Project. Universal Mobile Telecommunications System (UMTS); UTRA (BS) FDD; Radio Transmission and Reception (3GPP TS 25.104 version 4.7.0 Release 4); ETSI TS 125 104 V4.7.0, 2003, pp.23.

[36] Visan, T., Bosisio, R.G., Beauvais, J. (2000). New Phase and Gain Imbalance Correction Algorithm for Six-Port-Based Direct-Digital Millimetric Receivers. Microwave and Optical Technology Letters, 27, 6, 432-438.

[37] Radmanesh, M.M. *Radio frequency and microwave electronics illustrated.* Upper Saddle River, NJ : Prentice Hall PTR, 2001, 598-601.

[38] Proakis, J.G. *Digital Communications.* Boston : McGraw-Hill, 3rd Edtion, 1995, 271.

[39] Agilent Technology. ADS Documentation–Sinks, Sep. 2004, pp.1-7.

[40] The MathWorks Inc. Simulink–simulation and model-based design, version 6, ch.1.

[41] Sklar, B. *Digital communications fundamentals and applications*. Upper Saddle River, N.J : Prentice-Hall PTR, 2001,170.

[42] Voelker, K. (1995 Dec.). Apply Error Vector Measurements in Communications Design. Microwave & RF, 143-152.

[43] Agilent Technology. ADS Documentation–Introduction to circuit components, Sep. 2004, ch.5, pp.1-17.

[44] Proakis, J.G., Manolakis, D.G. *Digital signal processing : principles, algorithms, and applications*. Upper Saddle River, N.J. : Prentice Hall, 1996, 768-772.

[45] Minicircuits Company. Power splitter datasheet, [online]. Available: http://www.minicircuits.com/dg03-120.pdf .

[46] Anaren Inc. Hybrid couplers datasheet, [online]. Available: http://www.anaren.com/docs/pdf/1M703%20Rev%20A%2Epdf.

[47] Minicircuits Company. Switches datasheet, [online]. Available: http://www.minicircuits.com/dg03-216.pdf.

[48] Heroteck Inc. Zero-Bias Schottky Diode Detectors datasheet, [online]. Available: http://www.herotek.com/datasheets/pdf/Zero-Bias_Schottky_Diode_Detectors_100kHz-50Ghz.pdf

[49] Zhao, Y., Wang, L., Frigon, J. F., Nerguizian, C., Wu, K., Bosisio, R. G. (2006). A Software Defined Radio Receiver Architecture for UWB Communications and Positioning. IEEE Canadian Conference on Electrical and Computer Engineering, 197-200.

[50] Mano, M.M. *Digital design.* Upper Saddle River, New Jersey : Prentice-Hall, 2002, pp.139.

[51] Altera Corporation. Stratix EP1S80 DSP Development Board Data Sheet, [online].Availabe: http://www.altera.com/literature/ds/ds_stratix_dsp_bd_pro.pdf.

[52] Altera Corporation. Stratix Device Handbook, [online]. Availabe: http://www.altera.com/literature/lit-stx.jsp, July 2005, Vol.1, pp.2-6.

[53] Altera Corporation. Quartus II Handbook, [online]. Availabe: http://www.altera.com/literature/hb/qts/qts_qii5v1_01.pdf

[54] Boulet, B. *Fundamentals of signals and systems.* Hingham, Mass. : Da Vinci Engineering Press, 2006, 141-144.

[55] Misra, D. *Radio-frequency and microwave communication circuits analysis and design.* New York : Wiley, 2001, 517-518.

[56] Coulon, F.d. *Théorie et traitement des signaux.* Lausanne, Suisse : Editions Georgi, 1984, 77.

[57] Kissick, W.A. (2001 Jan). The Temporal and Spectral Characteristics of Ultrawideband Signals. U.S. National Telecommunications and Information Administration (NTIA) Report 01-383, pp.6-5, [online]. available: http://www.its.bldrdoc.gov/pub/ntia-rpt/01-383/01-383.pdf.

[58] Di Benedetto, M.-G., Giancola, G. *Understanding ultra wide band radio fundamentals.* Upper Saddle River, N.J. : Prentice Hall PTR, 2004, 163.

[59] Proakis, J.G. *Digital Communications.* Boston : McGraw-Hill, 3rd Edtion, 1995, 271.

[60] Pahlavan, K., Levesque, A.H. *Wireless information networks*. Hoboken, N.J. : Wiley-Interscience, 2005, pp.585.

[61] Agilent Technology. ADS Documentation–Timed components, Aug. 2005, ch.5, pp.65-66.

[62] Agilent Technology. ADS Documentation–Ptolemy simulation, Aug. 2005, ch.9, pp.8-11.

[63] Agilent Technology. ADS Documentation–Sinks, Aug. 2005, ch.1, pp.4-8.

[64] Jeruchim, M. (1984). Techniques for Estimating the Bit Error Rate in the Simulation of Digital Communication Systems. IEEE Journal on Selected Areas in Communications, 2, 1, 153-170.

[65] Schantz, H. *The art and science of ultrawideband antennas*. Boston, Mass. : Artech House, 2005, 30-33.

[66] Caminiti, F. (2005). Progetto e Realizzazione Di Antenne Per Sistemi UWB. Laurea Thesis, Univ. of Pavia, 71-86.

[67] Zhao, Y., Wang, L., Frigon, J.F., Nerguizian, C., Wu, K., Bosisio, R.G. (2006). UWB Positioning Using Six-Port Technology and a Learning Machine. IEEE Mediterranean Electrotechnical Conference, 352-355.

[68] Ghavami, M., Michael, L.B., Kohno, R. *Ultra-Wideband Signals and Systems in Communication Engineering*. Chichester : John Wiley & Sons, 2004, 15-18.

[69] Reed, J.H., Safari Tech Books Online *An Introduction to Ultra Wideband Communication Systems*. Upper Saddle River, NJ : Prentice Hall PTR, 2005, ch.6.1.4.

[70] Nguyen, H.V., Caloz, C. (2006). Dual-Band CRLH Six-Port Front-End in MIM Technology. 36th European Microwave Conference, 122-124.

[71] Iacobucci, M.S., Di Benedetto, M.-G., De Nardis, L. (2002). Radio Frequency Interference Issues in Impulse Radio Multiple Access Communication Systems. IEEE Conference on Ultra Wideband Systems and Technologies, 293-296.

[72] Murthy, C.S.R., Manoj, B.S. *Ad hoc wireless networks : architectures and protocols*. Upper Saddle River, NJ : Prentice Hall PTR., 2004, ch.14.2.

[73] Agilent Technology. Vector signal analysis basics – application notes 150-15, Jul. 2004, pp.34.

[online] available: http://cp.literature.agilent.com/litweb/pdf/5989-1121EN.pdf).

[74] Oppermann, I., Hämäläinen, M., Iinatti, J. *UWB Theory and Applications*. Chichester, England : Wiley, 2004, 61-63.

[75] Oppermann, I., Hämäläinen, M., Iinatti, J. *UWB Theory and Applications*. Chichester, England : Wiley, 2004, 89-93.

[76] Zhao, Y., Wang, L., Frigon, J. F., Nerguizian, C., Wu, K., Bosisio, R. G. (2006). A Software Defined Radio Receiver Architecture for UWB Communications and Positioning. IEEE Canadian Conference on Electrical and Computer Engineering, 197-200.

Appendix I Publication list

Journal papers:

[1] Zhao, Y., Frigon, J.-F., Ke Wu, Bosisio, R.G. (2006). Multi(Six)-Port Impulse Radio for Ultra-Wideband. IEEE Transactions on Microwave Theory and Techniques, 54, 4, 1707-1712.

[2] Zhao, Y., Viereck, C., Frigon, J.F., Bosisio, R.G., Wu, K. (2005). Direct Quadrature Phase Shift Keying Modulator Using Six-Port Technology. Electronics Letters, 41, 21, 1180-1181.

Conference papers:

[3] Zhao, Y., Frigon, J.-F., Ke Wu, Bosisio, R.G. (2006). RF Front-end for Impulse UWB Communication Systems. IEEE International Microwave Symposium, 308-311.

[4] Zhao, Y., Frigon, J.-F., Ke Wu, Bosisio, R.G. (2007). Numerical Model of Six-port and its Applications. 23rd International Review of Progress in Applied Computational Electromagnetics, accepted for publishing.

[5] Zhao, Y., Wang, L., Frigon, J.F., Nerguizian, C., Wu, K., Bosisio, R.G. (2006). UWB Positioning Using Six-Port Technology and a Learning Machine. IEEE Mediterranean Electrotechnical Conference, 352-355.

[6] Zhao, Y., Wang, L., Frigon, J. F., Nerguizian, C., Wu, K., Bosisio, R. G. (2006). A Software Defined Radio Receiver Architecture for UWB Communications and

Positioning. IEEE Canadian Conference on Electrical and Computer Engineering, 197-200.

[7] Zhao, Y., Gagne, J.-F., Wu, K. (2003). Adaptive Baseband Architecture for Software-Defined RADAR Application. IEEE Canadian Conference on Electrical and Computer Engineering, 2, 1087-1090.

Co-authored papers:

[8] Arshad, M., Frigon, J. F., Zhao, Y., Bosisio, R. G. (2007). Application of Six-Port Receiver for OFDM Signals. IEEE Canadian Conference on Electrical and Computer Engineering, accepted for publishing.

[9] Gerardi, L., Xu, Y., Zhao, Y., Bozzi, M., Perregrini, L., Wu, K., Bosisio, R. G. (2007). A New Six-port Circuit Architecture using Only Power Dividers/combiners," IEEE International Microwave Symposium, submitted.

[10] Xu, Y., Gerardi, L., Zhao, Y., Bozzi, M., Perregrini, L., Wu, K., Bosisio, R. G. (2007)., "Review of six-port interferometer technology," 23rd International Review of Progress in Applied Computational Electromagnetics, submitted.

[11] Gagne, J.-F., Xu, J.-J., Zhao, Y., Zhang, H., Wu, K. (2003). Software-defined Radar System: Concept and Application. Asia-Pacific Microwave Conference, 2, 1300-1303.